Spectroscopic studies of the human copper chaperone for superoxide dismutase: Probing the active cluster with selenocysteine variants

Amanda Nell Barry
Honors B.S., Biochemistry and Biophysics, Oregon State University (1999)
Honors B.S., Bioresource Research, Oregon State University (1999)
M.S., Bacteriology, University of Wisconsin-Madison (2002)

A dissertation submitted to the faculty of the

OGI School of Science & Engineering
at Oregon Health & Science University
in partial fulfillment of the
requirements for the degree

Doctor of Philosophy
In
Biochemistry and Molecular Biology

October 2007

The dissertation “Spectroscopic studies of the human copper chaperone for superoxide dismutase: Probing the active cluster with selenocysteine variants” by Amanda Nell Barry has been examined and approved by the following examination committee:

_____

Ninian J. Blackburn, Research Advisor
Professor

_____

James W. Whittaker
Associate Professor

_____

Matthew S. Sachs
Professor

_____

Megan M. McEvoy
Assistant Professor
University of Arizona

ACKNOWLEDGMENTS

I would like to thank my advisor, Dr. Ninian J. Blackburn, for accepting me as his student and for his guidance throughout my PhD research. I would also like to acknowledge the past and present members of the Blackburn lab, especially Jay Stasser and Martina Ralle for their teaching and advice on CCS and EXAFS.

I would especially like to thank my husband Matthew Hoffman, with whose help, patience, love, and expertise with Adobe Illustrator I could not do without.

TABLE OF CONTENTS

LIST OF FIGURES

LIST OF TABLES

ABSTRACT

Spectroscopic studies of the human copper chaperone for superoxide dismutase: Probing the active cluster with selenocysteine variants

Amanda Nell Barry
Thesis Advisor: Dr. Ninian J. Blackburn

Selenocysteine-containing mutants of human copper chaperone for superoxide dismutase (hCCS) were constructed using intein-mediated peptide ligation. These mutants were studied with respect to their ability to transfer Cu to E,Zn superoxide dismutase (SOD1) and their Cu-binding and X-ray absorption spectroscopic (XAS) properties. Previous studies have shown that three functionally distinct polypeptide domains are present in CCS: the N-terminal domain 1 (D1, residues 1-85) contains the copper-binding MXCXXC motif, domain 2 (D2, residues 86-234) has sequence homology to residues associated with the native SOD1 dimer interface, and the C-terminal domain 3 (D3, residues 235-274) contains a CXC motif. Recent results suggest the formation of a D3-D3 cluster within a dimeric or tetrameric protein and suggest that this cluster may be an important element of the copper transfer machinery. D3 cysteine-to-selenocysteine mutants of wild-type and D1 mutants of hCCS were constructed to investigate the D3 copper cluster in more detail. These mutants display similar activity to wild-type protein. The structure of the Cu centers of selenocysteine-containing mutants as shown by Cu EXAFS is similar to that of wild-type protein, with clear indications of a Cu cluster. Cu and Se EXAFS of these constructs reveal a unique adamantane-like cluster formed between two molecules of CCS at the D3-D3 interface. These results confirm the existence of a D3-D3 copper cluster in hCCS and suggest that a unique copper cluster may exist in this protein.

CHAPTER 1: INTRODUCTION

1.1 OVERVIEW

This thesis describes the characterization of the copper-binding site in domain 3 (D3) of the human copper chaperone for superoxide dismutase (hCCS). hCCS is necessary for the metalation of the copper-bound form of Cu,Zn-superoxide dismutase (SOD1) due to low amounts of intracellular free copper (Rae et al., 1999). The introduction of this thesis contains an overview of copper homeostasis in eukaryotes, including a discussion of copper transport into the cell, the copper chaperones, glutaredoxin, metallothioneins, copper export, and regulation. Three copper chaperones are discussed, and an in depth introduction to hCCS and SOD1 is provided. The copper binding sites of hCCS are reviewed. hCCS contains two copper-binding motifs in domain 1 (D1) (^{22}CXX^{25}C) and domain 3 (D3) (^{244}CX^{246}C), where a copper cluster is formed at a D3-D3 interface between a homodimer of reconstituted hCCS (Stasser et al. 2007). The structure of this cluster has not been previously established; it is the purpose of this thesis to elucidate this structure using a selenium probe in Cu and Se K-edge EXAFS.

Chapter 2 describes the materials and methods used in this thesis. Most notably, the creation of selenocysteine-containing hCCS variants using intein-mediated peptide ligation is discussed. The cloning and purification of truncation mutants of hCCS used for

single amino acid or peptide ligation is also discussed, as well as the expression of SOD1 used in SOD1-activation assays. Furthermore, this chapter includes a thorough discussion of Extended X-ray Absorption Fine Structure spectroscopy (EXAFS), a major method of this study to examine the semisynthetic hCCS constructs.

In Chapter 3, the ligation of a single selenocysteine and cysteine to a truncation variant of hCCS ending at amino acid 245 (CCS245Sec and CCS245Cys respectively) is discussed. Both of these constructs, along with a CCS246 truncation mutant, are characterized by copper binding, SOD1-activation assays, and EXAFS at the Cu and Se edge. This study not only confirms the presence of a D3-D3 copper cluster, but also provides evidence of residue 246 occupying a bridging position in the cluster. Furthermore, the transfer of copper to SOD1 by wild-type hCCS and the ligation mutants is investigated by EXAFS, showing that hCCS transfers copper to E,Zn-SOD1 from the D3 copper binding site. In Chapter 4, the creation and characterization of D1 double mutants of truncated hCCS ligated to a single selenocysteine or cysteine (C22,25A245Sec and C22,25A245Cys respectively) further elucidates the copper cluster structure in Cu K-edge EXAFS. Examination of these proteins provide compelling evidence for the existence of a trinuclear or tetranuclear copper cluster, as opposed to a dinuclear cluster. In Chapter 5, by examining peptide ligation variants of hCCS that replaced both Cys residues in the CXC copper-binding motif with Sec residues, conclusive evidence is given for a tetranuclear Cu_4S_6 adamantane-like copper cluster at the D3-D3 interface. Chapter 6 provides the final conclusions of the thesis, including a discussion of further studies to probe the D3-D3 copper cluster.

1.2 COPPER HOMEOSTASIS

Copper is an essential trace element, serving as a redox-active cofactor for a variety of metalloproteins involved in energy generation, protection against oxidative stress, iron uptake and distribution, and many other biological processes. Copper exists in two oxidation states, Cu(I) and the more stable oxidized form Cu(II). Proteins that require copper for activity include superoxide dismutase, cytochrome *c* oxidase, dopamine β-monooxygenase, tyrosinase, peptidylglycine alpha-amidating monooxygenase, and lysyl

oxidase. Due to its ability to reversibly donate and receive elections, copper possesses a potential toxicity to cells. Free copper is able to catalyze the generation of aggressive free radicals via the Fenton reaction:

$$O_2^- + O_2^- + 2H^+ \rightarrow H_2O_2$$
$$O_2^- + Fe^{3+} \rightarrow O_2 + Fe^{2+}$$
$$H_2O_2 + Fe^{2+} \rightarrow {}^{\cdot}OH + OH^- + Fe^{3+}$$

It has been demonstrated that a direct reduction of O_2 by Cu^+, the process referred to as the metal autoxidation reaction, may mediate ${}^{\cdot}OH$ generation (Urbanski and Beresewicz, 2000):

$$Cu^+ + O_2 \rightarrow Cu^{2+} + O_2^-$$

The production of ${}^{\cdot}OH$ can result in irreparable damage to proteins, lipids, and DNA through lipid peroxidation (Britton, 1996; Halliwell and Gutteridge, 1984). Lipid peroxides form by the attack of radicals on polyunsaturated fatty acid residues of phospholipids and can react with redox metals. This can produce mutagenic and carcinogenic malondialdehyde, 4-hydroxynonenal, and other exocyclic DNA adducts such as etheno and/or propano adducts. Also, by binding to proteins ectopically, copper can disturb protein structure (Uriu-Adams and Keen, 2005; Valko et al., 2005). There is essentially no free copper in the cytoplasm under normal physiological conditions (Rae et al., 1999). Due to its toxicity in both eukaryotic and prokaryotic cells, the uptake, transport, detoxification, storage, and elimination of copper are tightly regulated. Maintaining proper copper homeostasis provides the cell with essential copper levels without the production of damaging free radicals. In this way, copper is controlled through the import of Cu(I) into the cell via the copper transporter Ctr1, the shuttling of copper to specific proteins via copper chaperones, such as Cox17, Sco1, Cox11, the copper chaperone for superoxide dismutase (CCS), and Atox1, the sequestration of free copper in the cell by metallothioneins (MT), and the transcriptional regulation of copper controlling genes in the nucleus (Figure 1.1). Defects in these mechanisms can cause

severe or deadly diseases such as Menkes disease and Wilson disease (Culotta and Gitlin, 2001).

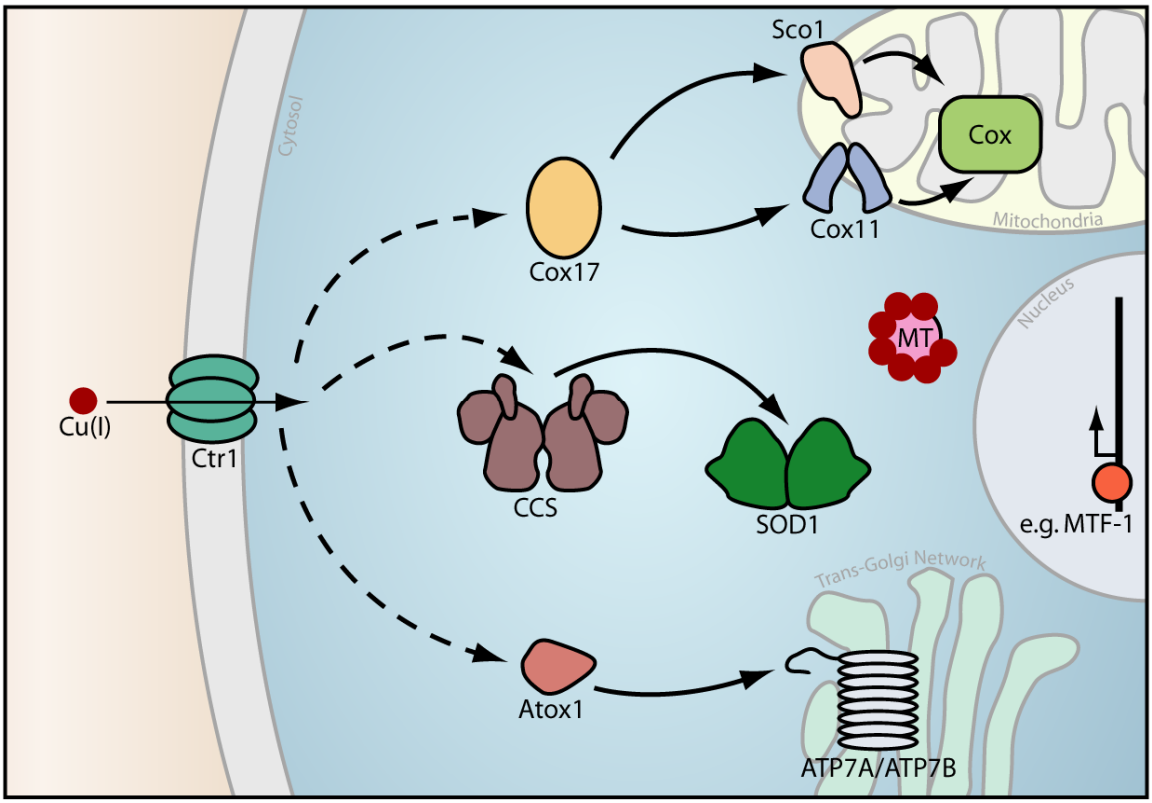

Figure 1.1. Copper homeostasis in the human cell.

1.2.1 TRANSPORT OF COPPER INTO THE CELL

In eukaryotic cells, copper uptake is performed by the copper transporter (Ctr)-family. These high-affinity, membrane-associated copper importers are relatively small proteins containing three transmembrane domains and transport Cu(I) rather than Cu(II). This is shown by the ability of silver, a Cu(I) mimetic, to strongly compete for transport (Lee et al., 2002) and by the requirement for metalloreductase activity at the yeast cell surface for high-affinity copper uptake (Hassett and Kosman, 1995). Ctr importers consist of four major domains. These proteins contain an N-terminal extracellular segment with one or more Met motifs, MXXM or MXM, that are important for survival under copper starvation (Guo et al., 2004; Petris, 2004) due to their involvement in the acquisition of

copper by directly coordinating Cu(I) (Jiang et al., 2005; Puig et al., 2002). Transport ability is stimulated by extracellular K^+ and does not require ATP for copper import (Lee et al., 2002; Petris, 2004). The first members of this family were identified in yeast, yCtr1 and yCtr3, and deletion mutant strains exhibit growth defects characteristic of copper depletion (Dancis et al., 1994a; Dancis et al., 1994b). In contrast to the three copper transporters found in yeast cells, human cells contain two Ctr proteins. Designated hCtr1 and hCtr2, both transporters contain a conserved C-terminal motif of a cysteine flanked by histidines (termed the HCH motif), located in the cytosolic domain. The cysteine in this motif, Cys189, is important for oligomerization of hCtr1 (Eisses and Kaplan, 2005). Only hCtr1, the main human cellular copper importer, is able to complement the defective copper uptake phenotype of the yeast *ctr1* and *ctr3* double mutant (Petris, 2004; Zhou and Gitschier, 1997). hCtr1 consists of 190 amino acids with three transmembrane domains. 2D crystallography and electron microscopy data show that hCtr1 forms a symmetrical homotrimer with a putative pore between the subunit interfaces (Nose et al., 2006) (Figure 1.2). Electron crystallography of hCtr1 2D protein crystals in a native phospholipid bilayer revealed a symmetrical trimer that is <40 Å wide with the center three-fold axis of each trimer forming a region of very low electron density that may form a channel that is likely to be involved in copper translocation (Aller and Unger, 2006). The amino terminus of both human and yeast Ctr1 is on the extracellular side of the plasma membrane, whereas the carboxyl terminus is in the cytosol (Eisses and Kaplan, 2005; Puig et al., 2002). The function of Ctr2 remains to be elucidated.

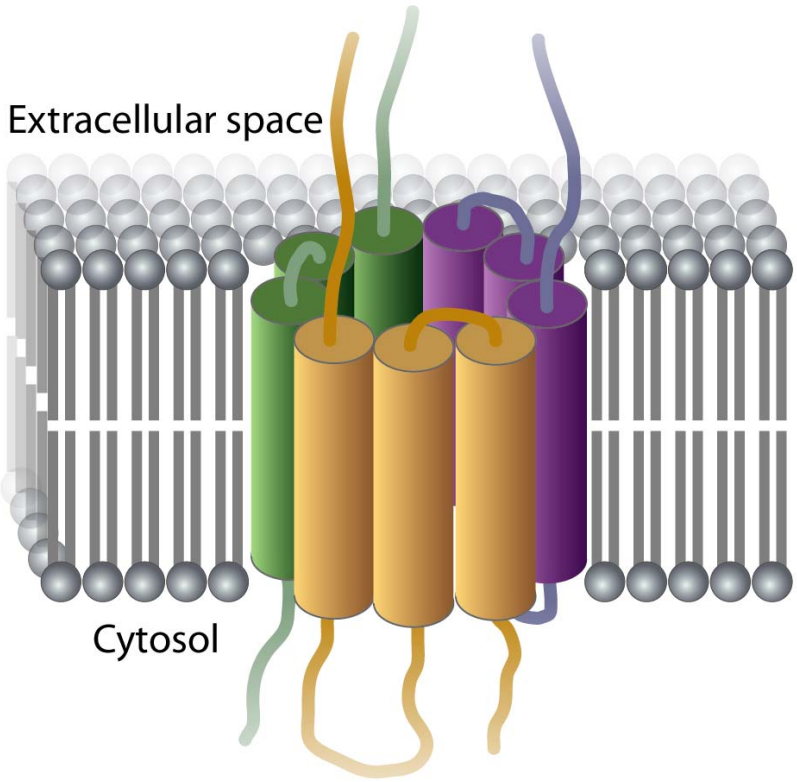

Figure 1.2. Putative structure of hCtr1. Modified from Nose et al., 2006.

1.2.2 COPPER CHAPERONES

After import, copper is provided to the copper chaperones from the Ctr proteins, which then traffic copper ions to specific intracellular proteins or compartments. These copper chaperones help in protecting the cell from the extreme toxicity of free intracellular copper by binding the copper with a high affinity and delivering it to target proteins. Unlike zinc, copper is required by a lower number of proteins, and therefore is needed at relatively low intracellular concentrations (Rae et al., 1999). Three functional groups of copper chaperones are conserved in eukaryotic cells: Atx1, Cox and CCS.

1.2.2.1 Atox1

In yeast, Atx1 delivers copper to the transport ATPase Ccc2 in the trans-Golgi network, where it translocates copper into vesicles that load into the multicopper containing

protein ferroxidase Fet3 (Lin et al., 1997). Human protein Atox1 is the homolog of Atx1 and is composed of 68 amino acids (Klomp et al., 1997). Atox1 belongs to a family of metal-binding domains characterized by a conserved MT/HCXXC sequence motif. The X-ray crystal structure of Atox1, in complex with either copper(I), cadmium(II), or mercury(II) metal ions, reveal a metal ion coordinated by three or four Cys residues derived from the metal-binding sites of two protein molecules in a metal:protein stoichiometry of 1:2 (Wernimont et al., 2000). Heteronuclear NMR methods showed that human Atox1 adopts the ferrodoxin fold both in the Cu(I)-loaded and apo forms. The solution structure of monomeric Cu(I)-Atox1 is different from the crystal structure of the same protein. Two protein molecules were found to coordinate a single metal ion in the crystal structure and only one protein molecule was found in the solution structure, although the protein fold is the same (Anastassopoulou et al., 2004) (Figure 1.3). Consistent with the solution structure of Atox1 where the S-Cu-S angle in Cu(I)-Atox1 was found to be $160^{o} \pm 25^{o}$, x-ray absorption spectroscopy revealed a linear two-coordinate Cu(I) center (Ralle et al., 2003).

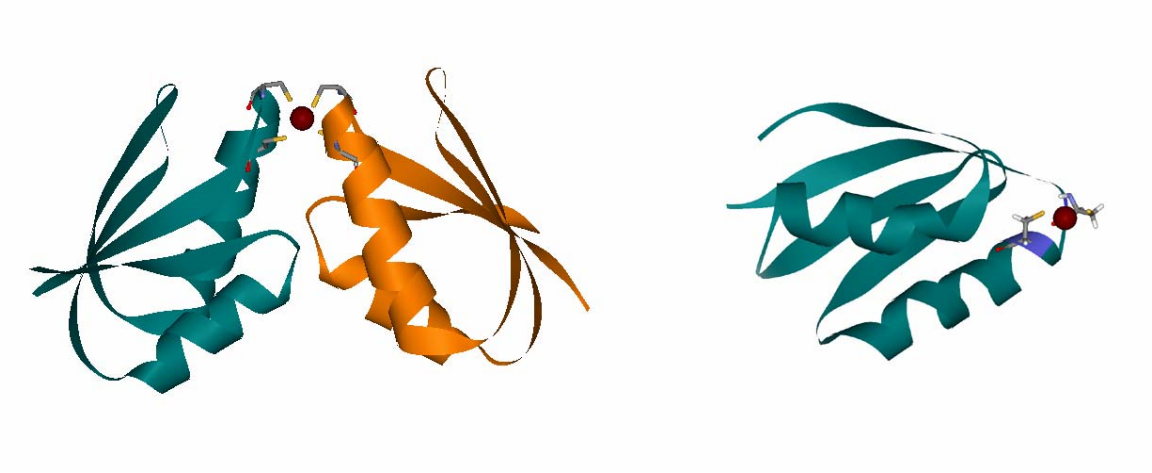

Figure 1.3. Left: Crystal structure of dimeric Cu(I)-bound Atox1 (Protein Data Bank file 1FEE); Right: Solution structure of monomeric Atox1 (Protein Data Bank file 1TL4). Copper atom in red.

Atox1 is responsible for delivering copper to Menkes and Wilson disease ATPase transporters, ATP7A and ATP7B respectively. After copper acquisition from Atox1, the copper transporting P-type ATPases ATP7A and ATP7B transport copper into the

secretory pathway for subsequent incorporation into essential cuproenzymes or export excess copper from the cell. ATP7A, the Menkes ATPase, transports copper across the placenta, the intestinal epithelium, and the blood-brain barrier (Chelly et al., 1993; Mercer et al., 1993; Vulpe et al., 1993). Disruption of ATP7A function results in copper deficiency in tissues, particularly in the brain, and leads to Menkes disease. The disease is associated with cerebral degeneration, abnormal hair structure and pigmentation, laxity of the skin and joints, and bony dysplasia. The Wilson ATPase, ATP7B, is expressed in the placenta, kidney, brain, and the liver (Bull et al., 1993; Muramatsu et al., 1998; Tanzi et al., 1993; Yamaguchi et al., 1993). The disruption of ATP7B function results in Wilson disease, which is characterized by impaired biliary copper excretion, excessive accumulation of copper in the cell cytoplasm, marked changes in liver morphology and function, as well as neurological and psychiatric abnormalities (Culotta and Gitlin, 2001). Furthermore, Atox1 is present at high concentrations in neurons and may serve a role in oxidative stress protection (Kelner et al., 2000). By isothermal titration calorimetry, binding affinities for Cu(I) of Atox1 and ATP7B domains indicate that the chaperone and the partner domains have similar binding constants (Wernimont et al., 2004).

Menkes and Wilson disease transporters have a long N-terminal cytosolic tail containing six CXXC copper-binding domains (Figure 1.4). The last two CXXC domains (counting from the N-terminus) are required for enzyme function, whereas the other copper-binding domains are involved in the regulation of activity, at least in ATP7B (Cater et al., 2004; Huster et al., 2003). The second copper-binding domain of ATP7B has been shown to act as the first entry point of Cu(I) upon delivery by Atox1 (Walker et al., 2004). An ATP-binding domain, composed of a phosphorylation domain and a nucleotide-binding domain, is present in both proteins and is essential for enzymatic function.

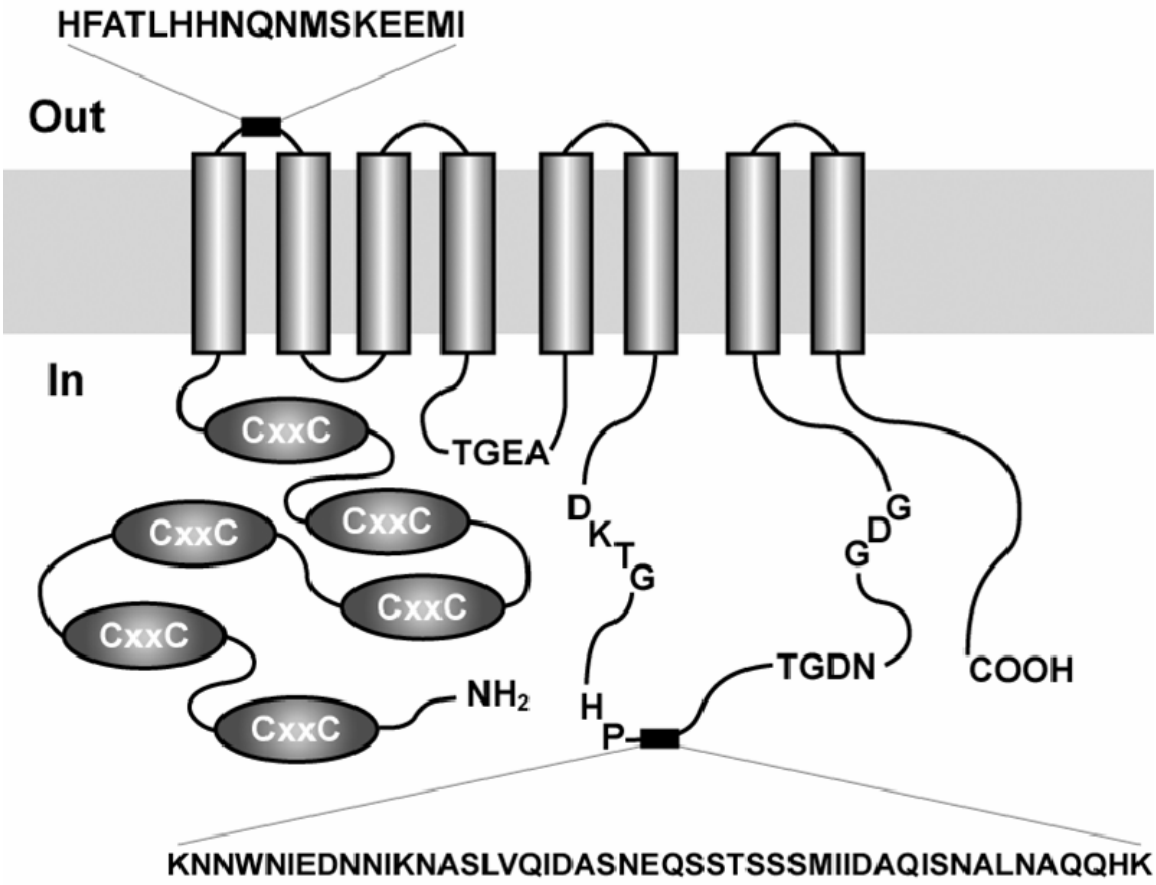

Figure 1.4. Diagram of ATP7A/ATP7B. Black boxes are insert sequences in ATP7A that are not present in ATP7B.

1.2.2.2 Cox

The mitochondrial pathway appears to be the most complex of the three currently known copper chaperone pathways. Cytochrome *c* oxidase (Cox) is a terminal multisubunit enzyme in the aerobic respiratory chain of eukaryotes and some bacteria. In eukaryotes, it is located on the inner mitochondrial membrane and requires multiple cofactors, including three copper ions, two heme molecules, zinc, magnesium and sodium ions for function (Carr and Winge, 2003). In yeast, Cox comprises three core catalytic subunits, Cox1, Cox2, and Cox3, which are encoded by the mitochondrial genome, and nine additional nuclear-encoded subunits (Taanman and Capaldi, 1992). The two copper centers, Cu_A and Cu_B, are essential for enzyme catalysis (Figure 1.5). Electrons

transferred from cytochrome *c* to the dinuclear, mixed-valence Cu_A center in Cox2 are used to reduce dioxygen to two molecules of water at a heterometallic heme a_3-Cu_B site in Cox1 (Ferguson-Miller and Babcock, 1996).

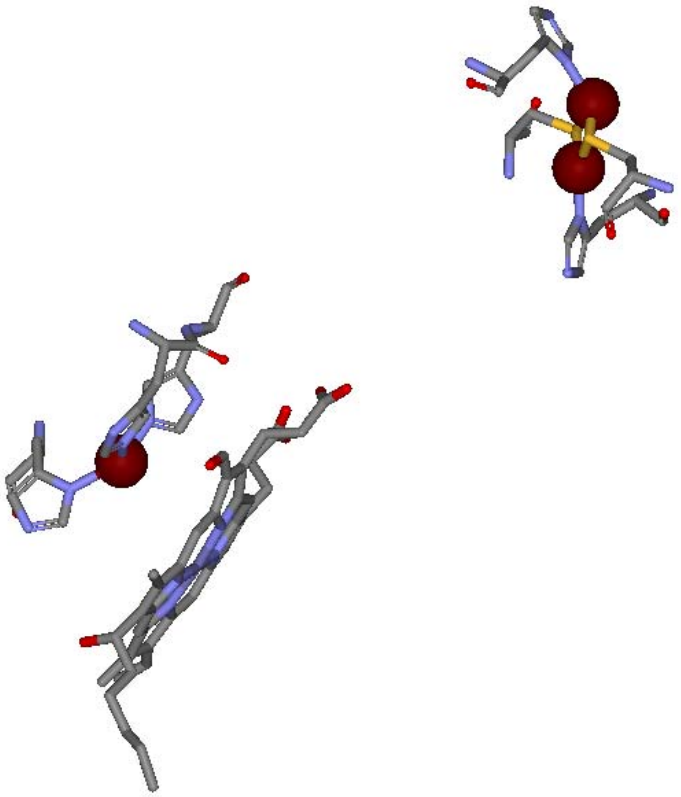

Figure 1.5. Cox Cu_A and Cu_B-heme a_3 sites (Protein Data Bank file 2OCC). Copper atom in red.

More than 30 nuclear-encoded accessory proteins have been implicated in the assembly of functional Cox (Tzagoloff and Dieckmann, 1990), including Cox17 (Glerum et al., 1996a; Punter and Glerum, 2003) and Sco1 (Dickinson et al., 2000; Glerum et al., 1996a) which are important for assembly of the Cu_A site and have been proposed to function specifically in copper transfer and loading. Although Cox17 in yeast was originally proposed to act as a mitochondrial copper shuttle on the basis of its copper-binding properties (Heaton et al., 2000) and dual localization to both the cytosol and the mitochondrial intermembrane space (IMS) (Beers et al., 1997), tethering of Cox17 to the

mitochondrial inner membrane (IM) does not affect its function, suggesting that it does not transfer copper ions between the cytosol and the IMS (Maxfield et al., 2004). Cox17 contains 69 amino acid residues, and it is currently believed to obtain copper from small, non-protein complexes within the mitochondrial matrix (Cobine et al., 2004). Prokaryotic homologs of Cox17 have not been identified (Arnesano et al., 2005). NMR analysis of copper-bound yeast Cox17 revealed two alpha-helices with an unstructured N-terminal domain with one Cu(I) ion coordinated by two cysteine residues (Abajian et al., 2004) (Figure 1.6). This is in contrast to EXAFS analysis of mitochondrial Cox17 which showed the formation of a polycopper cluster with three Cu(I) ions per monomer with predominantly trigonal coordination (Heaton et al., 2001).

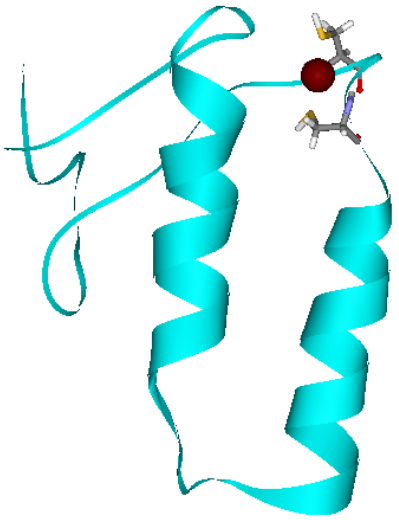

Figure 1.6. Solution structure of copper-bound yeast Cox17 (Protein Data Bank file 1U96). Copper atom in red; cysteine residues colored by atom.

Cox activity in Cox17-deficient yeast cells can be restored partially by both the addition of exogenous copper (Glerum et al., 1996a) and the overexpression of Sco1 (Glerum et al., 1996b), which receives copper directly from Cox17 (Horng et al., 2004). Although direct copper transfer to Cox2 has not been established, full-length yeast Sco1 has been shown to interact with Cox2 by coimmunoprecipitation and affinity chromatography (Lode et al., 2000). Sco1 contains both a transmembrane and a soluble domain (Buchwald et al., 1991). The N-terminal transmembrane helix domain is anchored to the

inner membrane. Extending into the intermembrane space, the soluble domain consists of about 200 residues and contains the conserved CXXXC motif domain that is essential for function (Mattatall et al., 2000; Rentzsch et al., 1999). Crystal structural analysis of Cu(I)-bound Sco1 showed that Cys-169 and Cys-173 in the CXXXC motif coordinate Cu(I) and that copper coordination creates a more rigid loop structure (Banci et al., 2006). Because Sco1 has a thioredoxin-like fold, it has been proposed that Sco1 can act both as a copper chaperone and a thioredoxin (Balatri et al., 2003; Williams et al., 2005; Ye et al., 2005). In this capacity, Sco would reduce the Cys residues in the CuA center for copper binding. In the crystal structure of oxidized Ni(II)HSco1, the two metal-binding Cys in the CXXXC motif are oxidized and form a disulfide bond with the Ni(II) ion interacting with the disulfide (Banci et al., 2006). Unlike Cox17, Sco1 is conserved in other eukaryotes as well as in bacteria (Chinenov, 2000). In soluble truncate preparations that lack a mitochondrial targeting sequence or the N-terminal transmembrane helix of *Saccharomyces cerevisiae* Sco1 (ySco1), human Sco1 (hSco1), and human Sco2 (hSco2), one copper ion, present as Cu(I) or Cu(II), is bound per protein (Beers et al., 2002; Horng et al., 2005; Nittis et al., 2001). For the cytochrome *c* oxidase assembly process, humans also contain another metallochaperone, Sco2. Both Sco1 and Sco2 may be involved in signaling for the regulation of cellular copper content (Leary et al., 2007). NMR analysis of Cu(I)-bound human Sco1 reveals the Cu(I) coordinated by two Cys residues of the CPXXCP motif and a His residue (Banci et al., 2006) (Figure 1.7). Similarly, in ySco1, X-ray absorption spectroscopic and mutagenesis studies indicate that the Cu(I) ion is trigonally coordinated by the two Cys residues, Cys148 and Cys152, in the CXXXC motif and by a conserved histidine, His239 (Nittis et al., 2001). However, in the crystal structure of ySco1, a Cu-binding site involving Cys181 and Cys216, cysteine residues present in ySco1 but not in other homologs, is formed (Abajian and Rosenzweig, 2006) (Figure 1.8).

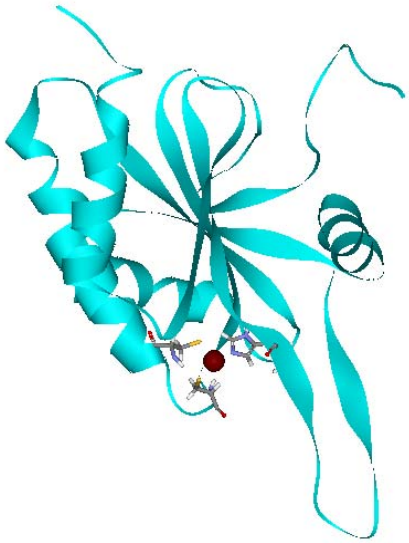

Figure 1.7. Crystal structure of Cu(I)-bound hSco1 (Protein Data Bank file 2GQM). Copper atom in red.

Figure 1.8. Crystal structure of Cu(I)-bound yScoI (Protein Data Bank file 2B7J). Copper atom in red.

Cox11 is required for the assembly of the Cu_B Cox site. Like Sco1, Cox11 receives copper from Cox17 (Horng et al., 2004). In *Rhodobacter sphaeroides* Cox11 knock-outs, cells lacked the Cu_B center but contained both hemes (Hiser et al., 2000). Similarly, *S.*

cerevisiae cells lacking Cox11 have impaired cytochrome *c* oxidase activity, are deficient in heme *a*, and are unable to assemble the holoenzyme (Tzagoloff et al., 1990). For yCox11, x-ray absorption spectroscopy reveals that three Cys residues coordinate the Cu(I) ion (Carr et al., 2002). EXAFS and NMR analysis of the *Sinorhizobium meliloti* Cox11 reveal that a copper cluster may be formed between two Cox11 monomers with two thiolates bridging two Cu(I) ions (Banci et al., 2004) (Figure 1.9).

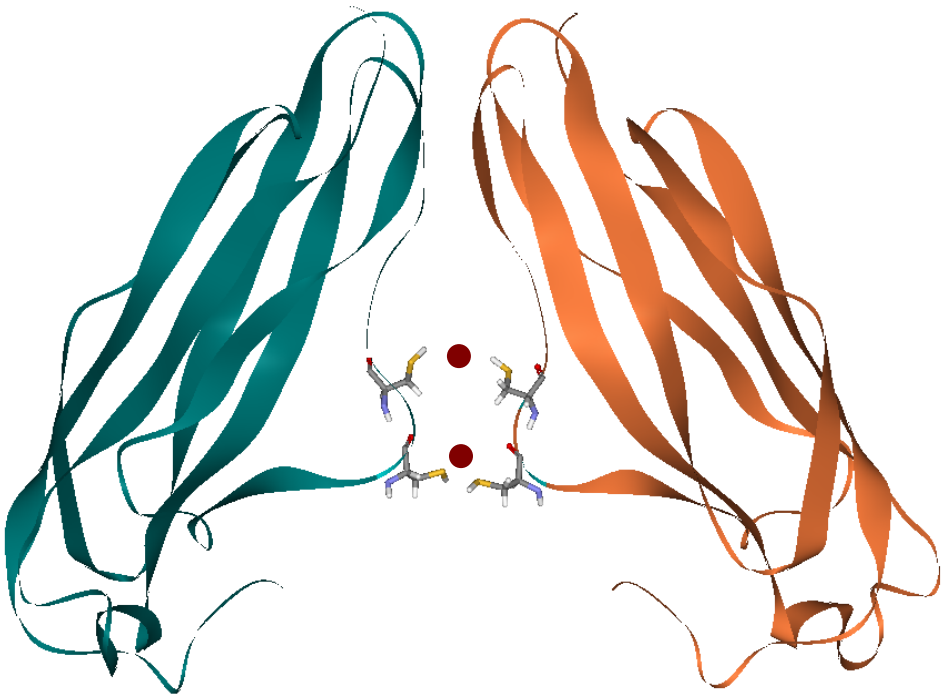

Figure 1.9. Putative structure of *S. meliloti* Cox11 (Protein Data Bank file 1SP0). Copper atom in red.

1.2.2.3 Copper Chaperone for Superoxide Dismutase (CCS)

Human copper, zinc-superoxide dismutase, SOD1, is a 32 kDa homodimer found in the cytoplasm of eukaryotic cells. SOD1 protects cells against oxidative damage by catalyzing the conversion of superoxide to dioxygen and hydrogen peroxide (Fridovich, 1995). Furthermore, superoxide dismutase may play a physiological role in copper

buffering in yeast (Culotta et al., 1995). SOD1 contains one Cu(II) ion and one Zn(II) ion in each of the two identical subunits which constitute the enzyme. The overall structure consists of an eight-stranded beta-barrel (Banci et al., 2002a; Strange et al., 2003) (Figure 1.10). The active site contains the two metal ions bridged by a common histidine ligand (Richardson et al., 1975). The Zn(II) ion is in a tetrahedral geometry, coordinated by three histidine residues and one aspartate residue. In the oxidized form of the protein, Cu(II) is in a square pyramidal geometry coordinated by four histidine residues and one solvent molecule (Blackburn et al., 1983; Boden et al., 1979; Hart et al., 1999; Strange et al., 2003). In the reduced form, the copper ion is bound to only the three histidyl residues (Banci et al., 2002b). Posttranslational modifications of SOD1 include copper and zinc binding and the formation of an intramolecular disulfide bond. In mammalian cells, copper incorporation has no essential role in the stability or turnover of SOD1 (Bartnikas and Gitlin, 2003). The production of mutant Cu, Zn-SOD1 that exhibits a gain of function in superoxide radical scavenging ability is known to be the cause of a fatal neurodegenerative disease, familial amyotrophic lateral sclerosis (Rosen et al., 1993). It has been hypothesized that copper released from the mutant SOD1 is responsible for the production of hydroxyl radicals via the Fenton reaction (Okado-Matsumoto et al., 2000).

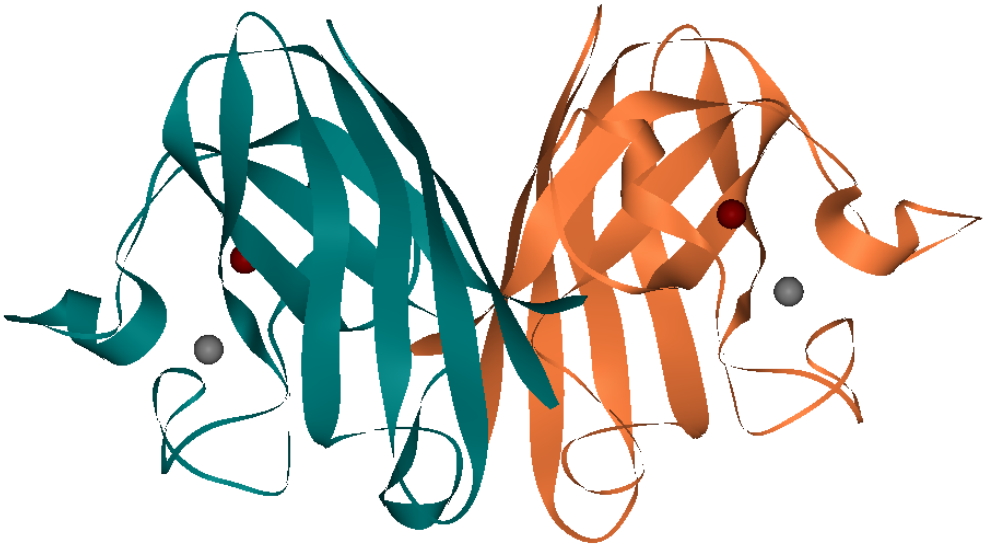

Figure 1.10. Crystal structure of human SOD1 dimer (Protein Data Bank file 1HL5). Copper atom in red; Zinc atom in silver.

The human copper chaperone, CCS (Copper Chaperone for SOD), is necessary to establish the copper-bound form of SOD1 due to low amounts of intracellular free copper (Rae et al., 1999). Furthermore, CCS may also facilitate the folding of SOD1 (Rae et al., 2001). CCS is highly specific for SOD1 and cannot deliver copper to other proteins that have different metallochaperones. However, when human SOD1 is expressed in CCS knockouts of either yeast or mammalian cells, it retains some activity due to the CCS-independent activation by glutathione (Carroll et al., 2004). In contrast, yeast SOD1 cannot obtain copper without CCS in vivo. In mammalian cells, CCS-dependent copper incorporation into SOD1 is rapid, and once copper is incorporated, it is unavailable for cellular exchange (Bartnikas and Gitlin, 2003). The structure of yeast CCS revealed a homodimer in which each monomer is composed of two structured domains (Lamb et al., 1999) (Figure 1.11). The N-terminal domain, domain I, contains a conserved Cu-binding motif, MXCXXC, similar to other copper chaperones such as Atox1. The second domain, domain II, is an SOD1-like domain but lacks all the catalytically-important structural aspects. Like SOD1, it forms an eight-stranded beta-barrel (Lamb et al., 2000). Unlike hCCS, yCCS does not contain any metal-binding sites in domain II. hCCS

contains both a Zn-binding site and a vestigial Cu-binding site. Although the CCS sequence from yeast is similar to human CCS, they are not identical. Sequence alignments show these differences, including two cysteine residues found in the SOD1-like domain II of the protein (Figure 1.12). CCS exhibits no detectable SOD1 activity, whereas a D200H mutation, targeting the fourth potential copper ligand in CCS, causes superoxide scavenging activity when this mutant was expressed in yeast (Schmidt et al., 1999). Conserved in hCCS are all the SOD1 zinc-binding ligands and three of the four histidine copper-binding ligands. The crystal structure of domain II from human CCS has these structural features that form two potential metal binding sites, and the site equivalent to the SOD1 zinc site was occupied by a zinc ion in the crystal with the zinc-binding site formed by two extended loops (Lamb et al., 2000). In the crystal structure, the yeast CCS C-terminal region, domain III was disordered. This region contains the unique CXC sequence, residues 244 to 246, that is essential for chaperone activity (Lamb et al., 1999). Both domains I and III are believed to bind metal ions, and based on XAS data, these domains are thought to interact via a cysteine-bridged dicopper cluster with copper coordinated to three S ligands and a Cu-Cu interaction seen at 2.72 Å (Eisses et al., 2000). Further examination of cysteine to serine CCS mutants by XAS revealed a copper cluster at the domain III dimer interface, and mutations in domain III (C244S/C246S) significantly reduced copper transfer activity to SOD1 (Stasser et al., 2005).

In mice and rats, copper deficiency increases the amount of CCS protein, but not mRNA levels (Bertinato et al., 2003; Bertinato and L'Abbe, 2003; Prohaska et al., 2003). Furthermore, CCS degradation was shown to be slower in copper-deficient rodent and human cell lines than when in copper-rich conditions, indicating a posttranslational mechanism of copper regulation in CCS expression (Bertinato and L'Abbe, 2003). Further examination of this posttranslational mechanism revealed a critical role for C244/246 in domain III in mediating the copper-dependent turnover of CCS, but no role for domain I (Caruano-Yzermans et al., 2006). This mechanism is independent of the mechanism of delivery of copper to SOD1 (Caruano-Yzermans et al., 2006), possibly due to the requirement of C244/246 in the transfer of copper to SOD1.

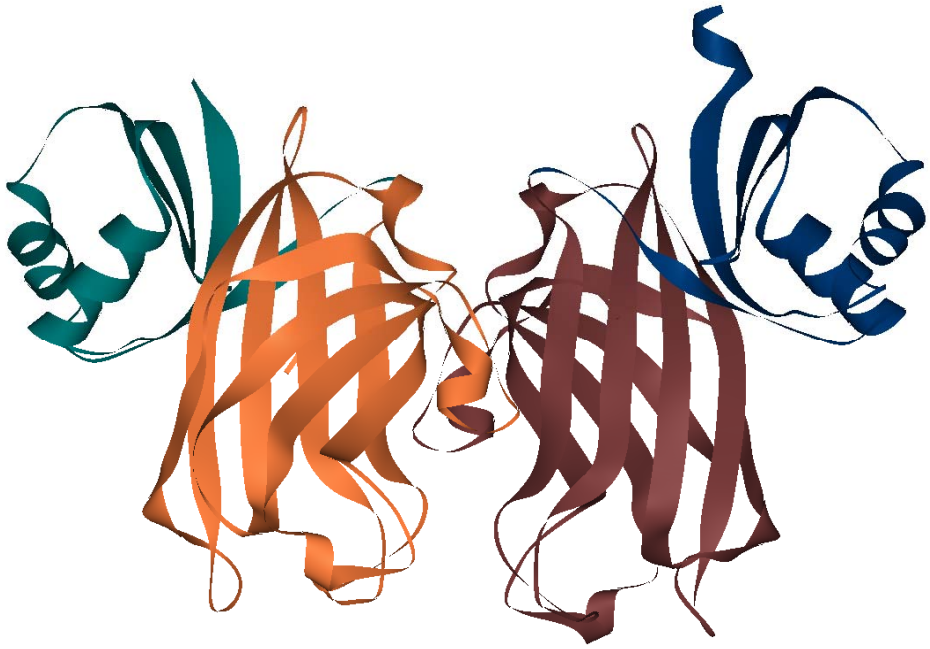

Figure 1.11. Structure of yCCS with domain 1 and domain 2 present. Domain 3 is unstructured and not indicated. (Protein Data Bank file 1QUP).

Figure 1.12. Alignment of hCCS (NP_005116), hSOD1 (CAG46542), and yCCS (P40202) (created using CLUSTALW).

The mechanism for copper loading of SOD1 by its partner metallochaperone CCS is not well understood. When mutations are introduced at the dimer interface of yeast SOD1, there is a loss of interaction with CCS, indicating that prefolded dimers of apoSOD1 serve as the substrate for CCS (Schmidt et al., 2000). Thus, when the SOD1 dimer interface is disrupted, the CCS-SOD1 heterodimer cannot form since it uses the same SOD1 dimer interface residues. H48A SOD1 mutants that are unable to bind copper form a stable complex with the yeast apo- and Cu-CCS in a heterodimer (Torres et al., 2001). It has been shown that CCS activates SOD1 by direct protein to protein transfer of the copper cofactor, and a mechanism of SOD1 activation by CCS was proposed (Rae et al., 2001). In this mechanism, the transfer process occurs through the cysteine pair of CCS domain III via ligand-exchange with copper-binding residues of the SOD1 active site. The mechanism was proposed to include either the formation of a heterodimer or a dimer of homodimers of CCS and SOD1 (Figure 1.13). Furthermore, the authors propose that domain III could interact alternatively with the domain I CXXC copper-binding site and

the SOD1 site in a presumed switch-like translocation of the copper ion. A crystal structure of SOD1(H48F) in complex with yeast CCS revealed that SOD1 interacts with its metallochaperone to form a complex comprising one monomer of each protein (Lamb et al., 2001) (Figure 1.14). The functionally essential C-terminal domain III of yeast CCS was shown to be well positioned to play a key role in the metal ion transfer mechanism and is linked to SOD1 by an intermolecular disulfide bond that may facilitate or regulate copper delivery. Although crystal structures of SOD1, CCS, and the SOD1-CCS complex are available, the details of chaperone-target protein recognition and docking for metal ion transfer are not fully understood. It was also suggested that CCS domains I and III transfer copper from the domain I sequestering site to the domain III translocation site (Eisses et al., 2000). These data are consistent with an earlier study of cobalt binding to human and tomato CCS (Zhu et al., 2000). In a yeast expression system, a mutant of CCS in which the zinc-binding residues H147 and D167 were substituted with Ala functioned less efficiently than wild-type CCS, leaving SOD1 in the apo-form. This suggests that the coordinated Zn ion in CCS is essential for CCS function (Endo et al., 2000).

Recently, it was shown that oxygen is required for the activation of SOD1 by CCS, indicating oxidant-responsive posttranslational regulation of SOD1 activity (Brown et al., 2004). In the presence of oxygen, kinetically stable disulfide formation in yeast SOD1 is accelerated by copper-bound CCS, facilitating the conversion of the immature form of yeast SOD1 to its active state (Furukawa et al., 2004). In fact, in *Caenorhabditis elegans*, the homolog of SOD1, wSOD-1, readily forms the disulfide bond and appears to exclusively use an alternative pathway to CCS activation that requires reduced glutathione (Jensen and Culotta, 2005).

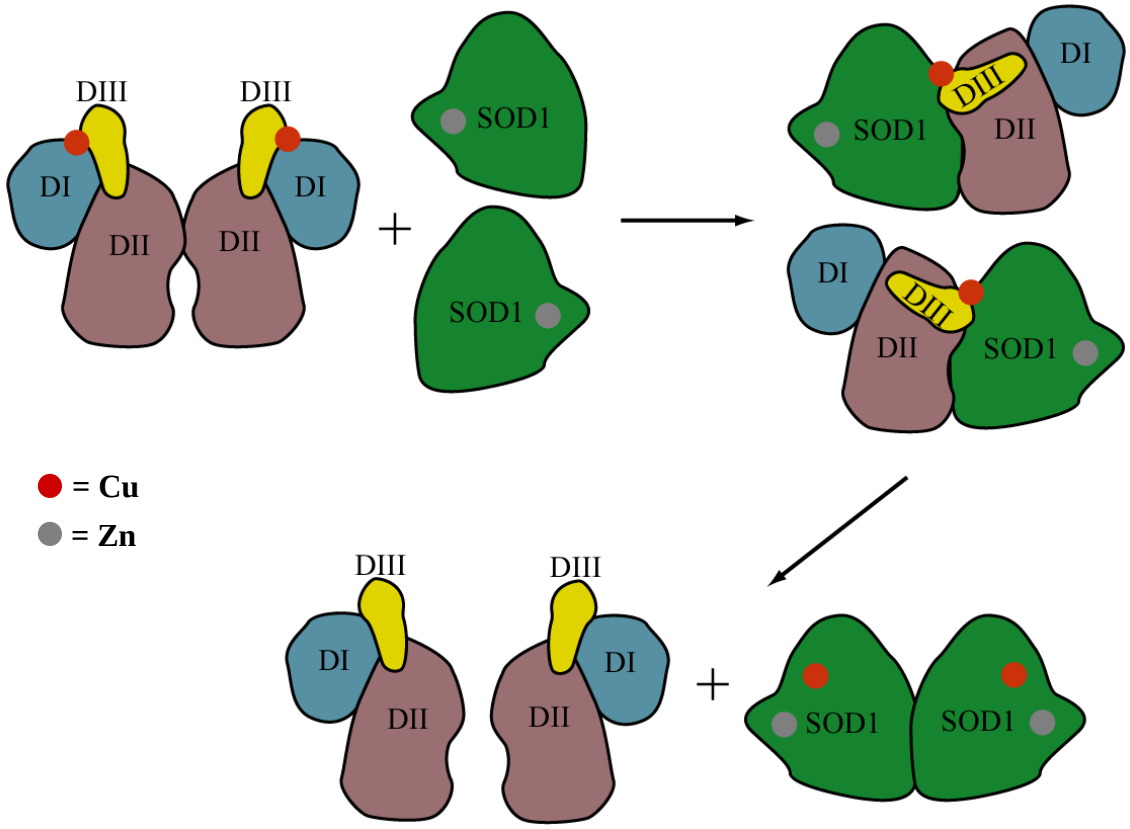

Figure 1.13. Proposed dimer mechanism of CCS activation. of SOD1.

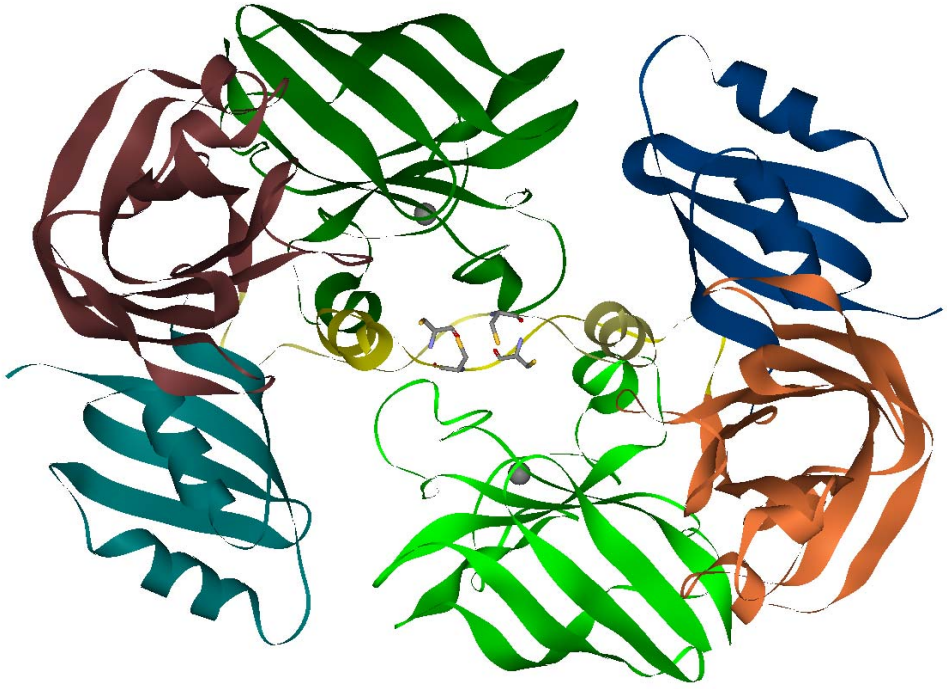

Figure 1.14. Crystal structure of yCCS in complex with SOD1 illustrating a dimer of dimers (Protein Data Bank file 1JK9). Zinc atom in silver.

Mutations in SOD1 are responsible for approximately 20% of familial amyotrophic lateral sclerosis (FALS). Although cytosolic protein aggregates appear to be common in FALS as well as in transgenic mouse models expressing mutant SOD1, the mechanisms leading to neurodegeneration in FALS are not well understood. Human FALS-linked SOD1 mutants (A4V, G37R, G41D, H46R, H48Q, G85R, G93C, and I113T) all bind copper and scavenge oxygen-free radicals in vivo under physiologic conditions, supporting a mechanism of SOD1 mutant-mediated disease arising from aberrant copper-mediated chemistry (Corson et al., 1998). CCS not only interacts with wild-type SOD1, but also SOD1 containing the common missense mutations resulting in FALS (Casareno et al., 1998). Both SOD1 and CCS are present together in cells that degenerate in FALS, with a 12-30-fold molar excess of SOD1 over CCS (Rothstein et al., 1999). CCS has also been shown to aggregate with SOD1 in SOD1-mutated FALS patients, which may

amplify neuronal Lewy body-like hyaline inclusions, resulting in a greater mutant SOD1-mediated toxicity (Kato et al., 2001; Watanabe et al., 2001). This aggregation has also been shown between CCS and mutant extracellular superoxide dismutase, SOD3, which is structurally similar to SOD1 (Son et al., 2003). However, completely deleting the CCS gene in FALS-linked SOD1 mutant mice does not modify the onset or progression of FALS, though copper-loaded mutant SOD1 was significantly reduced (Beckman et al., 2002; Subramaniam et al., 2002). Recently, it was shown that the yeast thiol oxidoreductase glutaredoxin preferentially targets the immature form of FALS mutant SOD1 lacking metal cofactors, indicating a role of a disulfide for the stability of SOD1 in vivo (Carroll et al., 2006).

CCS also interacts with the neuronal adaptor protein X11 α via the C-terminus of CCS domain III (residues PAHL) and the PDZ domain of X11 α (Duquesne et al., 2005). X11α binding to CCS appears to inhibit SOD1 activation (McLoughlin et al., 2001). This adaptor protein also binds to the Alzheimer's disease amyloid precursor protein. Cleavage of the amyloid precursor protein by the aspartic protease BACE1 results in the generation of Aβ peptides, major constituents of Alzheimer disease senile plaques. BACE1 binds a single Cu(I) atom and interacts with CCS domain I, and BACE1 expression reduces the activity of SOD1 in cells, indicating direct competition for available CCS (Angeletti et al., 2005). The interaction of CCS with Alzheimer plaque constituents and the importance of CCS and lack of availability for SOD1 activation in Alzheimer's disease should be further investigated.

1.2.3 GLUTAREDOXIN

Recently, it has been suggested that glutaredoxin, a small cytosolic protein that catalyzes the reduction of disulfide bridges, is a key component of the copper homeostatic machinery (Lim et al., 2006). This protein has been shown to preferentially target copper-deficient SOD1 that contains an oxidized disulfide in yeast (Carroll et al., 2006). By reducing the disulfide of SOD1, copper transport to SOD1 by CCS would be possible. It has also been proposed that human glutaredoxin, GRX1, is essential for ATP7A and

ATP7B function by catalyzing either the reduction of intramolecular disulfide bonds or the deglutathionylation of the cysteine residues within the CXXC motifs to facilitate copper-binding for subsequent transport (Lim et al., 2006).

1.2.4 METALLOTHIONEINS AND COPPER EXPORT

When copper is imported in excess, it is bound by metallothionein, a cysteine-rich low molecular weight protein. Found in all eukaryotes and some prokaryotes, metallothioneins are thought to be involved in the detoxification of metals including non-essential and excess essential metals, storage of essential metals, sequestration of reactive oxygen and nitrogen species and electrophiles, and intracellular trafficking of zinc (Feng et al., 2005; Shiraishi et al., 1982; Suzuki et al., 1993; Thornalley and Vasak, 1985; Yoshida et al., 2005). In mice, under Cu-deficient conditions induced by a Cu(I)-specific chelator, bathocuproine sulfonate (BCS), metallothionein is induced to maintain the activities of intracellular cuproenzymes (Ogra et al., 2006). Metallothioneins act as major intracellular Cu-binding proteins, especially in the presence of excess copper (Bremner, 1991; Lee et al., 1989; Thiele, 1988). These cysteine-rich proteins readily release metals in a redox-dependent fashion. It has been suggested that copper-bound metallothionein could potentially function in a nitric oxide-dependent pathway for the delivery of copper for apo-SOD in copper-challenged cells (Liu et al., 2000). These proteins typically have a one- or two-domain structure, and these structures and the nature of their metal binding reveal extensive evolutionary diversification (Vasak et al., 1980).

Most metallothioneins consist of two domains, α and β, separated by a short linker region, and these domains are capable of binding metals independently. Single-domain metallothioneins are present in fungi and early diverged metazoans, and these bind up to eight monovalent metal ions (Aschner et al., 2006). A metallothionein that sequesters free copper in the cytosol to increase resistance to high copper levels, Cup1, is the dominant mechanism by which *S. cerevisiae* detoxifies copper (Hamer et al., 1985). A second metallothionein, CRS5, is also present in *S. cerevisiae*, but it is not thought to play the dominant role in neutralizing excess intracellular copper (Culotta et al., 1994; Jensen et

al., 1996). Four metallothioneins are present in Drosophila, MtnA, MtnB, MtnC, and MtnD (Egli et al., 2003). While *MtnC* and *MtnD* are most likely duplicates from the *MtnB* gene, MtnA and Mtn B are expressed at different stages of development, with MtnA primarily expressed during embryogenesis and MtnB found in late stage embryos, larvae, and in adult flies within the gut, Malphigian tubules, fat body and hemocytes (Lastowski-Perry et al., 1985; Maroni et al., 1986; Silar and Wegnez, 1990). When all four metallothionein genes are knocked out, Drosophila mutants are highly sensitive to elevated copper concentrations (Egli et al., 2006). In vertebrates, metallothioneins are larger than those of Drosophila and yeast, consisting of 60 amino acids. Mammals contain four members of the metallothionein family, MT-I to MT-IV (Kagi, 1991; Palmiter, 1998). Each class of these MTs is composed of a number of different isoproteins, commonly referred to as MT-Ia, MT-Ib etc. The MT-I and MT-II isoforms are expressed in all tissues. At neutral pH, MT-I and MT-II differ by a single negative charge, and both are characterized by a single chain protein within which are approximately 20 cysteinyl residues (Aschner et al., 2006; Kille et al., 1994). Transcription of MT-I and MT-II is the primary level of regulation and is responsive to adverse conditions, such as heavy metal load, oxidative stress, and ionizing radiation (Andrews, 2000; Durnam and Palmiter, 1987; Kagi, 1991; Palmiter, 1998). MT-III is largely restricted to the central nervous system (Uchida et al., 1991), and expression of MT-III mRNA coincides with high concentrations of vesicular zinc, and has been postulated to factor in regulating glutamatergic neurotransmission and glutamate neurotoxicity (Yamada et al., 1996). MT-IV is solely expressed in squamous epithelial cells in skin and tongue. In general, events that induce MT-I and MT-II gene expression do not enhance the expression of MT-III or MT-IV (Aschner, 1996).

Sequestration of copper in organellar compartments where it can be stored until needed is another pathway of copper detoxification. In *Schizosaccharomyces pombe*, Ctr6 is responsible for storing copper in the vacuole (Bellemare et al., 2002). Localized to the vacuole membrane, Ctr6 is proposed to mobilize stored copper upon cytosolic copper depletion. Its sequence is most similar to Ctr2 in *S. cerevisiae*.

Another mechanism in modulating copper toxicity has been identified in *S. cerevisiae*. The iron permease Ftr1 and the multicopper oxidase Fet3 form a ferroxidase-dependent, high affinity iron uptake complex in the yeast plasma membrane (Askwith and Kaplan, 1998; Dancis et al., 1994b; De Silva et al., 1995; Kosman, 2002; Kosman, 2003; Stearman et al., 1996). Fre1 is a surface metalloreductase that is essential to the uptake of environmental Cu^{2+} and Fe^{3+}. In the uptake of Fe^{3+}, Fre1 produces Fe^{2+} that is a substrate for Fet3, and the Fe^{3+} produced by Fet3 is a ligand for the iron permease, Ftr1 (Kosman, 2003). Deletion of *fet3* leads to copper sensitivity (Szczypka et al., 1997). Deletion of *FRE1* in the *fet3Δ* background suppresses copper sensitivity, whereas deletion of *CTR1* and the expression of a ferroxidase-negative Fet3 does not suppress sensitivity in this background (Shi et al., 2003). The authors suggest that oxidation of Cu^{+} by Fet3 and the coordinated action of Fet3 and Fre1 plays an essential role in preventing toxicity from Cu^{+} ions before they enter the cell.

1.2.5 TRANSCRIPTIONAL REGULATION

A number of regulatory mechanisms ensure that copper is maintained at a level sufficient for, but not toxic to, cell growth. In fungi, copper homeostasis is mediated by the transcriptional regulation of genes involved in copper acquisition, mobilization, and sequestration (Ooi et al., 1996). Copper-responsive transcriptional regulation has been observed in insects and plants as well, suggesting this mechanism is widespread in nature (Himelblau et al., 1998; Ruzsa and Scandalios, 2003; Zhou et al., 2003). Six copper-responsive fungal factors have been characterized in detail. Mac1, GRISEA, and Cuf1 activate gene expression in response to copper deficiency, whereas Ace1, Amt1, and Crf1 activate gene expression in response to elevated copper levels. In *S. cerevisiae*, Mac1 is regulated by copper and has a copper-binding domain that acts as an intramolecular autoinhibitory domain (Jensen et al., 1998; Keller et al., 2005; Winge, 1998). This protein binds as a homodimer in the promoter regions of target genes to *cis*-acting elements in a site-specific manner (Joshi et al., 1999; Labbe et al., 1997; Serpe et al., 1999; Yamaguchi-Iwai et al., 1997). In the same organism, Ace1 consists of a copper-dependent DNA-binding domain and a carboxyl-terminal half that mediates contacts to

the transcription apparatus. This protein binds to *cis*-regulatory elements in the metallothionein gene promoters that mediate transcriptional activation by copper (Thiele, 1988). Ace1 induces expression of the metallothionein genes *CUP1* and *CRS5*, as well as *SOD1* (Culotta et al., 1994; Gralla et al., 1991; Thiele, 1988). X-ray absorption spectroscopy (XAS) analysis of Mac1 and Ace1 from *S. cerevisiae* reveal a polycopper cluster present in the copper-regulatory domains of both proteins, where each domain binds four Cu(I) ions in a trigonal geometry (Brown et al., 2002). Amt1 and Crf1 are functional orthologs of Ace1 that confer copper resistence in *Candida glabrata* and *Yarrowia lipolytica* respectively (Garcia et al., 2002; Zhou and Thiele, 1991). In the fission yeast *S. pombe*, Cuf1 is activated by copper starvation (Beaudoin et al., 2003). High-affinity copper uptake is regulated at the transcriptional level in *S. pombe* and *Podospora anserina* by Cuf1 and GRISEA respectively (Beaudoin and Labbe, 2001; Borghouts et al., 2002; Labbe et al., 1999). Cuf1 regulates the expression of the *CTR6* vacuolar efflux system (Bellemare et al., 2001), whereas GRISEA activated the expression of SOD2 that encodes a manganese SOD (Borghouts et al., 2002). Like Mac1, Cuf1 is controlled by a copper-dependent interaction between the DNA-binding domain and the copper-binding domain (Beaudoin et al., 2003). However, the N-terminal region of Cuf1 has a higher percentage of sequence identity with the corresponding Ace1 domain than with the N-terminal domain of Mac1. When introduced into an *ace1* null *S. cerevisiae* strain, Cuf1 can activate Ace1 target gene expression (Beaudoin and Labbe, 2001; Beaudoin et al., 2003). In higher eukaryotes, the main transcriptional regulator for handling heavy metal excess, including copper, is MTF-1 (metal-responsive element binding transcription factor-1 or metal-responsive transcription factor-1) (Auf der Maur et al., 2000; Egli et al., 2003; Giedroc et al., 2001; Heuchel et al., 1994; Lichtlen and Schaffner, 2001; Zhang et al., 2001). MTF-1 and its cognate binding site is the functional analog of yeast Ace1, but neither the polypeptides or their binding sites show evolutionary similarities (Lichtlen and Schaffner, 2001).

1.2.6 POSTTRANSLATIONAL REGULATION

Although transcription regulation appears to be the main source of control of copper homeostasis, posttranslational mechanisms of regulation exist in eukaryotes. Posttranslational control of transporters has been shown to exist in fungi in the copper-dependent endocytosis and degradation of *S. cerevisiae* Ctr1 (Ooi et al., 1996). This degradation of Ctr1 may be aided by Mac1 (Yonkovich et al., 2002). In mammals, the intracellular trafficking of copper transporters and the copper-stimulated endocytosis and degradation of Ctr1 are the currently known posttranslational regulatory mechanisms (Pena et al., 1999; Petris et al., 1996; Petris et al., 2003).

CHAPTER 2: MATERIALS AND METHODS

2.1 BIOLOGICAL METHODS

2.1.1 CLONING AND PURIFICATION OF WILD-TYPE TRUNCATED CCS PROTEINS

Truncated CCS constructs were initially made using wild-type intein-hCCS plasmid as a template. Professor Michiko Nakano of the Department of Environmental and Biomolecular Systems at the Oregon Health and Science University performed the initial cloning and transformation of the wild-type intein-hCCS containing plasmid. In this initial construction, wild-type hCCS cDNA was PCR-amplified from a maltose binding protein cell line used by our lab in previous studies using primers at the 5' and 3' terminus (5'-GAATTACCATGGCTTCGGATTCGGGGA-3 ', 5 '-AATTTTAAGCTCTTCCGCACGCTGACTCCTTTCGGC-3'). This expressed the full-length hCCS protein minus the last five amino acids (amino acids 1(Met) -269(Ala)). The amplified DNA was cloned into the pTXB3 expression vector (New England Biolabs) using restriction sites *NcoI* and *SapI* introduced in the 5' and 3' PCR primers respectively. The pTXB3 vector contains an intein/chitin binding protein from the *gyrA* gene of *Mycobacterium xenopi*. This tag allows the fusion protein to be bound to a chitin bead column and the target protein to be cleaved from the fusion protein by thiol-induced cleavage (Chong et al., 1997; Telenti et al., 1997). Truncated forms of the protein at amino acid 243 terminating in an Ala, just before the CXC motif, at amino acid

245 terminating in an Ala, just before the last cysteine in this motif, and at amino acid 246 just after this motif, were amplified from this construct. Truncated hCCS was PCR-amplified from this construct by use of primers at the 5' and 3' terminus (5'-ACCATGGCTTCGGATTCGGG-3' and 5'-TGCATCTGCTCTTCTGCAGGCCTGCTTGGGGTT-3' [CCS243] or 5'-AGATGGTGGCTCTTCCGCAAGCGCAGATCTG-3' [CCS245] or 5'-CCAGATGGCTCTTCCGCAGCAAGCGCAGATCT-3' [CCS246] or 5'-TCCTCCCAGGCTCTTCGGCAATCGCAAGCGCA-3' [CCS247] or 5'-GATGGGCCGGGCTCTTCCGCACCAGATGGTGA-3' [CCS252]). The cDNA was cloned into the pTXB-3 (New England Biolabs) by use of restriction sites *NcoI* and *SapI* introduced in the 5' and 3' primers respectively (Figure 2.1). All expression constructs were confirmed by automated DNA sequence analysis.

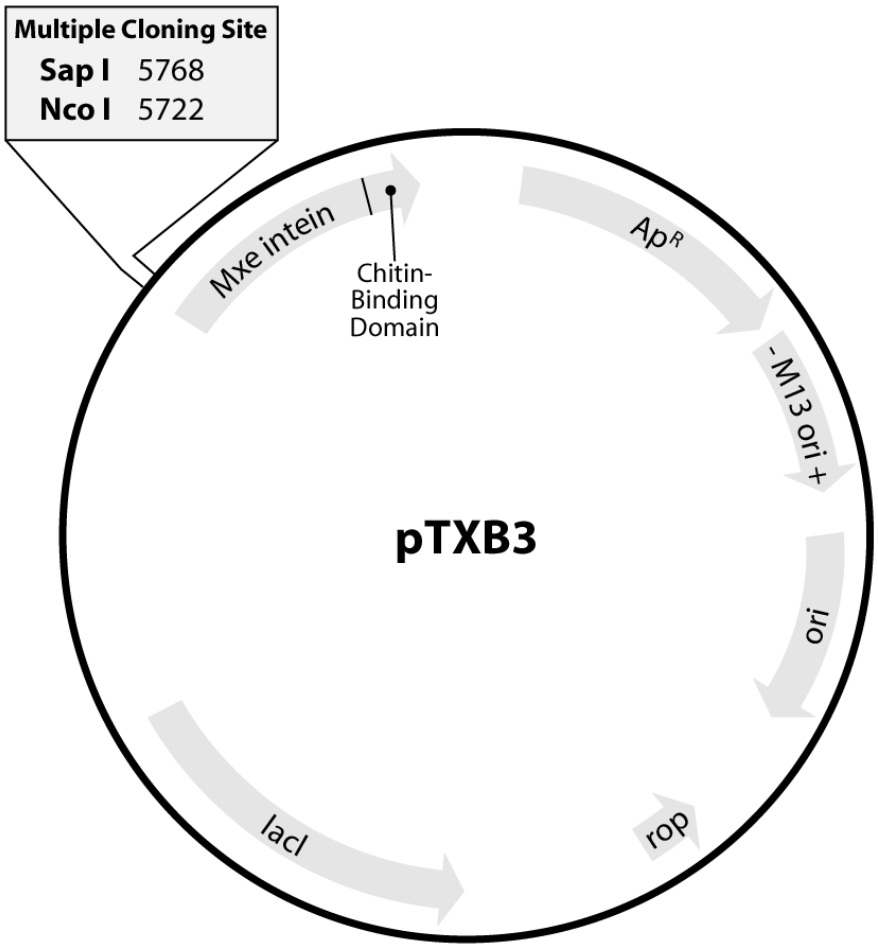

Figure 2.1. Intein expression vector, pTXB3 from New England Biolabs.

```
  1 MASDSGNQGT LCTLEFAVQM TCQSCVDAVR KSLQGVAGVQ DVEVHLEDQM VLVHTTLPSQ
 61 EVQALLEGTG RQAVLKGMGS GQLQNLGAAV AILGGPGTVQ GVVRFLQLTP ERCLIDGTID
121 GLEPGLHGLH VHQYGDLTNN CNSCGNHFNP DGASHGGPQD SDRHRGDLGN VRADADGRAI
181 FRMEDEQLKV WDVIGRSLII DEGEDDLGRG GHPLSKITGN SGERLACGII ARSAGLFQNP
241 KQICAC
      *
```

Figure 2.2. The expressed truncated hCCS protein amino acid sequence. Residues mutated from Cys to Ala in the C22,25A mutants are highlighted in grey. In the CCS243 construct, Ile243 is mutated to Ala, labeled with an asterisk. The underlined residues mark the domain 3 binding site, residues 244-246, where CCS245 ends at Ala245 and CCS246 ends at Cys246.

The fusion proteins were expressed in the *Escherichia coli* strain ER2566 (Novagen) after induction with isopropyl thio-β-D-galactoside (IPTG) in the presence of 500 μM $ZnSO_4$ (Figure 2.2). The cells were lysed with a French pressure cell press (SLM-Aminco). The fusion protein was purified from the soluble portion on a chitin column. The chitin beads (New England Biolabs) were packed into an XK 16/20 column with an AK 16 adaptor (Amersham Biosciences) and washed with 10 volumes of 50 mM sodium phosphate buffer and 500 mM sodium chloride, pH 7.2 (column buffer). The soluble portion was diluted three times with column buffer and run over the chitin column. The column was washed with another 10 volumes of column buffer followed by 3 volumes of column buffer plus 50 mM 2-mercaptoethanesulfonate (cleavage buffer). One volume of cleavage buffer was then added to the column and allowed to sit overnight. The cleavage buffer was removed from the column as the first fraction and another 3 volumes of cleavage buffer were added to the column. All of the fractions were saved and combined. When necessary, the protein was concentrated with an Amicon Centricon ultrafiltration cell of either 5000 or 10000 MWCO.

2.1.2 CLONING AND PURIFICATION OF C22,25A MUTANT TRUNCATED CCS PROTEINS

Using the initial wild-type intein-hCCS construct, mutations were made in the wild type hCCS-intein fusion by Mary Mayfield-Gambill of the Department of Environmental and Biomolecular Systems at the Oregon Health and Science University. Mutagenesis was accomplished using a site-directed technique. A Transformer Site-Directed Mutagenesis Kit (Clonetech) was used to create double Ala mutants C22,25A (Carter, 1987). The construct was confirmed by automated DNA sequence analysis. From this construct, truncated C22,25A hCCS was PCR-amplified by use of primers at the 5' and 3' terminus (5'-ACCATGGCTTCGGATTCGGG-3' and 5'-CCGTGATGGCTCTTCCGCAGATCTGCTTGGGGTT-3' [CCS243] or 5'-AGATGGTGGCTCTTCCGCAAGCGCAGATCTG-3' [CCS245] or 5'-CCAGATGGCTCTTCCGCAGCAAGCGCAGATCT-3' [CCS246]). The cDNA was cloned into the pTXB-3 (New England Biolabs) by use of restriction sites *NcoI* and *SapI* introduced in the 5' and 3' primers respectively. All expression constructs were confirmed by automated DNA sequence analysis.

The fusion proteins were expressed in the *Escherichia coli* strain ER2566 (Novagen) after induction with isopropyl thio-β-D-galactoside (IPTG) in the presence of 500 μM $ZnSO_4$ (Figure 2.2). The cells were lysed with a French pressure cell press (SLM-Aminco). The fusion protein was purified from the soluble portion on a chitin column. The chitin beads (New England Biolabs) were packed into an XK 16/20 column with an AK 16 adaptor and washed with 10 volumes of 50 mM sodium phosphate buffer and 500 mM sodium chloride, pH 7.2 (column buffer). The soluble portion was diluted three times with column buffer and run over the chitin column. The column was washed with another 10 volumes of column buffer followed by 3 volumes of column buffer plus 50 mM 2-mercaptoethanesulfonate (cleavage buffer). One volume of cleavage buffer was then added to the column and allowed to sit overnight. The cleavage buffer was removed from the column as the first fraction and another 3 volumes of cleavage buffer were added to the column. All of the fractions were saved and combined. When necessary, the protein was concentrated with an Amicon Centricon ultrafiltration cell.

2.1.3 SINGLE AMINO ACID AND PEPTIDE LIGATION

The plasmid used in this research for the cloning and purification of hCCS, pTXB-3, is part of the IMPACT™-system from New England Biolabs. In this vector, the target gene is cloned at the N-terminus of a modified intein, and an additional chitin binding domain from *Bacillus circulans* is fused to the C-terminus of the intein. In the intein-mediated purification with the affinity chitin binding tag, thiol induced self-cleavage of the intein causes the protein of interest to be eluted as a C-terminal thioester from the chitin column. The creation of this thioester can be utilized for peptide or single amino acid ligation.

In intein mediated protein ligation, the recombinant Cα-thioester formed from protein purification reacts with a peptide of single amino acid possessing an N-terminal Cys or Sec to form a native peptide bond (David et al., 2004; Evans and Xu, 1999; Hofmann and Muir, 2002; Muir, 2003; Muir et al., 1998; Severinov and Muir, 1998) (Figure 2.3). In the first step of this reaction, the unprotected Cα-thioester undergoes chemoselective transthioesterification with an N-terminal Cys of a second peptide or single amino acid. The thioester then spontaneously undergoes an *S*- to *N*-acyl transfer to form a native peptide bond and the resulting peptide product. The initial transthioesterification step is reversible and no side products are obtained, so no protecting groups are necessary on internal Cys residued within the protein or the ligation peptide. In our case, this allows the introduction of an unnatural amino acid, Sec, into the domain 3 copper-binding site of hCCS.

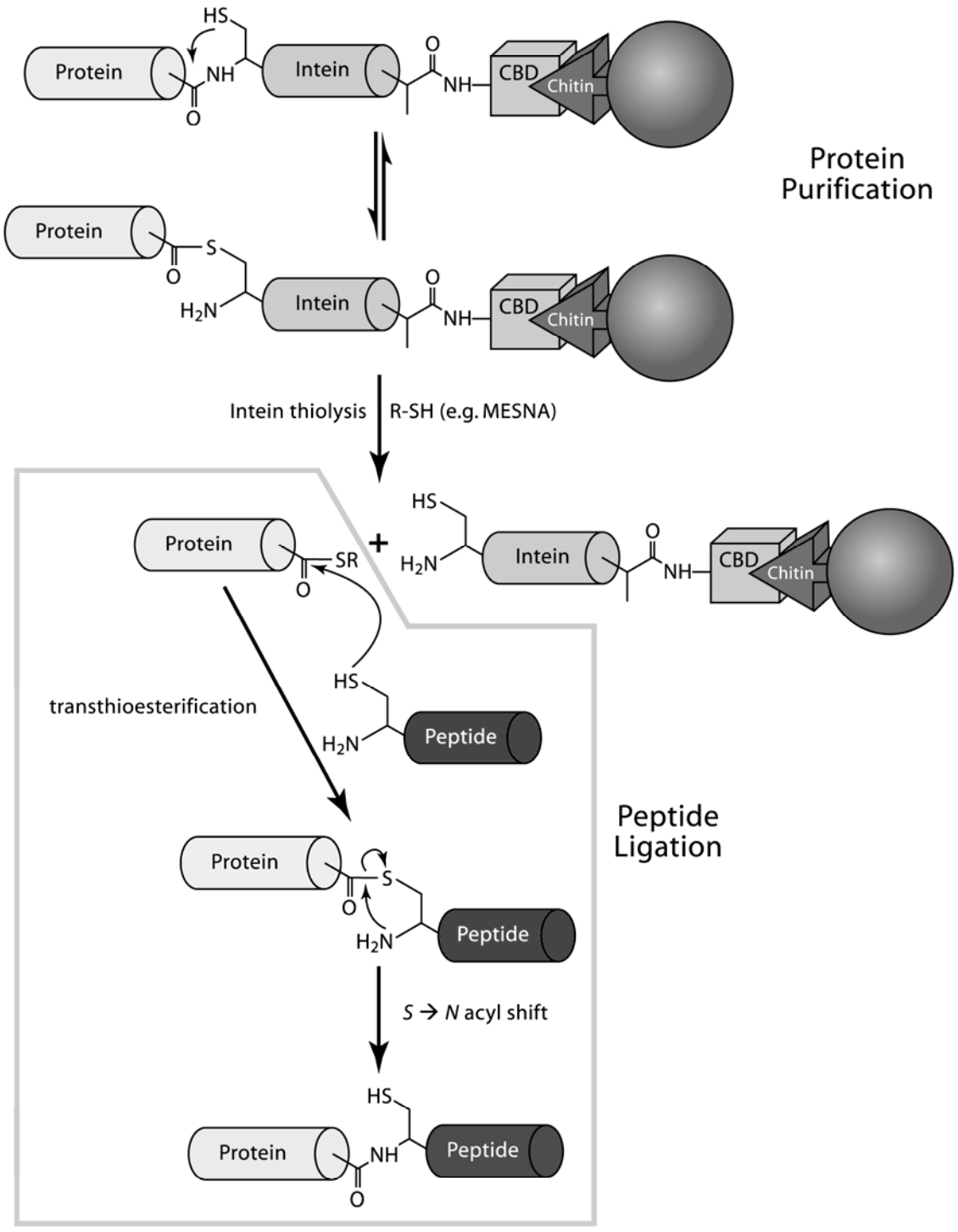

Figure 2.3. Protein purification and peptide ligation of CCS-intein fusion proteins.

We used the following method for single amino acid or peptide ligation. Peptides UAUA (U=selenocysteine), CAUA, UACA, and CACA were synthesized by Kevin M. Clark at the University of Illinois at Urbana-Champaign in the lab of Professor Wilfred Van der Donk. Initially, the hCCS mutant ending at amino acid 243 or 245 was brought into the anaerobic chamber for ligation. 10 mM seleno-DL-cystine (Sigma), cysteine (Sigma), or synthesized peptide was prepared. 10 mM seleno-DL-cystine (Sigma) was made by dissolving in concentrated HCl, cysteine in phosphate buffer, and the peptide in methanol. These solutions were then brought to pH 7.0 with 50 mM sodium phosphate buffer, pH 7.2. The selenocystine, cysteine, or peptide was reduced with 20 mM tris(carboxyethyl)phosphine (TCEP) (Sigma-Genosys) anaerobically. The reduced amino acid or peptide was added to the hCCS mutant in a final concentration of 1 mM and incubated for 4 days in the anaerobic chamber with gentle shaking followed by exhaustive dialysis at 5000 MWCO against Sec-free 50 mM sodium phosphate buffer, pH 7.2.

2.1.4 SOD1 EXPRESSION AND RECONSTITUTION

Recombinant human SOD1 was cloned as a *NdeI-SapI* fragment generated by PCR amplification of a cDNA clone obtained from Genome Systems (GB Accession Number AA702004). PCR primers that contained the restriction sites NdeI (5') and SapI (3') were used to amplify SOD1 cDNA (forward: 5'-GAGACCGCCATATGGCGACGAAGGC-3' and reverse: 5'-CTCCAAGCGGAAGAGCCTTGGGCGATC-3'). This fragment was cloned into the intein pTXB-1 vector from New England Biolabs at the *NdeI* and *SapI* restriction sites (Figure 2.4).

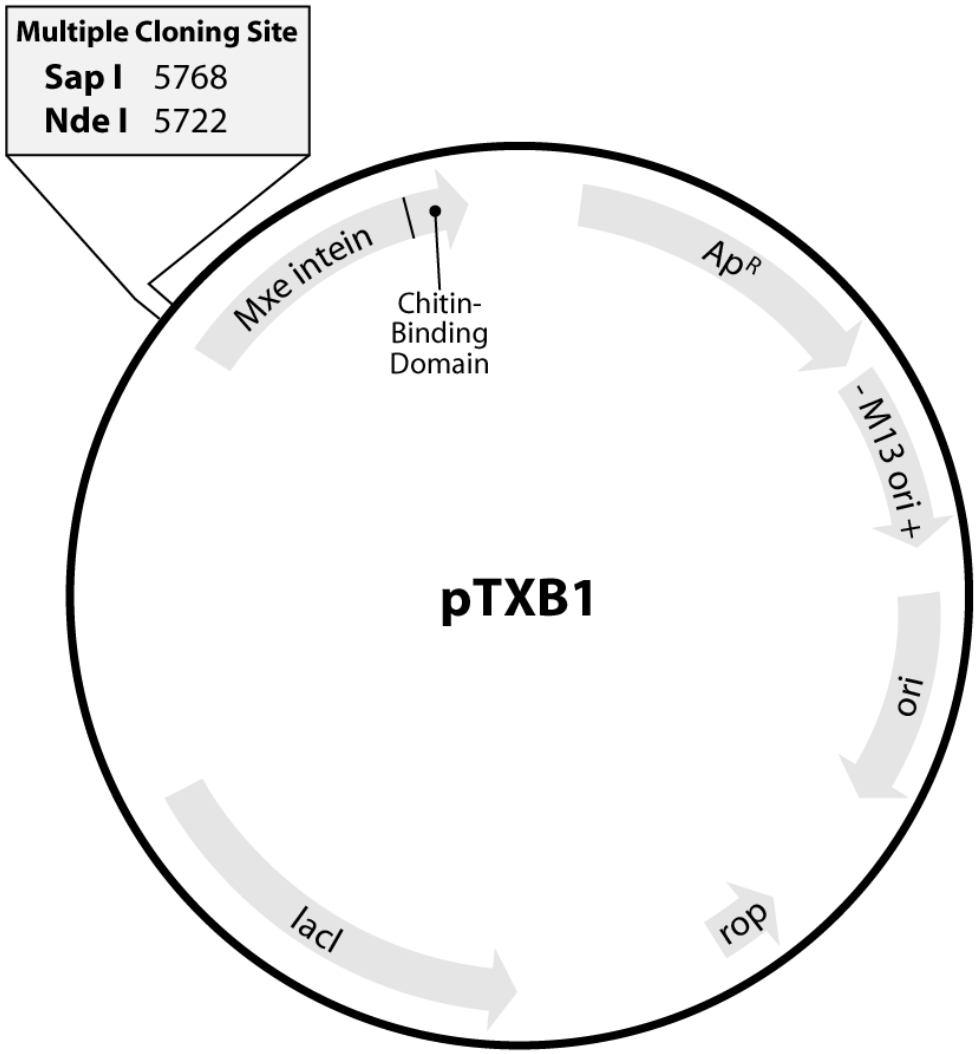

Figure 2.4. Intein expression vector, pTXB1, from New England Biolabs.

```
  1 MATKAVCVLK GDGPVQGIIN FEQKESNGPV KVWGSIKGLT EGLHGFHVHE FGDNTAGCTS
 61 AGPHFNPLSR KHGGPKDEER HVGDLGNVTA DKDGVADVSI EDSVISLSGD HCIIGRTLVV
121 HEKADDLGKG GNEESTKTGN AGSRLACGVI GIAQ
```

Figure 2.5. The expressed human SOD1 amino acid sequence.

Recombinant human SOD was expressed in the E. coli strain ER2566 (Novagen) after induction with IPTG in the presence of 500 uM $ZnSO_4$ (Figure 2.5). The cells were lysed

with a French pressure cell press. Recombinant human SOD was purified from the soluble portion with a chitin column as described above. The purified protein contained one Zn ion per monomer as determined by ICP-OES, and was presumed to be the E,Zn form. Fully metal-loaded Cu,Zn-SOD was obtained by adding excess $CuSO_4$ to the E,Zn-SOD followed by exhaustive dialysis against Cu-free column buffer.

2.1.5 CCS AND SOD1 ASSAYS OF ACTIVITY

The xanthine oxidase assay was used for the determination of the activity of both SOD1 and CCS originally developed by McCord and Fridovich (McCord et al. 1968; McCord et al. 1969). Xanthine oxidase catalyzes the conversion of xanthine to uric acid, producing high levels of superoxide anion as a by-product. In the assay, the superoxide released oxidizes cytochrome *c,* which can be followed by an increase of UV absorption at 420 nm. The addition of SOD1 to the reaction mixture removes the superoxide, thus decreasing the oxidation of cytochrome *c.* A unit of SOD is defined as the amount of SOD required to reduce the oxidation of cytochrome *c* by 50% under standard conditions. The ability of CCS to transfer copper to SOD1 was measured by incubating E,Zn-SOD1 with CCS for 15 to 30 minutes at 37^{o}C in a buffer of 50 mM sodium phosphate containing 10 μM bathrocuprine sulfonate and 10 μM EDTA at pH 7.8. The activity of CCS is defined as the amount of CCS required to activate one unit of activity of SOD.

In order to examine the success of transfer from CCS to E,Zn-SOD1 by Cu K-edge EXAFS, SOD1 was expressed and purified with a Strep-tag in the pASK-IBA3 plasmid (IBA, Göttingen, Germany) in *E. coli* BL21/DE3 and separated from the mixture with CCS on a Streptactin sepharose column (Sigma-Genosys). For each liter of SOD1 expressed in the presence of 500 μM $ZnSO_4$, 5 ml of Streptactin sepharose were used. The column was equilibrated with 2 column volumes of 100 mM Tris-HCl pH 8.0, lysate was loaded onto the column, and the column was washed with 5 column volumes of 100 mM Tris-HCl pH 8.0. SOD1 was eluted with 6 half column volumes of 100 mM Tris-HCl pH 8.0 with 2.5 mM desthiobiotin. After purification and determination of Zn

concentration, E,Zn-SOD1 was mixed with CCS and incubated as previously described. After incubation, the mixture was loaded onto a Streptactin sepharose column and SOD1 was separated from the mixture as described above. After elution and examination of purification by SDS-PAGE, SOD1 was concentrated for Cu K-edge EXAFS analysis.

2.2 PHYSICAL METHODS

2.2.1 COPPER RECONSTITUTION OF CCS

Fully metal-loaded hCCS truncation mutants were obtained by reducing the ligated protein over Immobilized TCEP Disulfide Reducing Gel (Pierce Biotechnology, Inc.) in an equal column volume as protein and immediately adding a known amount of tetrakis(acetonitrile)copper(I)hexafluorophosphate (Aldrich) dissolved in acetonitrile to a final solution of 10% acetonitrile. The protein and Cu(I)-acetonitrile solution were left to sit at room temperature in the anaerobic chamber for one hour. This was followed by exhaustive dialysis at 5000 MWCO against buffer to remove any free Cu or acetonitrile.

2.2.2 DETERMINATION OF PROTEIN AND METAL CONCENTRATION

Protein concentration was measured by Bradford assay (Bio-Rad Laboratories) using bovine serum albumin (BSA) as a standard. Copper was measured by atomic absorption/emission spectrophotometry on a Varian-Techron AA-5 atomic absorption spectrophotometer or on a Perkin-Elmer Optima 2000 DV inductively coupled plasma optical emission spectrophotometer (ICP OES). The oxidation state of the copper was determined by electron paramagnetic resonance spectroscopy (EPR) versus a Cu(II)-ethylenediaminetetraacetic acid (EDTA) standard on a Bruker Elexys 500 EPR spectrometer. The zinc concentration was measured by atomic absorption spectroscopy and ICP OES spectroscopy.

2.2.3 MASS SPECTROMETRY

Mass spectrometry was performed by Dr. Martina Ralle in the Department of Biochemistry at OHSU. Protein masses were determined by electrospray ionization mass spectrometry. Proteins were injected onto a 0.3 x 10mm C4 column (214MS53.10;Vydac), and masses were determined on-line using an ion trap (model LCQ Deca XP plus by Thermo Finnigan). The flowrate was 9 µl/min with a linear gradient of 2-75% acetonitrile over 55 minutes in a mobile phase containing 0.1% formic acid. Samples were injected using the Surveyor autosampler (Thermo Finnigan) and concentrated/purified using a protein micro trap cartridge (Michrom BioResources). Mass spectra of proteins eluted from the C-4 column were deconvoluted using BioWorks Browser (Themo Finnigan). Mass accuracy better than 0.02% was confirmed using horse myoglobin.

2.2.4 EXAFS

X-ray absorption spectroscopy (XAS) offers us a powerful tool for the study of metalloproteins in solution. X-rays are electromagnetic radiations with relatively short wavelengths in the range of 10 to 0.001 nanometers, corresponding to frequencies in the range 30 to 30 000 PHz that lie between ultraviolet light and gamma rays in the electromagnetic spectrum(Koningsberger and Prins, 1988; Teo, 1986). Soft to hard X-rays are generated as synchrotron radiation, emitted when charged particles such as electrons or positrons travel with a speed approaching that of light in curved paths in a magnetic field. Synchrotron radiation provides a high intensity X-ray source with tunability over a wide energy range with a continuous spectrum, high collimation, and plane-polarization. X-ray absorption spectra are generally produced in the range of 200-35 000 eV (λ=62.1-0.355 Å) (Koningsberger and Prins, 1988; Teo, 1986). In this energy range, the main process for X-ray absorption is such that the photon is completely absorbed by an atom and the incident radiation has sufficient energy to remove an electron from its shell (1s (K-edge), 2s or 2p (L-edge)), leaving a core hole. Fluorescence X-ray photons are then emitted from the excess energy produced from electrons falling into the core hole. The electron ejected from its shell will have an energy equal to the

energy of the incoming photon less its binding energy when in the core, and this photoelectron will interact with the surrounding atoms. An X-ray absorption edge is formed when the electron is excited from core state to continuum. The minimum photon energy required to eject an electron out of a particular atomic state is equal to the absolute value of the binding energy of the electron and is called the threshold energy (Koningsberger and Prins, 1988; Teo, 1986). As with all electromagnetic radiation, X-rays can be treated as either waves or particles. Electrons also possess wave-particle duality. Considering the wave nature of the ejected photoelectron and regarding the atoms as point scatterers, backscattered waves, produced when the waves interact with a point scatterer, interfere with the forward wave of the photoelectron to produce either peaks or troughs (Figure 2.6). Extended X-ray absorption fine structure (EXAFS) refers to this oscillatory variation of the X-ray absorption as a function of photon energy beyond an absorption edge (Koningsberger and Prins, 1988; Teo, 1986). Therefore, EXAFS only appears when the absorbing atom is closely surrounded by other atoms so that scattering is observed.

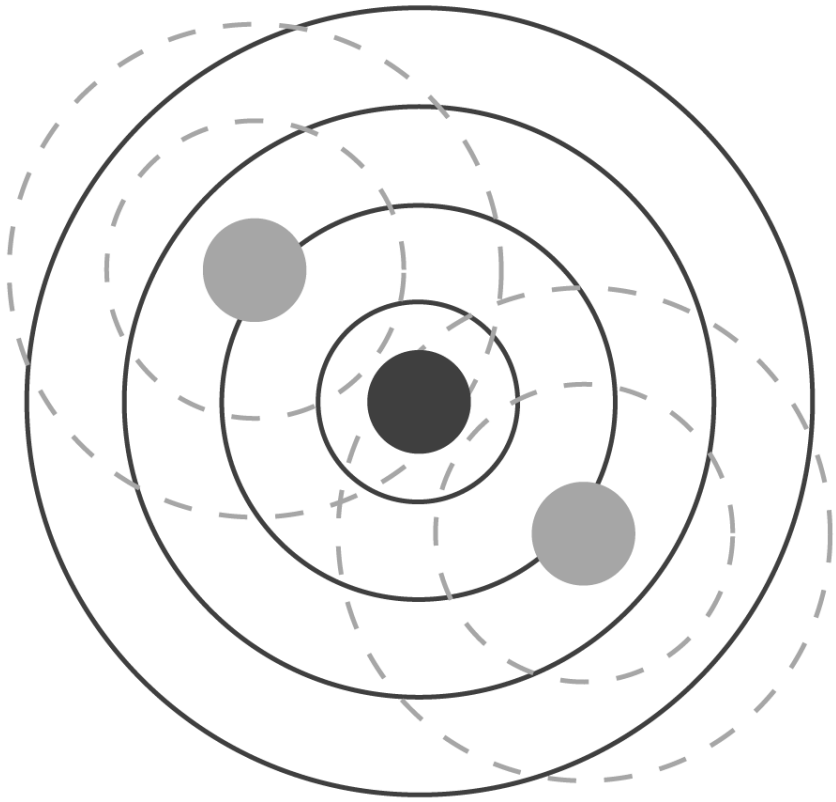

Figure 2.6. Diagram of photoelectron waves from a central atom (solid line) being backscattered by neighboring atoms (dashed lines).

In general, EXAFS spectra refer to the region 40-1000 eV above the absorption edge (Koningsberger and Prins, 1988; Teo, 1986). Absorption peaks due to excitation of core electrons to some bound states generally appear near or below the edge. Bonding information such as the energetics of virtual orbitals, the electronic configuration, and the site symmetry are contained within the pre-edge region. Between the pre-edge region and the EXAFS region is the X-ray Absorption Near Edge Structure (XANES) region (Koningsberger and Prins, 1988; Teo, 1986). EXAFS spectroscopy is plotted as a function of the X-ray absorption coefficient μ as a function of photon energy E above the threshold of an absorption edge. The interference between the outgoing and incoming photoelectron waves give rise to the sinusoidal variation of μ vs. E known as EXAFS (Koningsberger and Prins, 1988; Teo, 1986). The photoelectron ejected by absorption of

an X-ray photon can be viewed as an outgoing spherical wave centered at the excited atom with a wavelength $\lambda = 2\pi/k$ where

$k = \sqrt{2m/\hbar^2}(E-E_o)$ (Equation 2.1)

E is the incident photon energy and E_o is the inner-shell binding energy or the threshold energy of that particular absorption edge. Normalization of the oscillatory part of the absorption coefficient by the smooth atomic absorption background (μ_o) defines the EXAFS signal as:

$\chi(E) = \mu(E)- \mu_o(E)/\mu_o(E)$ (Equation 2.2)

To relate $\chi(E)$ to structural parameters, we must convert energy E into the photoelectron wavevector k. If we consider only the contribution of single scattering from the surrounding atoms with each term representing a contribution of a spherical shell of equivalent atoms at a distance R_i from the absorbing atom, the transformation of $\chi(E)$ in E space gives rise to $\chi(k)$ in k space where (Koningsberger and Prins, 1988; Teo, 1986):

$\chi(k) = \sum A_i(k)\sin(2kR_i+\delta_i)$ (Equation 2.3)

with δ_i as the atom-specific phase shift and the amplitude factor ($A_i(k)$) as:

$$A_i(k) = \left(\frac{N_i}{kR_i^2}\right)S_o^2 F_i(k)\exp(-2k^2\sigma^2)\exp(-R_i\lambda_i) \quad \text{(Equation 2.4)}$$

EXAFS results give information about the types and numbers of atoms surrounding the absorbing atom and the distance between absorber and scatterer (Koningsberger and Prins, 1988; Teo, 1986). In the above equation, R refers to the distance between the absorber and scatterer, N the number of atoms, the amplitude factor ($A_i(k)$) representing the atom type, S_o^2 describes the effects of multielectron excitations accompanying the

photoeffect in the inner shell, and σ^2 is the Debye-Waller factor, measuring the thermal and structural disorder in the shell. In this thesis, Debye-Waller factors (DW) are given as $2\sigma^2$.

For all samples, Cu K-edge (8.979 keV) and Se K-edge (12.658 keV) extended X-ray absorption fine structure (EXAFS) data were collected at the Stanford Synchrotron Radiation Laboratory operating at 3 GeV with currents between 100 and 50 mA. All samples were measured on beam line 9-3 by use of a Si[220] monochromator and a Rh-coated mirror upstream of the monochromator with a 13 keV energy cutoff to reject harmonics (Figure 2.7). A second Rh mirror downstream of the monochromator was used to focus the beam. Data were collected in fluorescence mode on a high-count-rate Canberra 30-element Ge array detector with maximum count rates below 120 kHz. A 6 μ Z-1 metal oxide (Ni, Cu; As, Se) filter and Soller slit assembly were placed in front of the detector to reduce the elastic scatter peak when needed. Three to nine scans of a sample containing only sample buffer (50 mM $NaPO_4$ and 500 mM NaCl, pH 7.2) were collected at each absorption edge, averaged, and subtracted from the averaged data for the protein samples to remove Z-1 Kβ fluorescence and produce a flat pre-edge baseline. This procedure allowed data with an excellent signal-to-noise ratio to be collected down to 100 μM total copper in the sample. The samples (80 μL) were measured as aqueous glasses (>20% ethylene glycol) at 15^{o}K. Energy calibration was achieved by reference to the first inflection point of a copper foil (8980.3 eV) for Cu K-edges and an arsenic foil (11867 eV) for Se K-edges, placed between the second and third ionization chamber. Data reduction and background subtraction were performed with the program modules of EXAFSPAK (George, 2001). Data from each detector channel were inspected for glitches or drop-outs before inclusion in the final average.

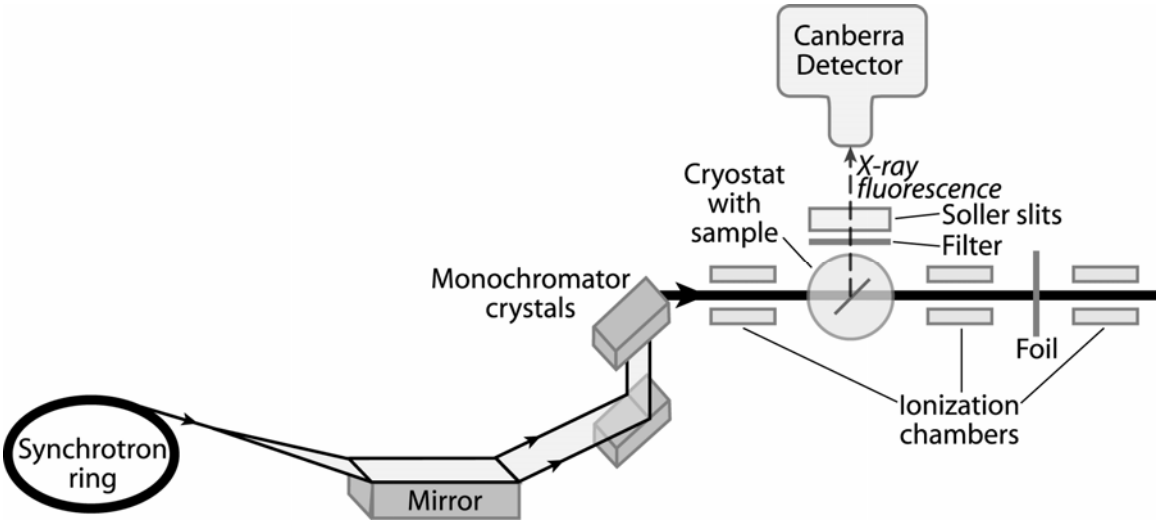

Figure 2.7. Schematic view of X-ray beamline experimental set-up at the Stanford Synchrotron Radiation Laboratory for EXAFS data collection.

Spectral simulation was carried out with the program EXCURVE98 (Binsted and Hasnain, 1996; Gurman, 1995; Ralle et al., 1999). EXAFS data are simulated by fitting the background subtracted data to a chemical model for the protein active site, which assumes an initial set of structural parameters, and then refines these by least squares minimization. For example, if it is believed that the protein site has Cu coordinated to three cysteine residues, the theoretical EXAFS spectrum corresponding to 3 Cu-S interactions at a specific distance R will be computed using equations 2.3 and 2.4, and the "goodness of fit" will be assessed by calculating the sum of the squares of the difference between theory and experiment at each data point. This sum is called the F value, and is defined as:

$$F^2 = \frac{1}{N}\sum_{i=1}^{N} k^6 \left(Data - Model \right)^2 \quad \text{(Equation 2.5)}$$

The program then adjusts the parameters in the fit until F reaches a minimum.

As seen in equations 2.3 and 2.4, there are a number of adjustable parameters which contribute to the amplitude and phase of the EXAFS oscillation. The parameters which

have structural significance are the coordination number, N, which determines the amplitude of the EXAFS wave, the metal-ligand distance, R, which determines the frequency and phase of the wave, and the Debye-Waller factor, DW, which is a measure of the statistical variation of the metal bond length about its mean position, R. The DW factor, (equal to $2\sigma^2$ in equation 2.4) acts as an exponential damping factor which attenuates the amplitude of the wave as k increases. An additional parameter E_0 is also refined in the fitting process, and allows the starting energy of the EXAFS oscillation to be adjusted by a few eVs in order to match the phase of the experimental and theoretical waves.

The following plots show the effect of varying each of these parameters. Figure 2.8 compares waves for 3 Cu-S interactions at 2.0 and 2.5 Å. It can be seen that the frequency of the wave increases as the distance increases. Figure 2.9 shows the effect of increasing the coordination number from 1 Cu-S at 2.5 Å to 2 Cu-S at the same distance. Here it can be seen that the amplitude of the wave doubles, while the frequency remains the same. Figure 2.10 shows the effect of increasing the DW factor from 0.003 $Å^2$ to 0.03 $Å^2$. Here the waves have similar amplitude at low k, but the amplitude decreases more rapidly with increasing k for the large DW value, i.e. the wave experiences increasing damping as the DW factor increases.

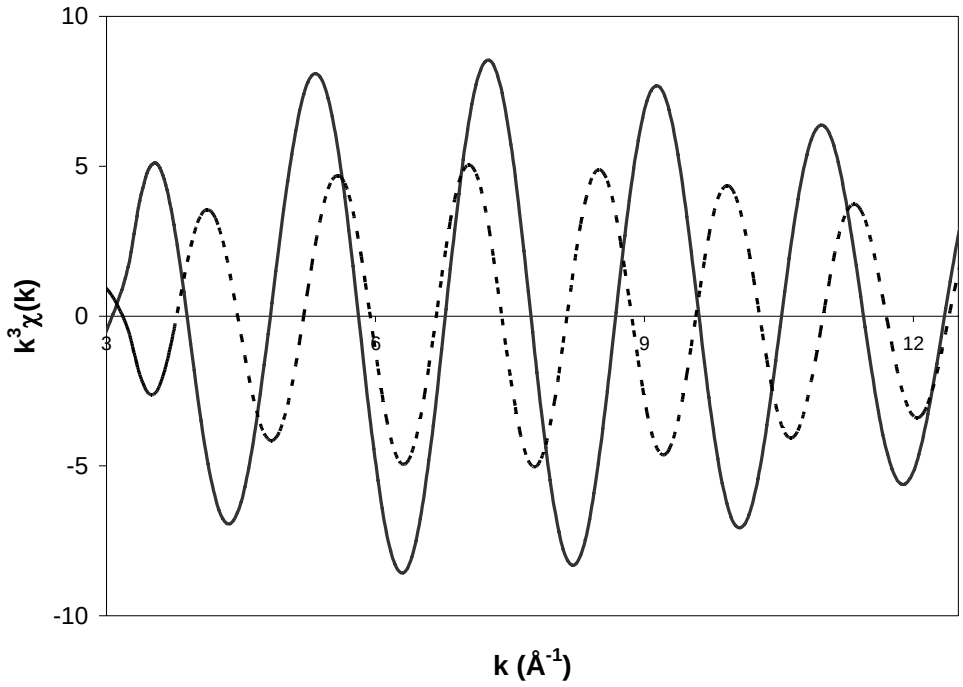

Figure 2.8. Simulation EXAFS of 3 Cu-S at 2.0 Å (solid line) and 2.5 Å (dashed line).

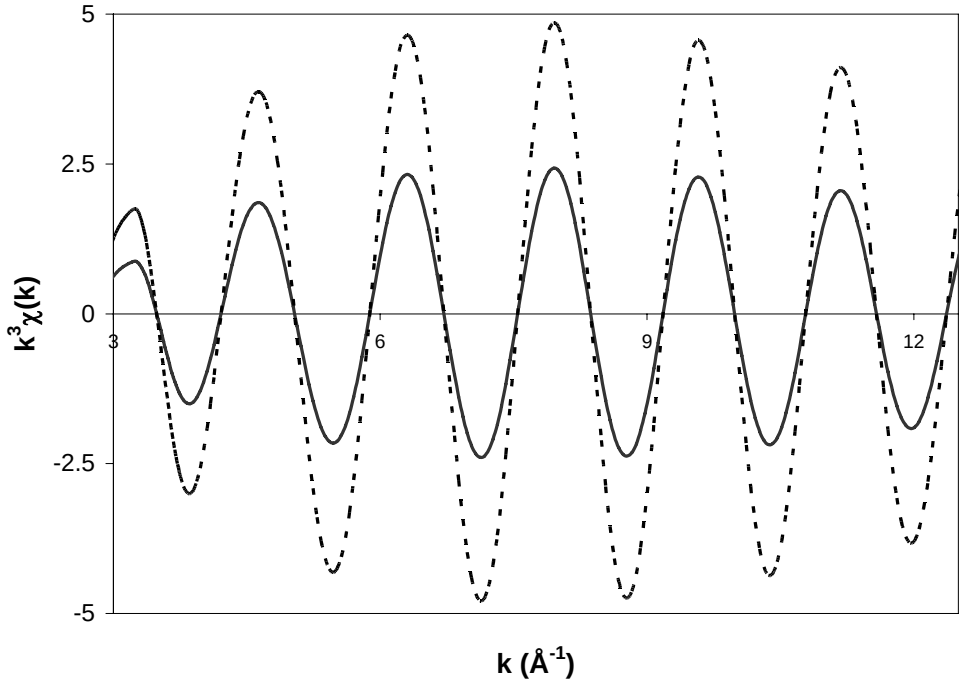

Figure 2.9. Simulation EXAFS of 1 Cu-S (solid line) and 2 Cu-S (dashed line).

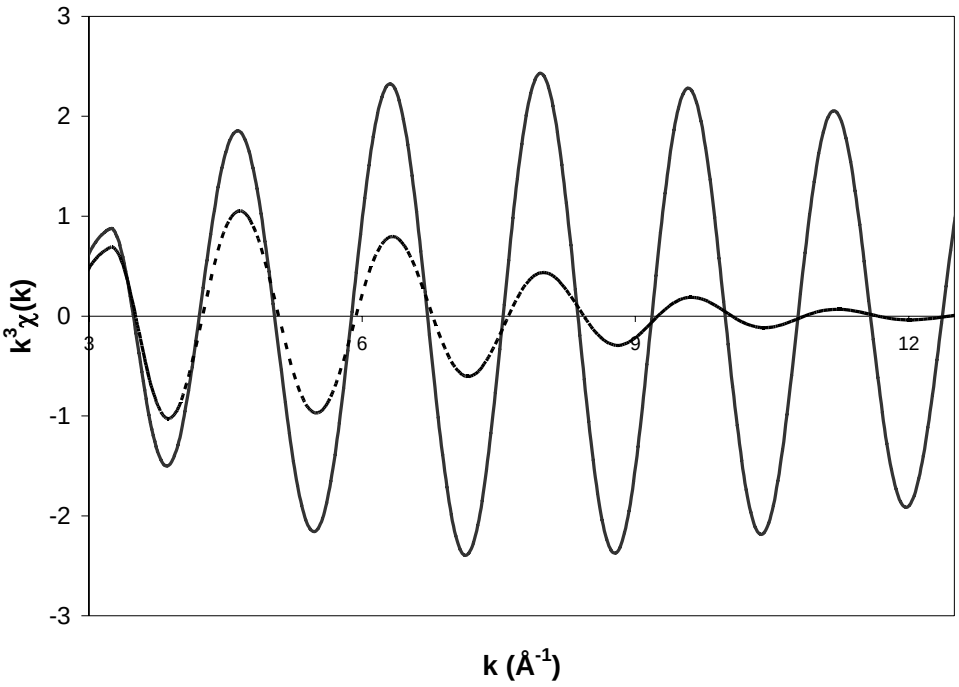

Figure 2.10. Simulation EXAFS of a Cu-S interaction with a DW=0.003 Å^2 (solid line) and DW=0.030 Å^2 (dashed line).

Typically EXAFS data are also represented by their Fourier transform (FT). The FT is defined by the equation:

$$\int_{-\infty}^{+\infty} \chi(k) \exp(-ikR) dk \quad \text{(Equation 2.6)}$$

and corresponds to the "spectrum" of frequencies contained within the EXAFS oscillation. The transform contains peaks which correspond to the distance of each shell of scatterers from the metal absorber. A good example relevant to the work in this thesis is the situation that occurs in Cu(I)-thiolate clusters (Pickering et al. 1993). These clusters contain shells of Cu-S(thiolate) atoms at 2.3 Å, and further shells of Cu-Cu interactions at ~ 2.7 Å, such as in hexakis-(μ-benzenethiolato)tetracuprate(I) (Figure 2.11). Figure 2.12 shows the EXAFS and FT of this system. The EXAFS oscillations contain a beat at ~9 Å due to the interference between the waves corresponding to Cu-S

at 2.25 Å, and Cu-Cu at ~2.7 Å. The two waves are clearly denoted in the FT by two resolved peaks at 2.3 and 2.7 Å respectively.

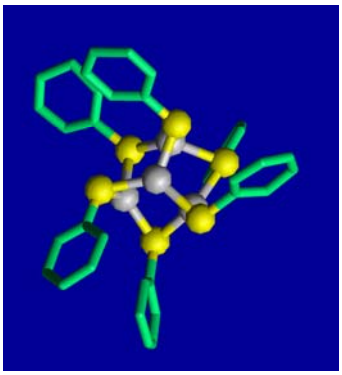

Figure 2.11. Hexakis-(μ-benzenethiolato)tetracuprate(I) (Courtesy of Graham N. George, University of Saskatchewan)

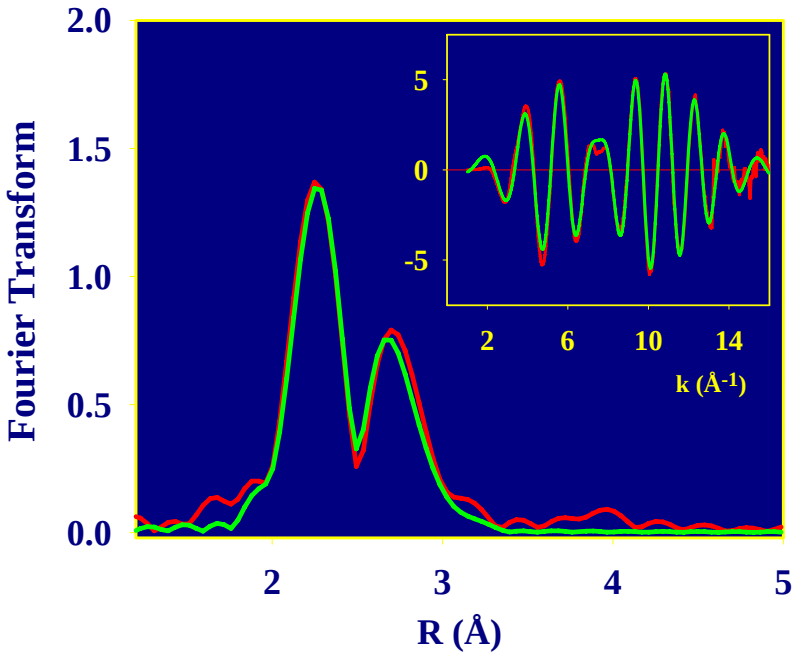

Figure 2.12. EXAFS and FT of a Cu(I)-thiolate system. Red line = Experimental data; Green line = Theoretical Fit. (Courtesy of Graham N. George, University of Saskatchewan)

CHAPTER 3: STUDIES ON THE CCS245CYS AND CCS245SEC PROTEINS

3.1 Initial characterization of CCS245Cys and CCS245Sec

Copper binding and XAS studies have been performed on wild-type hCCS (Eisses et al., 2000) and Cys to Ser single and double mutants of the D1 CXXC and D3 CXC motifs in a maltose binding protein fusion (Stasser et al., 2005). Other experiments have also been performed in an untagged hCCS with Cys to Ala mutations isolated using an intein self-cleaving vector (Stasser et al., 2007). These studies identified the coordination chemistry at each of the D1 and D3 Cu(I) binding sites and showed that Cu(I) forms a monomeric 3-coordinate CuS_2X (X= exogenous thiol, or solvent) complex at the MTCQSC site in D1 and a multinuclear cluster at the interface of two D3 polypeptides. Analysis of the intensity of the Cu-Cu cluster interaction in the Cys to Ala variants, suggested that the nuclearity of the cluster was greater than two, and was most consistent with a Cu_4S_6 adamantane-type species. The XAS data, in conjunction with studies of oligomerization equilibrium as a function of copper loading, led to a model for hCCS function in which Cu(I) binding converts the apo-dimer with a D2-D2 interface to a new dimer connected by cluster formation at two D3 CSC motifs. The predominance of dimer over tetramer in the cluster-containing species, strongly suggested that the D2 dimer interface remains open and available for sequestering a SOD1 monomer. The work implicated the copper

cluster in the reactive form, but fell short of providing any mechanistic detail concerning the reactivity of the cluster in the redox-driven copper/thiol-disulfide exchange between hCCS and its SOD1 partner.

If SOD activation is correlated with cluster formation, then it follows that the chemistry of the activation process is likely to depend critically on the cluster composition and geometry. To date, Cu K-edge EXAFS is the only spectroscopic technique to reveal the existence of the Cu(I) cluster, but it has not exposed details of cluster nuclearity and structure. Ligand-directed XAS probes, such as Se, can provide important additional information on metal coordination. This has been seen in the study of a selenocysteine substituted azurin derivative, where Se EXAFS was used in conjunction with Cu EXAFS to provide important new information on the cupredoxin site (Ralle et al., 2004). The semisynthesis of hCCS substituted with selenocysteine to produce a CXU copper-binding motif in D3 is described in this chapter. The protein binds Cu(I) to produce the first example of a multinuclear Cu(I) cluster containing a Cu-Se bond in a protein. By analyzing both Cu and Se EXAFS data, additional structural information on the cluster is obtained.

3.1.1 Semisynthesis of CCS245Cys and CCS245Sec

Since peptide synthesis and ligation yield becomes increasingly challenging with increasing length of the oligopeptides, the first step in creating a selenocysteine-containing hCCS mutant was to discover the shortest C-terminus that would allow retention of metal transfer activity. Therefore, truncated versions were made of hCCS after Cys246 (CCS246), 247 (CCS247), and 252 (CCS252) by PCR amplification of a wild-type hCCS template. Protein-coding regions were ligated into the pTXB-3 intein-containing plasmid and overexpressed in *E. coli* ER2566 with IPTG and Zn addition. After purification on chitin beads and intein cleavage, the truncation mutants were analyzed for activity and metal content by ICP-OES. Typically, all of the proteins bound 1 Zn per mole protein, such that copper-binding stoichiometries could be determined from the Zn:Cu ratios. Copper reconstitution was performed anaerobically by addition of

a 3-fold excess of $Cu[CH_3CN]_4^+$ followed by dialysis to remove remaining free copper and acetonitrile. CCS246 bound 2.3 Cu/Zn, CCS247 bound 2.7 Cu/Zn, and CCS252 bound 2.4 Cu/Zn. Activity was assayed by measuring the ability of the truncation mutants to transfer copper to E,Zn-SOD1 and the results are listed in Table 3-1.

Sample	Activity (units)
Cu,Zn-SOD1	2000
hCCS	1500
CCS246	1282
CCS247	1326
CCS252	1238

Table 3-1. SOD1-activation activity of hCCS truncation mutants.

As reported previously (Stasser et al., 2005), the amount of SOD1 activity recovered by reconstitution of E,Zn-SOD1 with hCCS (1500 units) is less than that of E,Zn-SOD1 reconstituted with inorganic cupric ions (2000 units). However, the activities of CCS246, CCS247 and CCS252 truncation mutants were the same within experimental error, and each mutant retained ~90 percent of the wild-type hCCS activity. Further analysis of the time course of SOD1 activation by CCS246 suggested that activity levels close to that of the Cu^{2+} reconstituted SOD could be achieved by increasing the time of incubation (Figure 3.1). Therefore, the CXC motif is essential to induce SOD1 activation, whereas the additional C-terminal sequence is not required but may accelerate the metal transfer.

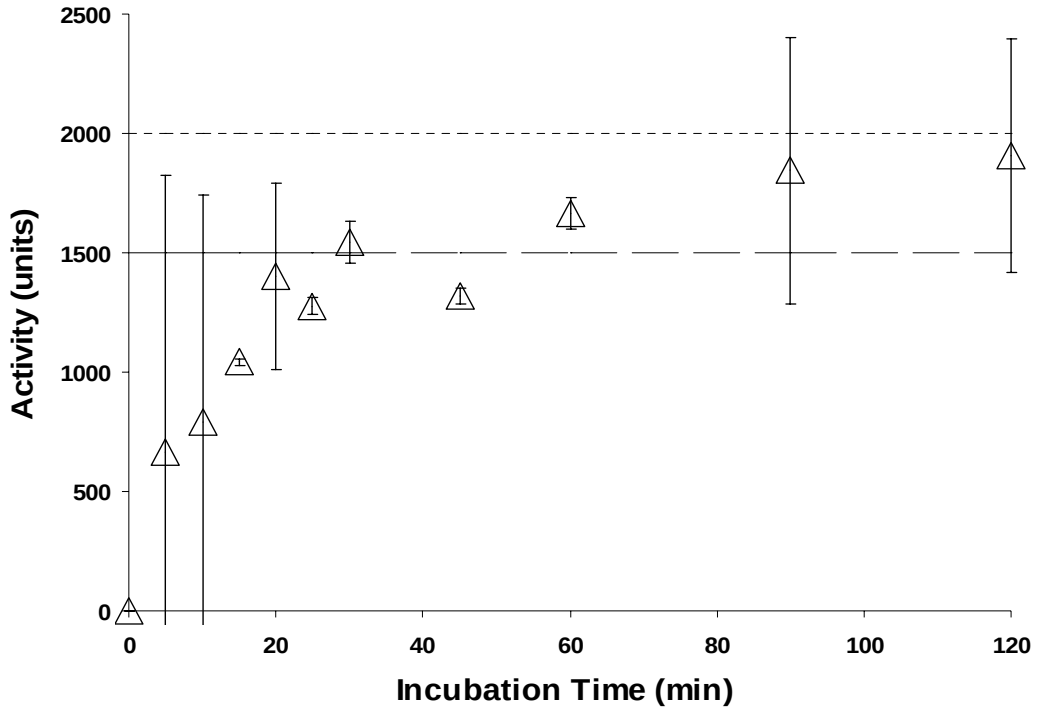

Figure 3.1. SOD1-activation activity of CCS246 at different incubation times. Error bars at 95% confidence intervals (equivalent to 3 standard deviations of the sample data). (small dashed line = reconstituted SOD1; large dashed line = hCCS; triangles = CCS246)

Since the CXC motif was both necessary and sufficient for SOD maturation, we chose initially to create a CAU motif as the C-terminal sequence since this could be achieved by ligating a single selenocysteine onto a 245-truncation mutant (CCS245) substituting Sec for Cys246. Thus, a ^{245}Ala truncation mutant, where the Ser245 was mutated to an Ala for more efficient ligation, was created by PCR amplification of hCCS. Ligation of an amino acid or peptide to a protein ending in Ala results in more efficient ligation, presumably due to the lack of an interfering side chain. The CCS245 truncation was then expressed in *E. coli* ER2566 and purified on a chitin column with intein cleavage by MESNA. Single amino acid ligation of selenocysteine or cysteine (as a control) to the truncated protein was performed anaerobically. Seleno-DL-cystine was first reduced with TCEP and then added 1:10 (protein:Sec) to the truncated protein. After 96 hours of anaerobic incubation, free selenocysteine and TCEP were removed by dialysis. Cys ligation was performed in a similar fashion.

3.1.2 Copper reconstitution

Reconstitution of the newly synthesized protein with Cu(I) was initially difficult due to diselenide formation even under anaerobic conditions in the CCS245Sec truncation, thereby preventing binding of Cu(I) to the CAU motif. To avoid this oxidation, it was necessary to reduce the diselenide with TCEP followed by rapid addition of the Cu(I) under anaerobic conditions. This was achieved by use of an immobilized TCEP-reducing gel (Pierce). Protein was added to the TCEP-bound agarose in a column and left to reduce for one hour. After elution with two volumes of buffer, three mole-equivalents of $[Cu(I)(CH_3CN]_4^+$ in acetonitrile were immediately added to the protein. Reconstituted proteins were then dialyzed against decreasing amounts of acetonitrile in 50mM phosphate buffer in order to remove free copper and acetonitrile. Metal analysis by ICPOES showed that the concentrations of Cu, Zn and Se in the selenocysteine-substituted h-CCS were 900, 400 and 409 μM respectively. Thus the CCS245Sec protein bound one Se per Zn, indicating efficient Sec ligation and 2.2 Cu per Zn and Se.

3.1.3 Ligation Efficiency

Mass spectral data give an independent estimate of the efficiency of the ligation process. Figure 3.2 shows the mass spectral data for Cys and Sec ligations respectively. The mass for the Cys-ligated (*m/z* = 25837) protein is the expected mass CCS245Cys with two disulfide crosslinks and the N-terminal methionine residue cleaved (m/z calc: 25837). The two disulfides probably correspond to the C141-C227 disulfide observed in the hCCS D2 crystal structure and a C22-C25 disulfide which is seen in the apo-yCCS structure. The Sec-ligated protein exhibits an intense peak at *m/z* = 25880. The mass corresponding to the analogous Sec-substituted protein with Met1 cleaved and two disulfides is *m/z* = 25884. This suggests that at least one additional S-S, Se-S exists in the Sec protein and is consistent with formation of a Se-S bond between C244 and C246 of the D3 CXC motif. Conspicuously absent are peaks that represent the unligated protein in the Sec-ligated spectrum. The low intensity peak in the Cys-ligated spectrum at 25663 does not correspond to unligated CCS245 truncation with Met1 cleaved (m/z calc: 25737, +MESNA: 26248) but could represent a form of the Met1-cleaved CCS245 truncation protein with the C-terminal alanine cleaved (m/z calc = 25663). The absence

of any species with mass representative of the CCS245 truncated starting material suggests close to 100% efficiency of the ligation process.

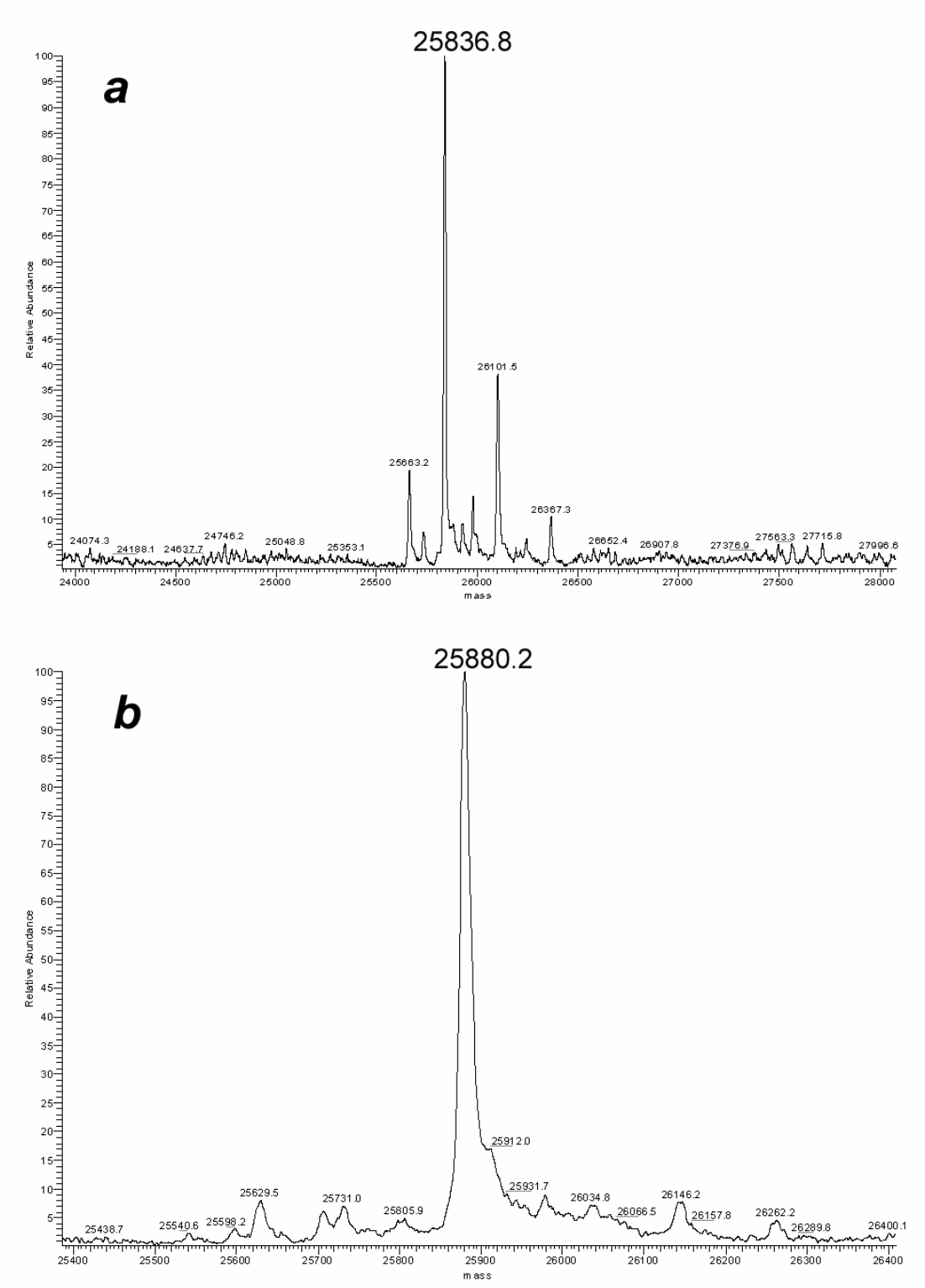

Figure 3.2. Mass spectral data of the (a) CCS245Cys ligated protein and (b) CCS245Sec ligated protein with major molecular weight peak indicated.

3.1.4 SOD-activation activity of semisynthetic CCS245Cys and CCS245Sec

Both ligation constructs were assayed for activity by measuring their ability to transfer copper within a 30 minute incubation period to apo-E-ZnSOD1 at a ratio of 1:1 hCCS:SOD1 in 3 replicate runs (Table 3-2). Both Cys and Sec-ligated proteins had the same transfer activity within experimental error, but appeared to have a slightly lower activity than the plasmid-expressed controls. The cysteine-ligated hCCS retained 81% of its activity compared to CCS246, whereas the selenocysteine-ligated protein retained 78% compared to CCS246. The slightly decreased activity of the ligation mutants could be due to less than 100% ligation efficiency or slower transfer kinetics. Since the Se:Zn ratio was unity, and mass spectrometric analysis indicated no observable unligated CCS245 truncated precursor, the former explanation seems unlikely.

Sample	Activity (units)
Cu,Zn-SOD1	2000
hCCS	1500
CCS246	1282
CCS245Cys	1042
CCS245Sec	1006

Table 3-2. SOD-activation activity assays for CCS245Cys and CCS245Sec in comparison to wild-type hCCS, CCS246, and reconstituted SOD1.

When the ratio of CCS:SOD1 is increased in the CCS245Cys and CCS245Sec SOD1-activation assays, slightly increased transfer activity is seen (Figure 3.3). This effect is more marked when the incubation time of CCS245Sec with SOD1 is increased (Figure 3.4). This increased transfer activity with protein concentration and incubation time indicate that slower transfer kinetics are the likely origin of the decreased activity of the 245-X ligated proteins. It is clear however, that substitution of Se for S has no affect on the SOD maturation activity.

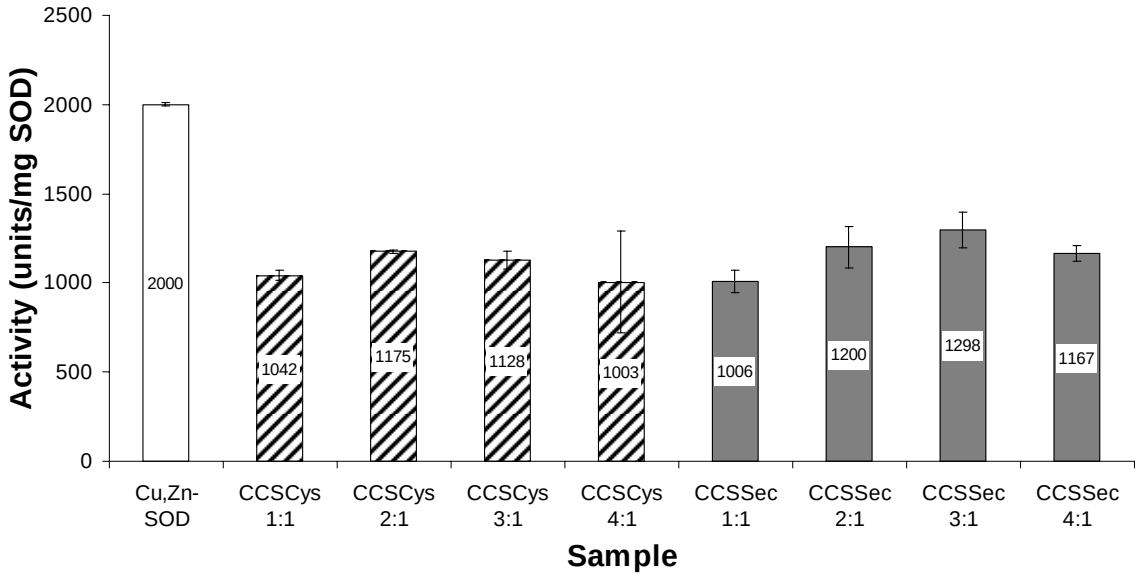

Figure 3.3. SOD1-activation activity of CCS245Cys and CCS245Sec with differing CCS:SOD1 ratios. Error bars at 95% confidence intervals (equivalent to 3 standard deviations of the sample data).

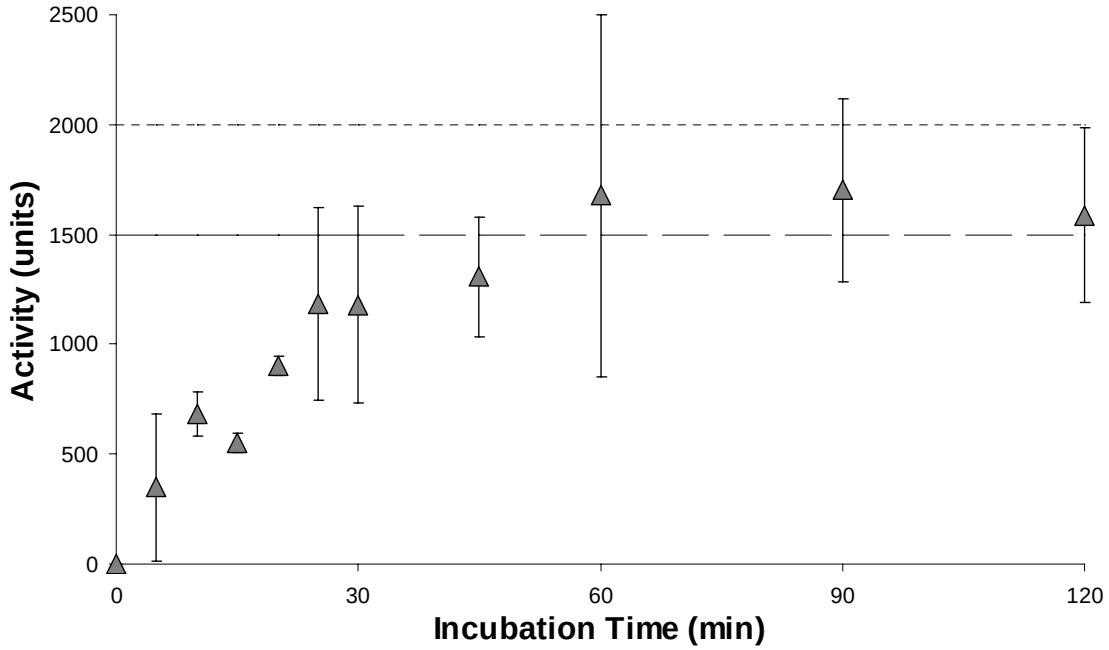

Figure 3.4. SOD1-activation assays of CCS245Sec with differing incubation times. Error bars at 95% confidence intervals (equivalent to 3 standard deviations of the

sample data). (small dashed line = reconstituted SOD1; large dashed line = hCCS; triangles = CCS245Sec)

3.2 Cu-EXAFS on CCS245Cys and CCS245Sec

3.2.1 CCS245Cys Cu EXAFS

Cu K-edge EXAFS of the Cys-ligated hCCS are shown in Figure 3.5. As expected the CCS245Cys protein is very similar to the previously reported XAS of the wild-type protein (untagged, residues 1-268, (Stasser et al., 2007)). Two shells of scatterers are observed at ~2.2 and 2.7 Å, corresponding to Cu-S and Cu-Cu respectively. Curve fitting analysis leads to a best fit with 3 Cu-S interactions (R, $2\sigma^2$) at 2.24 Å (0.006 $Å^2$) and 1 Cu-Cu at 2.71 Å (0.011 $Å^2$). From previous work on the C244A/C246A double mutant constructed in the full length (untagged) protein, it was concluded that a multinuclear Cu(I) cluster was formed at the interface of two D3 polypeptides, with a characteristic DW of 0.012 $Å^2$ for the Cu-Cu interaction (Stasser et al., 2007). Since both D1 and D3 Cu binding sites are presumed to be occupied in a 1:1 ratio, this would equate to 2 Cu-Cu interactions per Cu center in the D3 cluster, or a nuclearity ≥ 3.

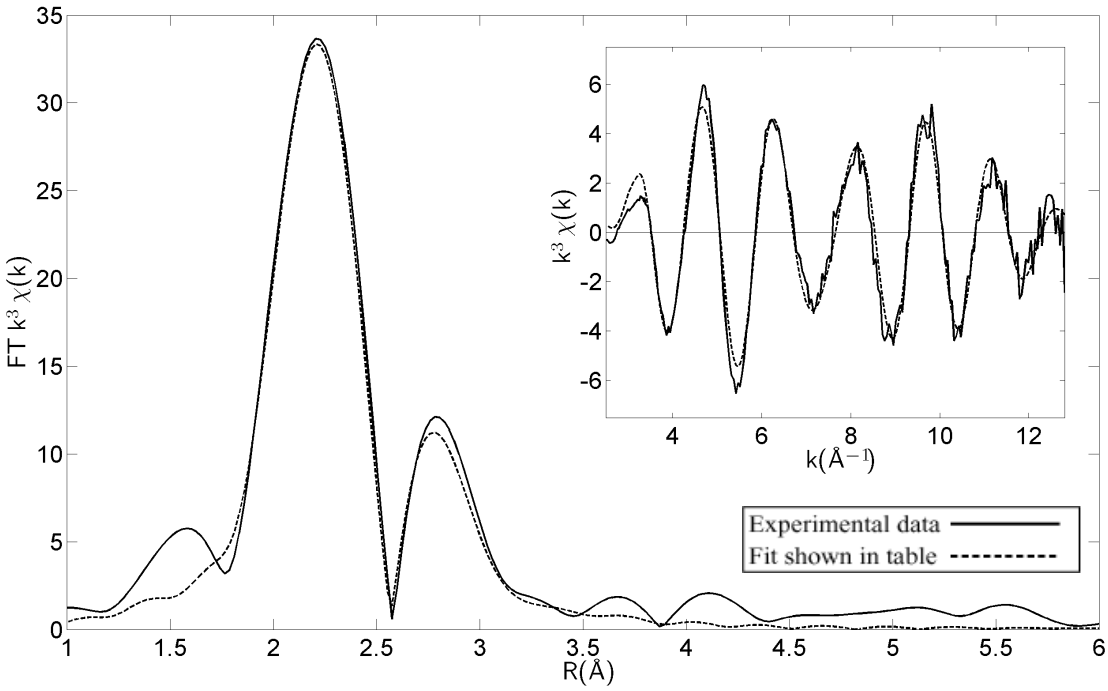

Scatterer	Distance (Å)	Debye-Waller (Å²)	-E_0 (eV)	F
3.0 S	2.24	0.012	4.12	0.372
1.0 Cu	2.71	0.011		

Figure 3.5. Cu K-edge EXAFS of CCS245Cys.

In contrast to CCS245Cys, the CCS246 protein routinely showed a low intensity ~2.7 Å outer-shell feature, suggestive of less cluster formation (Figure 3.6). Since the semisynthetic CCS245Cys behaves normally (i.e. is identical with full length (1-268) hCCS) with respect to cluster formation, it is possible that the plasmid-based protein may be unstable with respect to cleavage of the C-terminal Cys residue from the protein within the cell, which would result in incomplete cluster formation. On the other hand, it is unclear why the protein would exhibit the high levels of SOD activation observed in the reconstitution assay. At present, we have no clear explanation for the anomalous behavior of the expressed CCS246 protein relative to CCS245Cys.

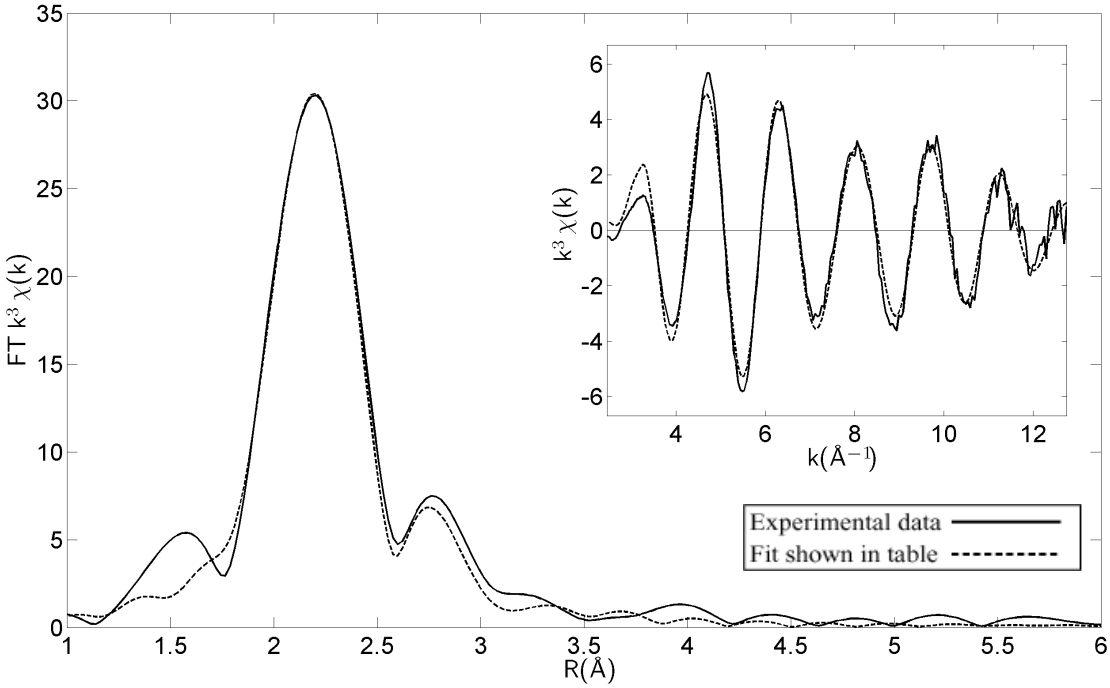

Scatterer	Distance (Å)	Debye-Waller (Å²)	-E_0 (eV)	F
3.0 S	2.24	0.013	4.71	0.327
1.0 Cu	2.68	0.021		

Figure 3.6. Cu K-edge EXAFS of CCS246.

3.2.2 CCS245Sec Cu EXAFS

With Cu bound at D1 in a predominately Cu-S environment, and the expected coordination of Cys244 from each D3 polypeptide, analysis of the Cu EXAFS was performed with Cu-S, Cu-Se, and Cu-Cu shells. The best fit (using Cu-Se = 2.38 ± 0.2 Å, and $2\sigma^2$(Cu-Cu) = 0.012 Å^2) gave 2.2 Cu-S at 2.240 Å (0.010 Å^2), 0.7 Cu-Se at 2.400 Å (0.007 Å^2), and 1.4 Cu-Cu at 2.705 (0.012 Å^2) (Figure 3.7). These parameters lead to full consistency of metrical parameters at both Cu and Se absorption edges.

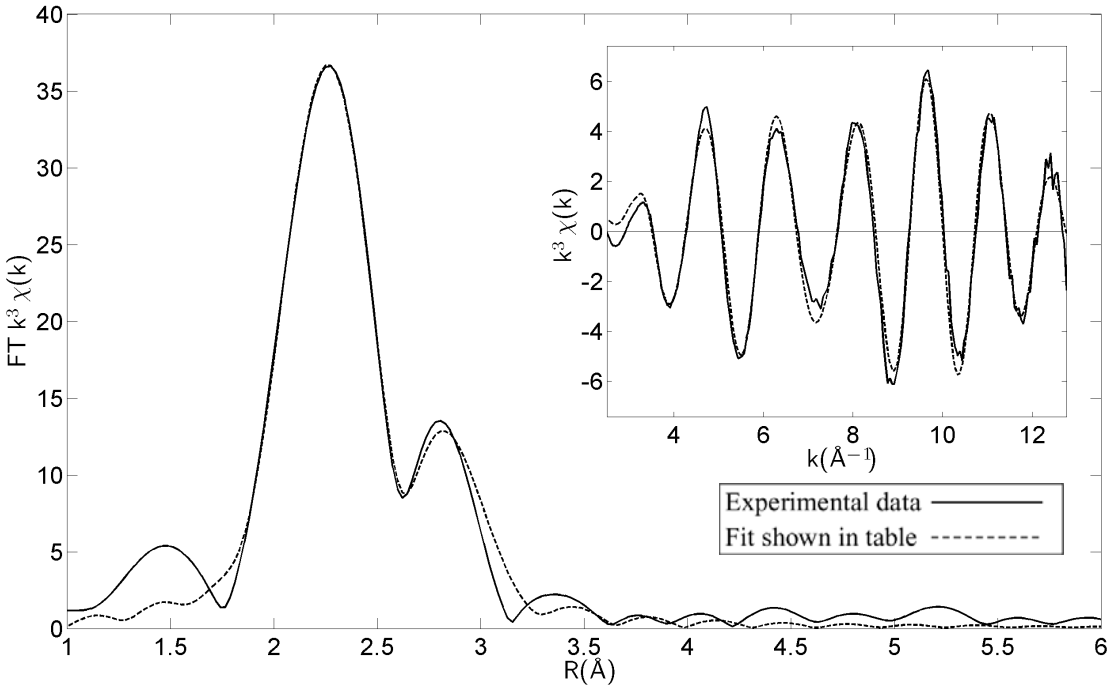

Scatterer	Distance (Å)	Debye-Waller (Å²)	-E_0 (eV)	F
2.0 S	2.23	0.009	3.06	0.246
1.2 Cu	2.70	0.011		
0.8 Se	2.40	0.007		

Figure 3.7. Cu K-edge EXAFS of CCS245Sec.

3.2.3 CCS245Sec copper titration

Due to the ability of the CCS245Sec mutant to bind more than 2 coppers per protein, we decided to investigate the structure of the copper cluster using Cu-EXAFS when increasing equivalents of copper to protein are added. Up to four coppers per protein were successfully added to CCS245Sec, but no more than 3.2 coppers per protein could be added to CCS245Sec. When comparing the experimental Cu K-edge EXAFS data at each stoichiometric addition of copper, all appeared identical except for that of 1:1 Cu:protein (Figure 3.8). Not surprisingly, the fits are also identical, except for that of the 1:1 protein which shows less Cu present, indicating an incomplete copper cluster formation.

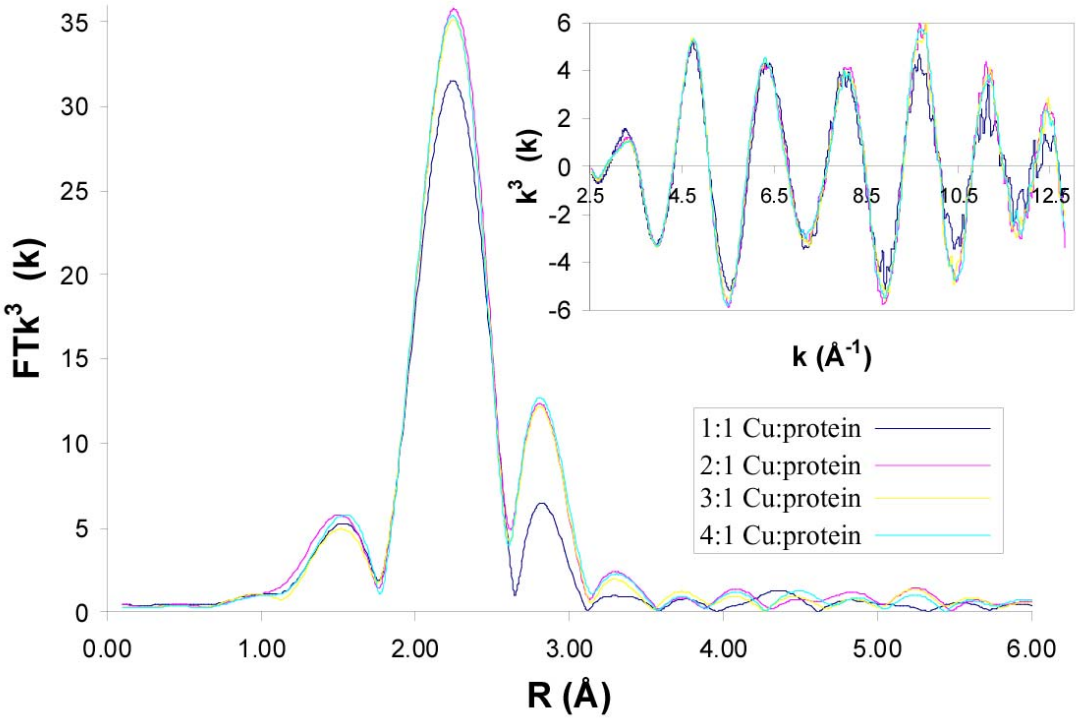

Figure 3.8. Cu K-edge EXAFS experimental data for CCS245Sec with different ratios of Cu:protein added.

3.3 Se-EXAFS on CCS245Cys and CCS245Sec

3.3.1 Apo CCS245Sec

Due to the presence of selenocysteine as the C-terminal residue of CCS245Sec, it was possible to probe the speciation of the Se by Se K-edge EXAFS without copper present. A number of structural environments were considered possible. First the Se could be present as a reduced selenol or selenide which would result in predominant Se-C first-shell scattering. Alternatively, as suggested by the mass spectral data, oxidation could lead to a sulfido-selenide (S-Se) in which case Se-S would accompany the Se-C interactions in the first shell. Finally, a Se-Se interaction might occur if CAU motifs from two domain 3 polypeptides could crosslink. This latter situation would be reminiscent of the Cu(I)-cluster formation shown to occur at a D3 – D3 dimer interface (Stasser et al., 2005; Stasser et al., 2007). EXAFS spectra for the apo-CCS245Sec are shown in Figure 3.9. Fits using either Se-C, or mixed Se-C/Se-S were unable to

reproduce the increase in amplitude of the EXAFS oscillations maximizing at k~9 $Å^{-1}$. This pattern of EXAFS amplitude envelope is typical of scattering from heavy atoms such as transition metals and heavier chalcogenides. Therefore, we also considered fits with Se-Se interactions arising from D3 dimerization. The best fit was found to be a mixture of both Se-S (0.3) and Se-Se (0.7) with an F value of 0.340. This shows that, as isolated, the ligated protein appears to be oxidized, and exists as an equilibrium mixture of monomers with Se-S distances of 2.21 Å, and dimers with Se-Se distances of 2.32 Å. These results emphasized the need for reduction of the ligated proteins on the immobilized TCEP column prior to reconstitution with Cu(I). Se-EXAFS was also used to probe the Se oxidation state after this TCEP reduction step (data not shown), but the results could not be interpreted in terms of a simple model such as a single Se-C shell as expected for a reduced selenol. The reasons for the complexity of the Se EXAFS after reduction remain unclear (since all steps were performed anaerobically), but it is possible that further reaction/oxidation might have occurred during the time needed to concentrate the samples for XAS analysis. This aspect of apo-CCS245Sec chemistry was not explored further.

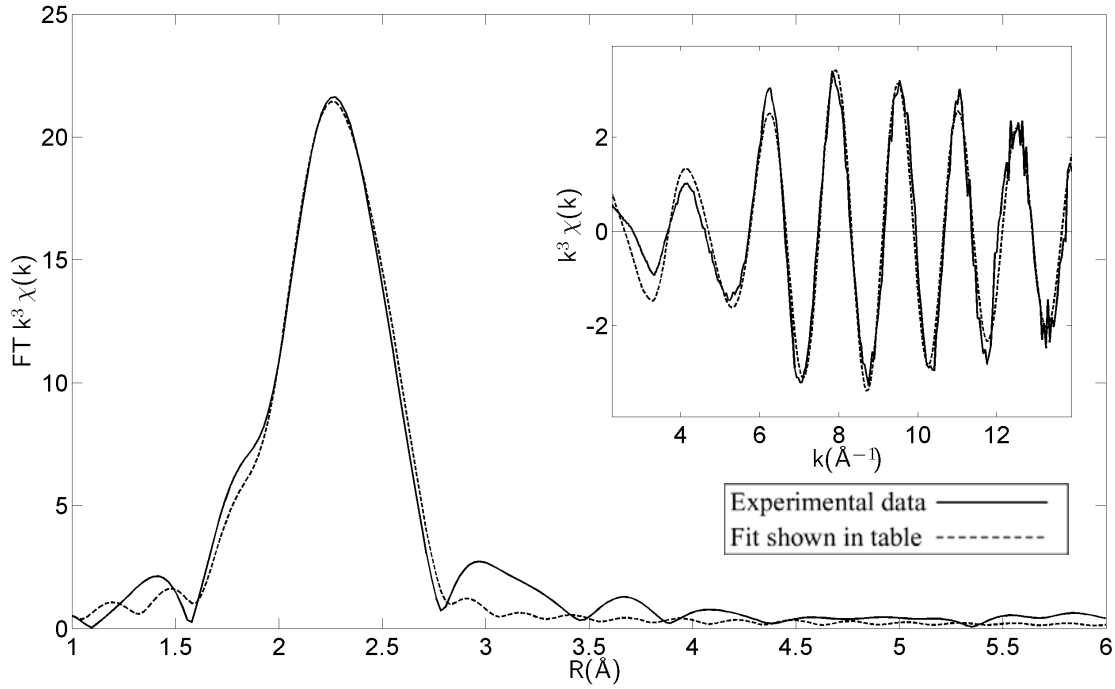

Scatterer	Distance (Å)	Debye-Waller (Å²)	-E_0 (eV)	F
1.0 C	1.99	0.006	6.28	0.342
0.7 Se	2.32	0.006		
0.3 S	2.21	0.006		

Figure 3.9. Se K-edge EXAFS of apo-CCS245Sec.

3.3.2 CCS245Sec Se-EXAFS

The Se K-edge EXAFS (Figure 3.10) should contain contributions from 1 Se-C and a number of Se-Cu interactions, depending on the cluster structural composition. As expected, the data show strong contributions from a heavy atom scatterer maximizing at k ~ 9 $Å^{-1}$. Simulations were attempted with 1 Se-C and a varying number of Se-Cu interactions. A single Se-Cu gave a F value of 0.507 with Se-C and Se-Cu [R, ($2\sigma^2$)] of 2.01 Å (0.002 $Å^2$) and 2.38 Å (0.001 $Å^2$) respectively. In this fit, the EXAFS amplitude was not adequately fit even with the extremely low Se-Cu DW factor. A much improved fit, F= 0.421 was obtained with 1 Se-C and 2 Se-Cu with $R(2\sigma^2)_{Se\text{-}C}$ = 2.04 Å (0.006 $Å^2$) and $R(2\sigma^2)_{Se\text{-}Cu}$ = 2.40 Å (0.007 $Å^2$). When the Se-Cu occupation number and DW were allowed to float freely, the Se-Cu coordination number refined to 1.9 with $2\sigma^2$=0.006 $Å^2$.

These simulations lead to the unambiguous conclusion that each Se is bound by 2 Cu atoms at 2.38 Å in the D3 cluster.

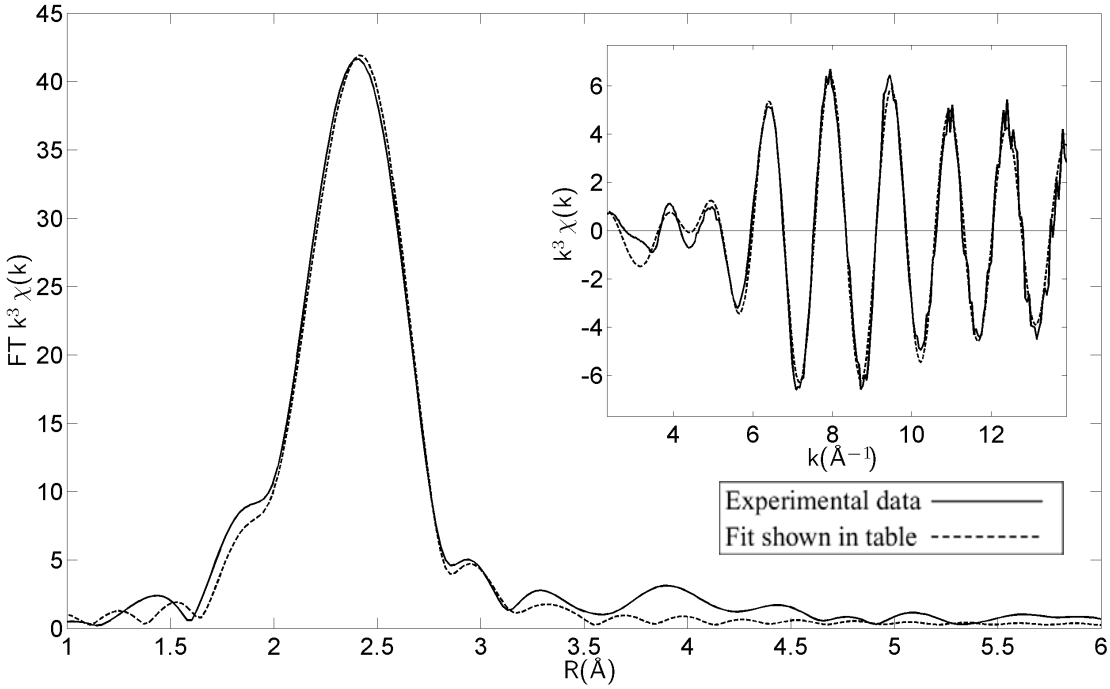

Scatterer	Distance (Å)	Debye-Waller (Å²)	-E_0 (eV)	F
1.0 C	2.04	0.006	9.23	0.421
2.0 Cu	2.40	0.007		

Figure 3.10. Se K-edge EXAFS of CCS245Sec.

3.3.3 CCS245Sec copper titration

As seen in the Cu-EXAFS, when copper was added stoichiometrically to CCS245Sec, the copper edge did not change significantly after 2 or more equivalents of copper to protein were bound. However, when comparing the Se-EXAFS experimental data of the differing Cu:protein preparations, changes with each addition can be seen (Figure 3.11). When fit, more copper is seen at the Se K-edge as more is added to the protein, indicating a more complex Cu-Se cluster forming with increasing amounts of added copper. When simulating increasing amounts of Cu at the Se K-edge, differences can be observed in the K-edge at ~4.5 $Å^{-1}$, and waves with increasing amplitude above 4.5 $Å^{-1}$ are seen (Figure 3.12). The 4.5 $Å^{-1}$ feature can also be seen to change significantly in simulations with increasing amounts of Se-S at ~3.9 Å in Se-Cu clusters with only one Cu present (Figure 3.13). At that distance, Se-S could represent non-bonded interactions across the cluster.

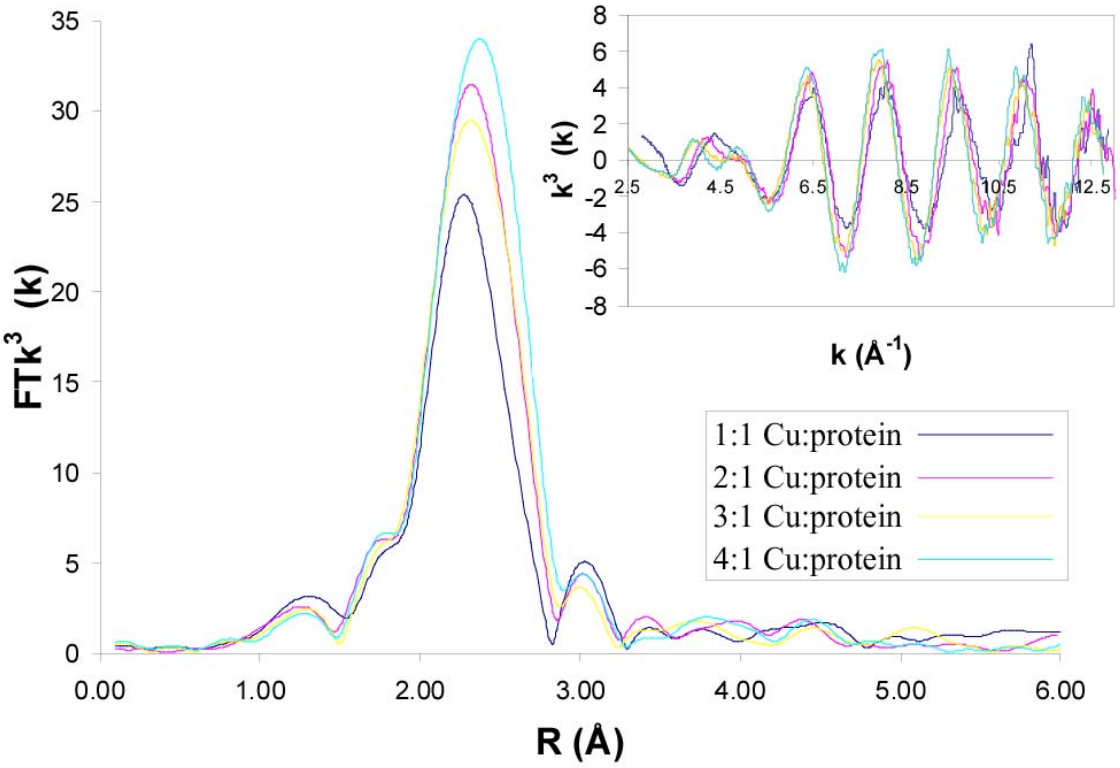

Figure 3.11. Se K-edge EXAFS experimental data of CCS245Sec with different ratios of Cu:protein added.

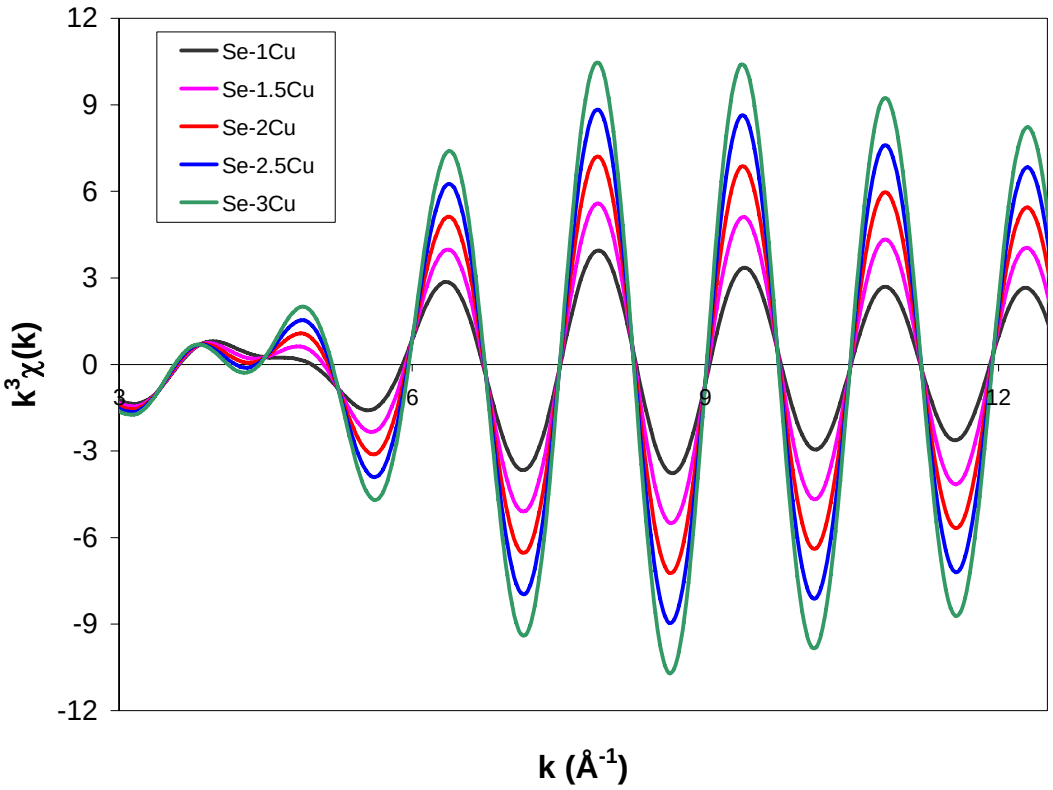

Figure 3.12. Simulated EXAFS of Se-Cu complexes.

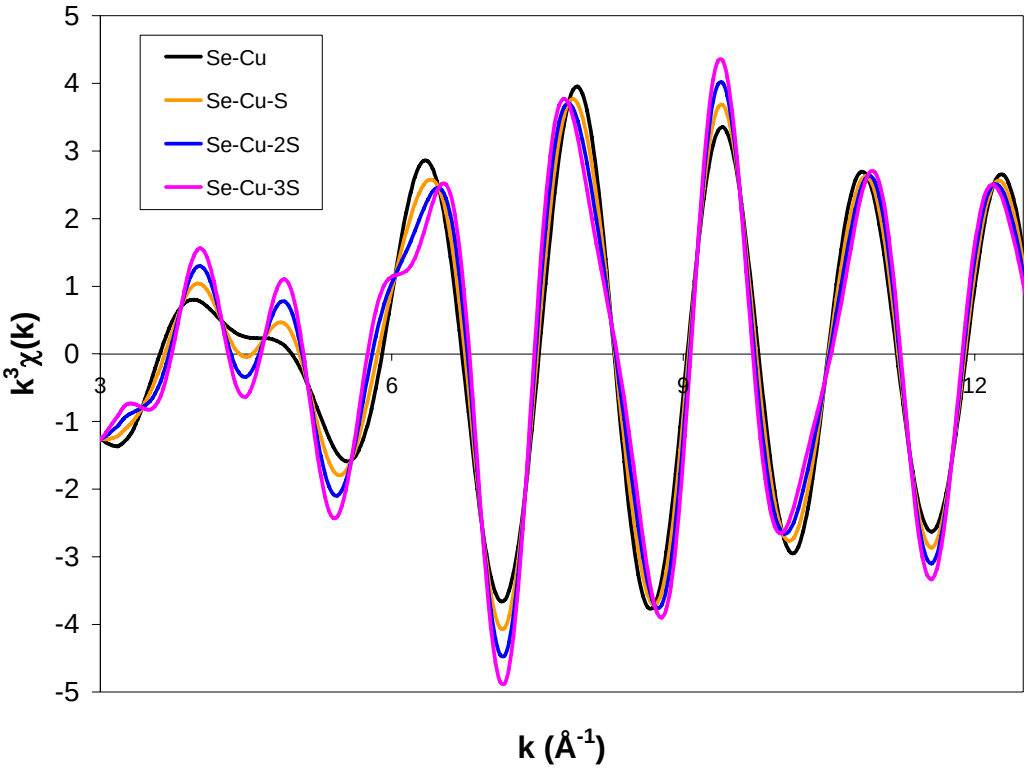

Figure 3.13. Simulated EXAFS of Se-Cu-S complexes with increasing amounts of S.

3.4 EXAFS studies of copper-transfer to SOD1 by wild-type hCCS and CCS245Sec

3.4.1 Wild-type hCCS

In order to examine the transfer of copper from hCCS to SOD1 using EXAFS, we initially began with studies of wild-type hCCS. Two ways of measuring copper transfer were considered. First, either CCS or SOD1 could be tagged, the two proteins mixed, separated, and EXAFS could be collected for each separate protein. Second, either CCS or SOD1 could be labeled with a spectroscopic probe, proteins could be mixed, and EXAFS of the mixed solution measured, interrogating transfer via the changes in the spectral features of the probe. This second method gives the advantage of not having to separate the two proteins after they were mixed. To begin, Cu-EXAFS of hCCS with SOD1 in a mixture of 1:1 was examined. Fully metallated wild-type hCCS was combined

with E,Zn-SOD1 in a ratio of 1:1 and incubated at 37°C for 30 minutes. This mixture showed a spectrum (Figure 3.14) that looked almost identical to that of the C244A CCS mutant (Stasser et al., 2007). This spectrum is thought to represent CCS protein with copper present in D1 and missing from D3, since there is no Cu-Cu interaction.

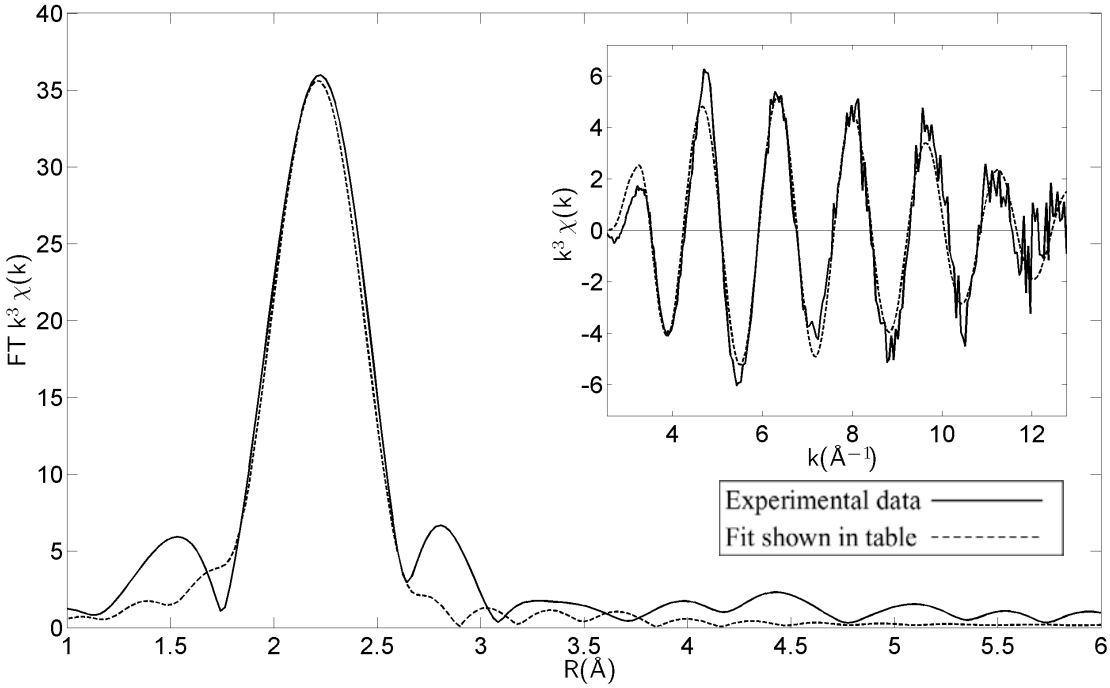

Scatterer	Distance (Å)	Debye-Waller (Å²)	-E₀ (eV)	F
3.0 S	2.24	0.011	3.09	0.555

Figure 3.14. Cu K-edge EXAFS of a mixture of hCCS with E,Zn-SOD1.

Although copper has appeared to have left CCS, no histidine contribution to the Cu-edge from reconstituted SOD1 can be seen, even though the two proteins have not been separated. This could be due to the strong Cu-S signal from CCS that dominates the spectrum.

In a second experiment, the transfer of copper from hCCS to SOD1 is confirmed when SOD1 is anaerobically separated from the wild-type hCCS-SOD1 mixture and Cu-EXAFS are analyzed. Utilizing the presence of a Strep-tag on SOD1, SOD1 was purified from hCCS on a Streptactin sepharose (Sigma-Genosys) column after incubation as done

previously. The mixture was loaded onto the column, washed with 3 volumes of column buffer, and tagged SOD1 was eluted from the column with elution buffer containing desthiobiotin. The eluted protein was concentrated and Cu K-edge EXAFS were measured. Cu-histidine features are seen in Cu EXAFS of the purified SOD1, indicating that SOD1 has been reconstituted by hCCS

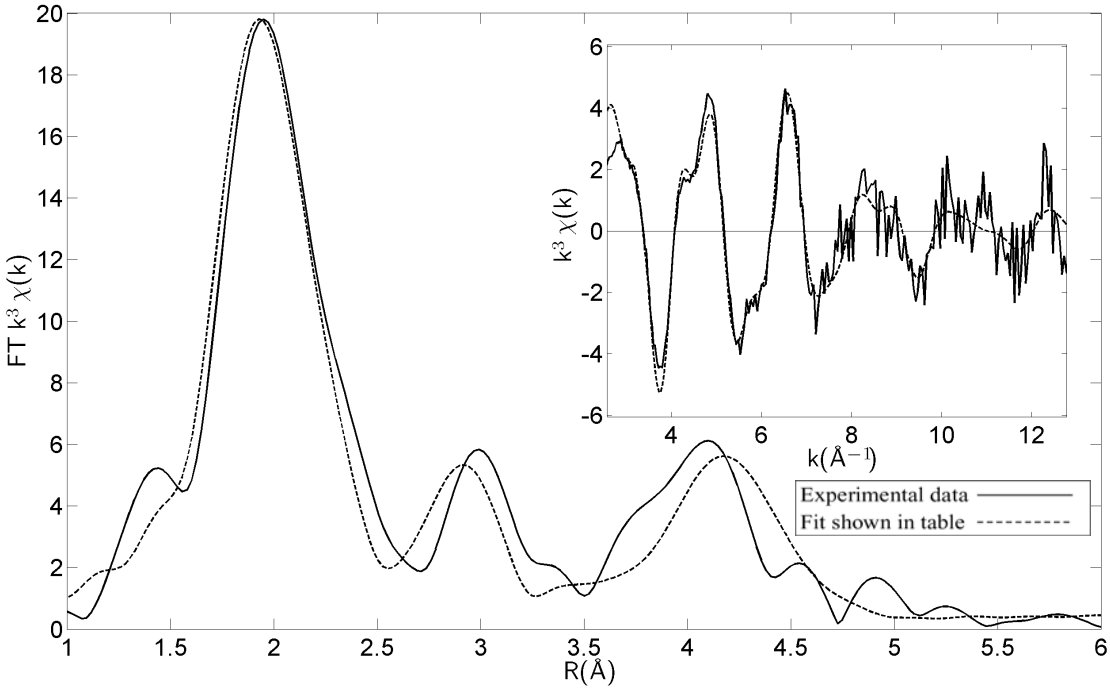

Scatterer	Distance (Å)	Debye-Waller (Å²)	-E_0 (eV)	F
3.0 N	1.96	0.012	2.64	0.713
3.0 C	2.93	0.016		
3.0 C	3.02	0.016		
3.0 N	4.18	0.024		
3.0 C	4.22	0.024		
0.4 S	2.24	0.009		

Figure **3.15**). When compared to a spectrum of E,Zn-SOD1 reconstituted with Cu(II) (Figure 3.16), the two spectra look similar with four histidine residues present in the Cu(II)-reconstituted SOD1 and three present in the hCCS-reconstituted SOD1. Three-coordinate SOD1 indicates that the Cu is reduced (Blackburn et al. 1983). The reduced Cu binding site present in the hCCS-reconstituted SOD1 is probably due to the anaerobic purification of hCCS-reconstituted SOD1. In addition, the best fit of the hCCS-reconstituted SOD1 Cu K-edge EXAFS, F = 0.713, contains some Cu-S (0.4 S) with an $R(2\sigma^2)_{Cu\text{-}S}$ = 2.24 Å (0.009 Å^2), probably due to the presence of some hCCS in the

purified SOD1. The spectra indicate that E,Zn-SOD1 was successfully reconstituted with copper by hCCS and that hCCS may lose copper from the D3 cluster to SOD1.

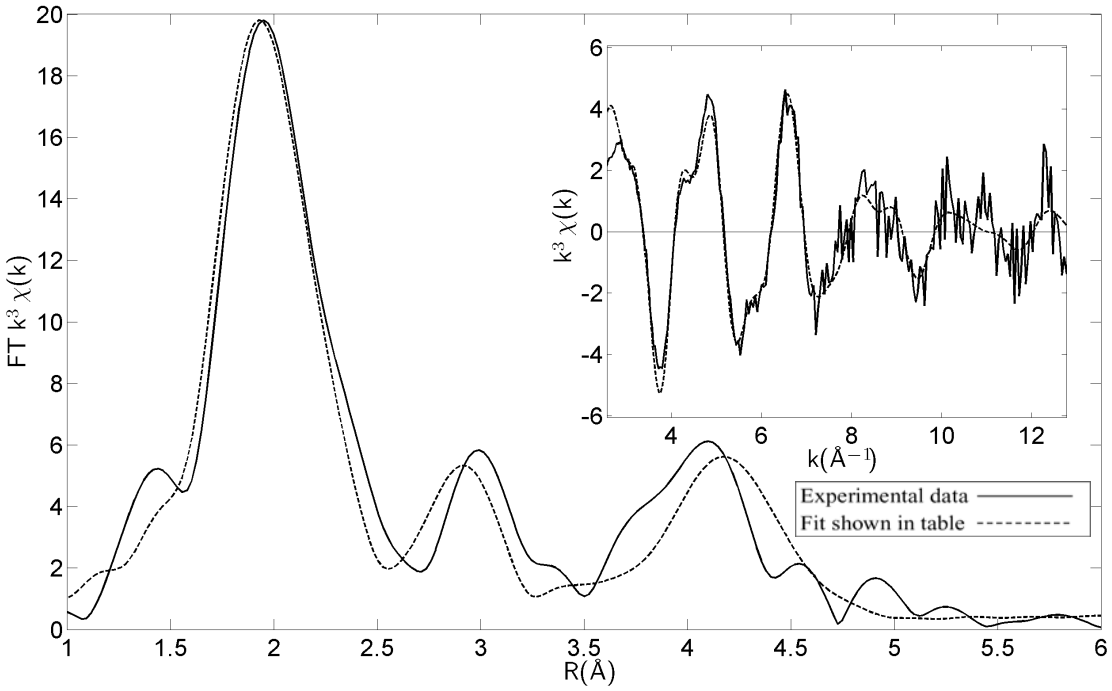

Scatterer	Distance (Å)	Debye-Waller (Å²)	-E_0 (eV)	F
3.0 N	1.96	0.012	2.64	0.713
3.0 C	2.93	0.016		
3.0 C	3.02	0.016		
3.0 N	4.18	0.024		
3.0 C	4.22	0.024		
0.4 S	2.24	0.009		

Figure 3.15. Cu K-edge EXAFS of SOD1 purified from the hCCS and E,Zn-SOD1 mixture.

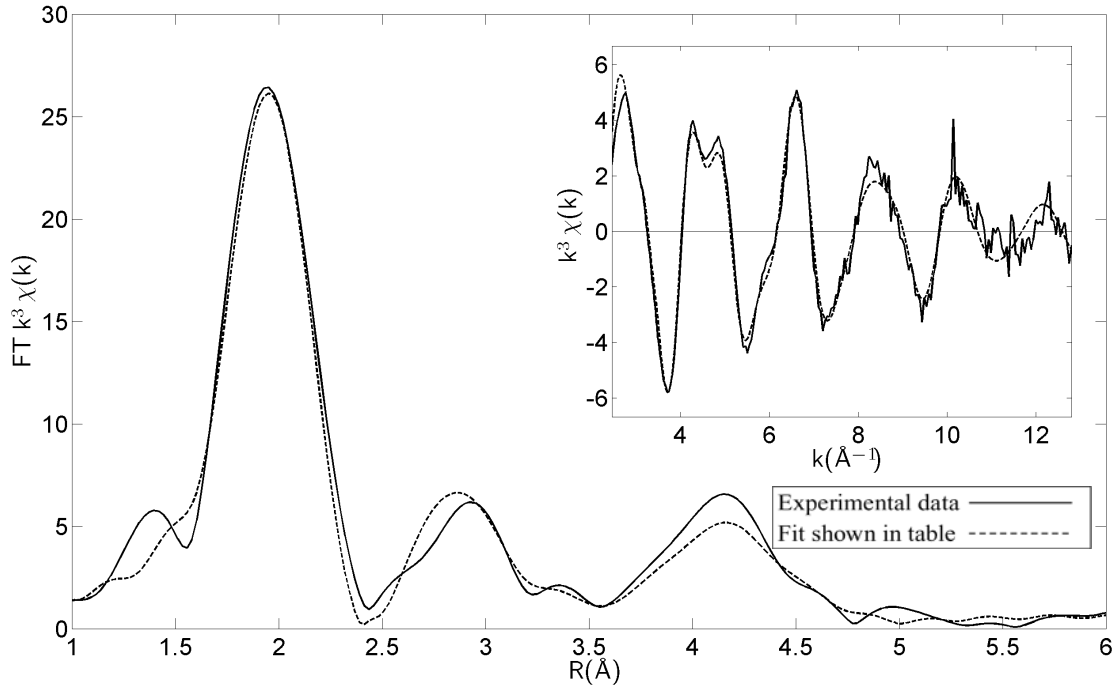

Scatterer	Distance (Å)	Debye-Waller (Å²)	-E_0 (eV)	F
4.0 N	1.99	0.011	4.90	0.274
4.0 C	2.93	0.018		
4.0 C	3.00	0.018		
4.0 N	4.21	0.033		
4.0 C	4.14	0.033		

Figure 3.16. Cu K-edge EXAFS of reconstituted SOD1.

3.4.2 CCS245Sec

In order to examine how the D3 site is affected by the transfer of Cu to SOD1, we examined the Cu and Se-EXAFS of a mixture of CCS245Sec and apo-SOD1. In order to see the histidine contribution to the spectrum by reconstituted SOD1, we added 5:1 SOD1:CCS. Although there was an excess of SOD1, copper was not completely removed from the Cu-Se cluster. Cu EXAFS revealed a mixture of Cu-histidine, Cu-S, Cu-Cu, and Cu-Se (Figure 3.17). The best fit, F = 0.297, showed 1.0 histidine scatterer with $R(2\sigma^2)_{Cu-N}$ = 1.93 Å (0.005 Å^2), 1.0 S with $R(2\sigma^2)_{Cu-S}$ = 2.19 Å (0.003 Å^2), 1.3 Cu with $R(2\sigma^2)_{Cu-Cu}$ = 2.69 Å (0.012 Å^2), and 0.8 Se with $R(2\sigma^2)_{Cu-Se}$ = 2.42 Å (0.007 Å^2). With the Se-labeled

proteins, separation of SOD1 from the CCS245Sec and SOD1 mixture were unsuccessful, with concentrations of CCS245Sec still present (data not shown). It is unclear why separation of SOD1 from the hCCS-SOD1 mixture was successful, whereas separation of SOD1 from the CCS245Sec-SOD1 mixture was not. Perhaps the Se-containing copper cluster binds more tightly to SOD1.

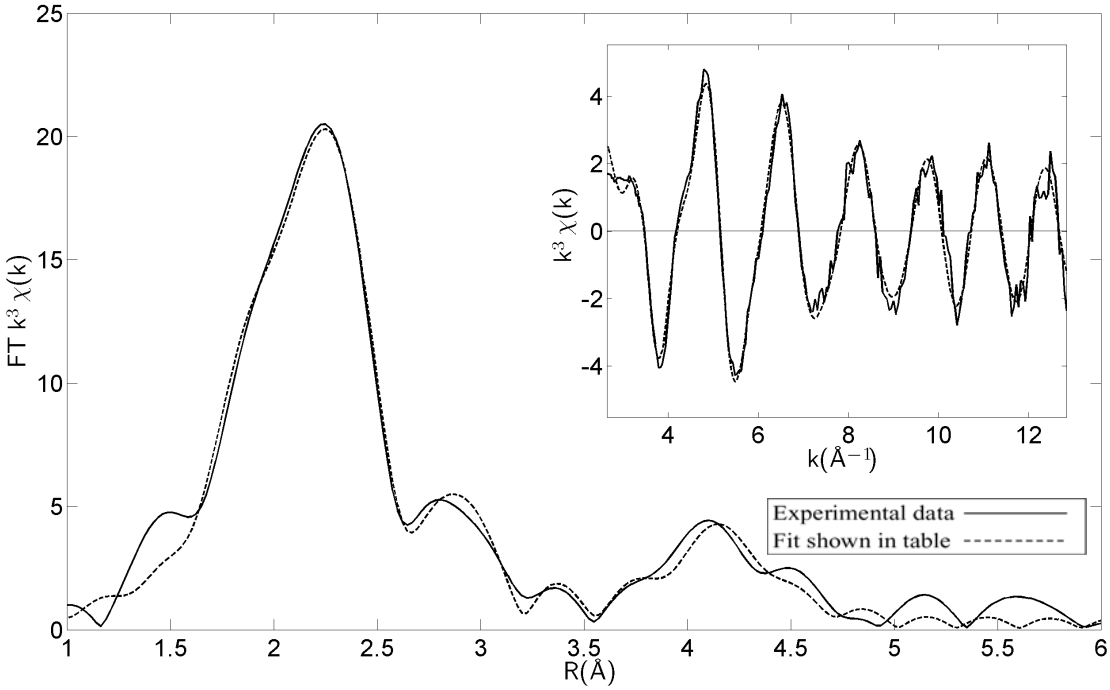

Scatterer	Distance (Å)	Debye-Waller (Å²)	-E_0 (eV)	F
1.0 N	1.93	0.005	0.72	0.297
1.0 C	2.87	0.010		
1.0 C	2.98	0.010		
1.0 N	4.16	0.015		
1.0 C	4.19	0.015		
1.0 S	2.19	0.003		
1.3 Cu	2.69	0.012		
0.8 Se	2.42	0.007		

Figure 3.17. Cu K-edge EXAFS of a mixture of CCS245Sec and E,Zn-SOD1.

Se EXAFS of the CCS245Sec and SOD1 mixture looked similar to that of CCS245Sec alone, indicating that the environment of Se in the cluster did not change upon transfer of copper to E, Zn-SOD1 (Figure 3.18). This could be due to the presence of more than one copper in the D3-D3 copper cluster and the presence of a Se-Cu cluster with a lower nuclearity after transfer. Another possibility is that, in the presence of SOD1, a complex

is formed between CCS245Sec and SOD1 in which the copper cluster is maintained as the copper is transferred to the histidine site of SOD1.

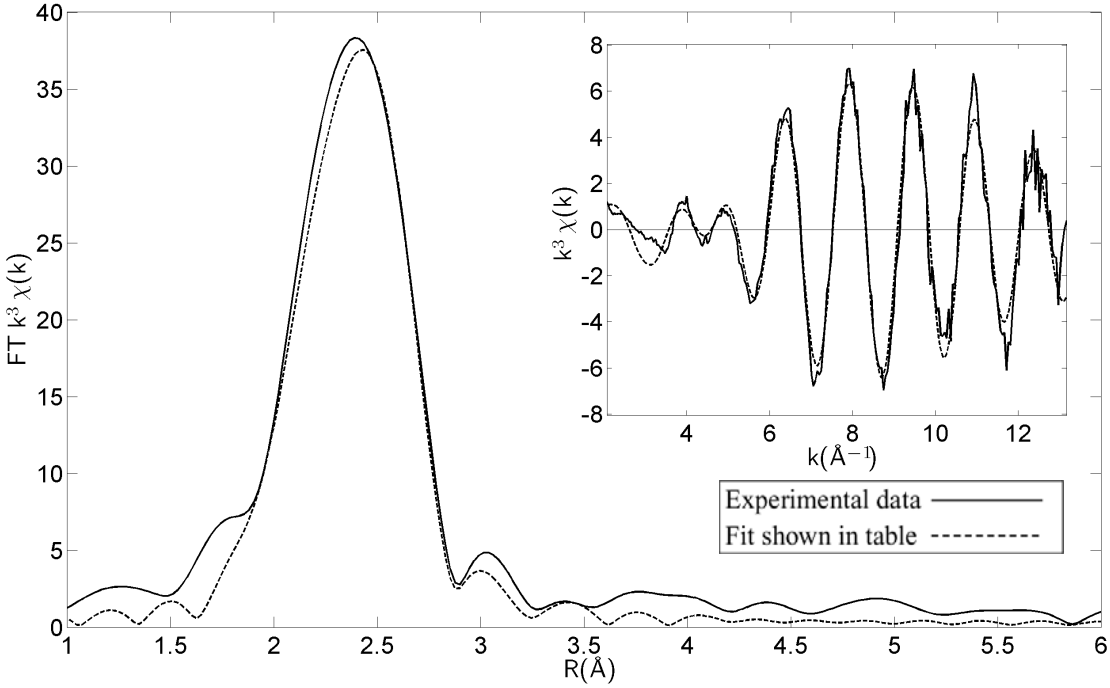

Scatterer	Distance (Å)	Debye-Waller (Å²)	-E_0 (eV)	F
1.0 C	2.01	0.006	4.08	0.484
2.0 Cu	2.38	0.007		

Figure 3.18. Se K-edge EXAFS of a mixture of CCS245Sec and SOD1.

3.5 Conclusions

This chapter reports the semisynthesis of a selenocysteine derivative of the human copper chaperone for superoxide dismutase, substituted with Sec at the C-terminal Cys246 residue. Measurements of CCS246-induced SOD1 activation have shown that the CXC D3 sequence is both necessary and sufficient for E,Zn-SOD maturation, such that the formation of the Sec derivative could be achieved by protein ligation of a single selenocysteine amino acid to a CCS245 truncation. This reaction proceeded in high yield, and generated the desired CCS245X (X=Cys, Sec) protein of the expected mass, using both Cys and Sec.

Apo-CCS245Sec was found to be present in forms containing both Se-S and Se-Se cross links. The Se-S selenylsulfido form could represent either intramolecular crosslinking between Cys244 and Sec246 or intermolecular dimerization. The Se-Se interaction identified in the Se EXAFS of the apo-CCS245Sec can only arise from an intermolecular diselenide formed via dimerization of the D3 polypeptide. This feature of CCS245Sec mimics the D3-D3 dimer formation induced by Cu(I) cluster formation, and thus suggests that D3 dimerization involves favorable protein-protein interactions. Also, comparisons of the redox potential of disulfides, selenylsulfides and diselenides clearly show a decrease in potential throughout the series, providing an alternative driving-force for the D3-D3 diselenide crosslink.

CCS245Sec binds up to 3.2 mole equivalents of Cu(I), as determined by copper titration studies. The consistent increase in Cu:CCS monomer ratios above 2.0, suggests that the D3-D3 cluster has a nuclearity greater than 2. Cu and Se K-edge EXAFS have been analyzed to provide metrical details of the coordination environments of the Cu and Se atoms. Since Cu-Se and Se-Cu interactions (determined from the Cu- and Se-datasets to have identical coordination numbers) must necessarily have bond-lengths and DW factors, these constraints should produce a more accurate picture of the multinuclear Cu(I) cluster, and the positions of the Se atoms (and hence, residue 246) within the cluster. The Se-Cu interaction extracted form the Se K-edge data shows 2 Se-Cu interactions at 2.41 Å. Fits using lower Se-Cu coordination numbers produce higher least squares residuals, and more importantly, lead to parameters which lead to unacceptable fits to the Cu-edge data. This allows us to conclude with some degree of certainty that each Se sees 2 Cu atoms in its first shell, and therefore must occupy a bridging position in the cluster. Possible cluster structures for the D3-D3 interaction with residue 246 occupying a bridging position in the cluster are shown in Figure 3.19. These include a bis-cysteine bridged dinuclear cluster, a trinuclear cluster based on a Cu_3S_3 hexagonal ring with one additional bridging cysteine, and a Cu_4S_6 tetranuclear cluster composed of three fused Cu_3S_3 hexagonal rings. A dinuclear cluster with two bridging Se atoms would require each Cu to be coordinated to 2 Se and 1 S. Attempts to fit the Cu K-edge data to this model, using the Cu-Se distances and DW factors extracted from the Se edge were

routinely unsuccessful, leading to inconsistent analyses at the Cu and Se K-edge respectively. However, when higher cluster nuclearity was introduced, the Cu and Se K-edge data could be simulated with parameters which were consistent at both edges. The presence of Cu(I) bound in D1 still contributes to the Cu K-edge data, introducing some ambiguity into the fitting results. Use of D1 C22,25A mutants at the CXXC Cu(I) binding site will help resolve the remaining ambiguity concerning the Cu-edge data.

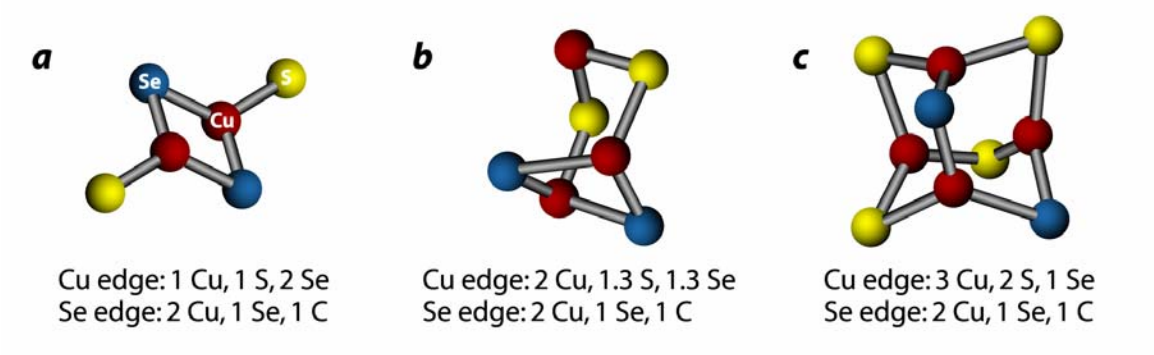

Figure 3.19. Possible structures for the D3-D3 Cu cluster and edge environments if Se were present in the cluster. (a) bis-cysteine bridged dinuclear cluster (b) trinuclear cluster based on a Cu_3S_3 hexagonal ring with one additional bridging cysteine (c) Cu_4S_6 tetranuclear cluster composed of three fused Cu_3S_3 hexagonal rings

Copper was shown to be successfully transferred to E, Zn-SOD1 from hCCS and CCS245Sec using Cu and Se K-edge EXAFS. Transfer from wild-type hCCS appeared to cause the D3 copper cluster to disappear, whereas a cluster was still present in CCS245Sec. Furthermore, SOD1 could not be completely purified from the CCS245Sec/SOD1 mixture. This may indicate a stronger CCS245Sec/SOD1 complex compared to that of hCCS/SOD, resulting in a more complex EXAFS spectra at the Cu K-edge and the appearance of an intact Cu cluster at the Se edge.

CHAPTER 4: STUDIES ON THE C22,25A245CYS AND C22,25A245SEC PROTEINS

4.1 Initial characterization of C22,25A-245Cys and C22,25A-245Sec

In the last chapter, the characterization of CCS245Sec revealed that Se in residue 246 occupies a bridging position in the D3-D3 copper cluster. This was made clear from the Se K-edge EXAFS data. However, the presence of Cu(I) bound in D1 still contributed to the Cu K-edge data, introducing some ambiguity into the fitting results at the Cu K-edge. This chapter describes the use of D1 C22,25A mutants at the CXXC Cu(I) binding site to help resolve the remaining ambiguity concerning the Cu-edge data. The C22,25A-245Sec protein binds copper and provides further proof for the existence of a Cu_4S_6 adamantane-type species at the D3-D3 dimer interface of hCCS.

4.1.1 Semisynthesis of C22,25A245Cys and C22,25A245Sec

As we learned with the study of CCS245Sec, the CXC motif was both necessary and sufficient for SOD maturation. The C22,25A-245 truncation mutant, where the Ser245 was again mutated to an Ala for more efficient ligation, was created by PCR amplification of C22,25A hCCS. The 245 truncation polypeptide was then expressed in *E. coli* ER2566 and purified on a chitin column with intein cleavage by MESNA. Single

amino acid ligation of selenocysteine or cysteine (as a control) to the truncated protein was performed anaerobically. Seleno-DL-cystine was first reduced with TCEP and then added 1:10 (protein:Sec) to the truncated protein. After 96 hours of anaerobic incubation, free selenocysteine and TCEP were removed by dialysis. Successful ligation was confirmed by ICP analysis of zinc and selenium concentrations and by mass spectrometry analysis. Cys ligation was performed in a similar fashion.

4.1.2 Copper reconstitution

As with CCS245Sec, to circumvent the tendency towards oxidation, it was necessary to reduce the diselenide with TCEP followed by rapid addition of the Cu(I) under anaerobic conditions. This was most conveniently achieved by use of an immobilized TCEP reducing gel. Protein was added to the TCEP-bound agarose in a column and left to reduce for one hour. After elution with two volumes of buffer, two mole-equivalents of $[Cu(I)(CH_3CN]_4^+$ in acetonitrile were immediately added to the protein. Reconstituted proteins were then dialyzed against decreasing amounts of acetonitrile in 50mM phosphate buffer in order to remove free copper and acetonitrile. Metal analysis by ICPOES showed that the concentrations of Cu, Zn and Se in the selenocysteine-substituted C22,25A245Sec were 1000, 550 and 555 μM respectively. Thus, the C22,25A245Sec protein bound approximately one Se per Zn, indicating efficient Sec ligation and 1.8 Cu per Zn and Se.

4.1.3 Ligation Efficiency

Mass spectral data give an independent estimate of the efficiency of the ligation process (Figure 4.1). The mass for the Cys-ligated protein (*m/z* = 25793) is 20 units higher than that expected for a Met1 cleavage of the C22,25A245Cys protein with two disulfides (*m/z* = 25773) and does not correspond to C22,25A245 unligated protein with or without Met1 cleavage (*m/z* = 25674 and 25805 respectively). Interestingly, there is also a peak at *m/z* = 25655, which is around 20 units higher than that expected for unligated protein. It is unclear why this discrepancy exists. The mass for the Sec-ligated (*m/z* = 25817) protein is closest to the mass corresponding to the Sec-substituted protein with Met1 cleaved and two disulfides (*m/z* = 25820). Like the CCS245Sec protein, this suggests that at least one additional S-S, Se-S exists in the Sec protein and is consistent with formation of a

Se-S bond between C244 and C246 of the D3 CXC motif. Although there is a peak at *m/z* = 25647, this mass does not correspond to unligated protein with Met1 cleaved (*m/z* = 25674). The identity of this peak is unclear.

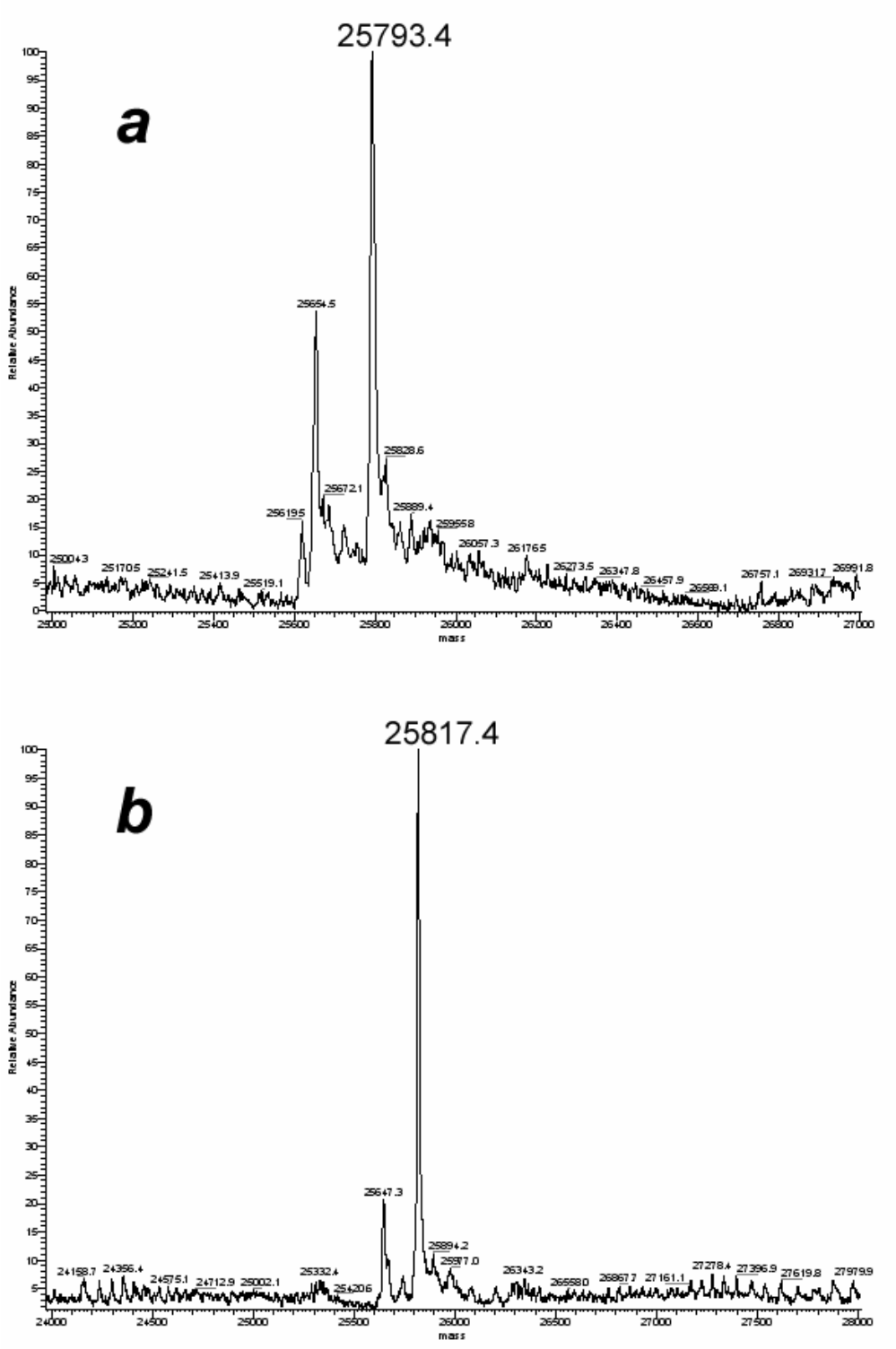

Figure 4.1. Mass spectral data of the (a) C22,25A245Cys ligated protein and (b) C22,25A245Sec ligated protein.

4.1.4 SOD-activation activity of semisynthetic C22,25A245Cys and C22,25A245Sec

Both ligation constructs were assayed for activity by measuring their ability to transfer copper within a 30 minute period to E-ZnSOD1 at a ratio of 1:1 hCCS:SOD1 (Table 4-1). Both Cys and Sec-ligated proteins had the same transfer activity within experimental error, but appeared to have slightly lower activity than the plasmid-expressed wild-type hCCS truncated at CCS246. The cysteine-ligated hCCS retained 84% of its activity compared to CCS246, whereas the selenocysteine-ligated protein retained 89% compared to CCS246. As with CCS245Sec, the slightly decreased activity of the ligation mutants could be due to slower transfer kinetics. The substitution of Se for S appears to have no affect on the SOD maturation activity.

Sample	Activity (units)
Cu,Zn-SOD1	2000
hCCS	1500
CCS246	1282
C22-25A245Cys	1075 ± 110
C22-25A245Sec	1136 ± 142

Table 4-1. SOD1-activation activity assays for C22,25A245Cys and C22,25A245Sec in comparison with CCS246, hCCS, and reconstituted SOD1.

When the ratio of CCS:SOD1 is increased in the C22,25A245Cys and C22,25A245Sec SOD1-activation assays, slightly increased transfer activity is seen (Figure 4.2), but not within significant error.

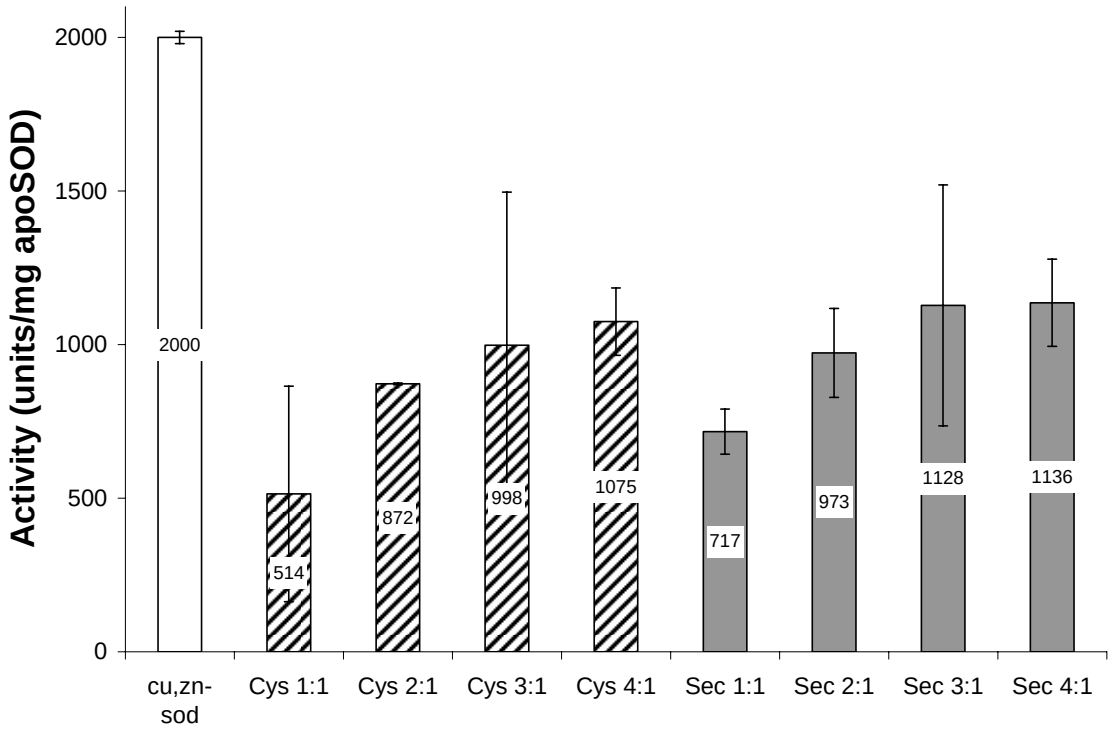

Figure 4.2. SOD1-activation assays of C22,25A245Cus and C22,25A245Sec with varying ratios of CCS:SOD1. Error bars at 95% confidence intervals (equivalent to 3 standard deviations of the sample data).

4.2 Cu-EXAFS on C22,25A245Cys and C22,25A245Sec

4.2.1 C22,25A245Cys

Cu K-edge EXAFS of the Cys- ligated C22,25A hCCS are shown in Figure 4.3. As expected, the spectrum of the C22,25A245Cys protein is very similar to the previously reported XAS of the wild-type C22,25A protein (Stasser et al., 2007). Two shells of scatterers are observed at ~2.2 and 2.7 Å, corresponding to Cu-S and Cu-Cu respectively. Curve fitting analysis leads to a best fit with 3 Cu-S interactions (R, $2\sigma^2$) at 2.27 Å (0.010 $Å^2$) and 2 Cu-Cu at 2.72 Å (0.011 $Å^2$).

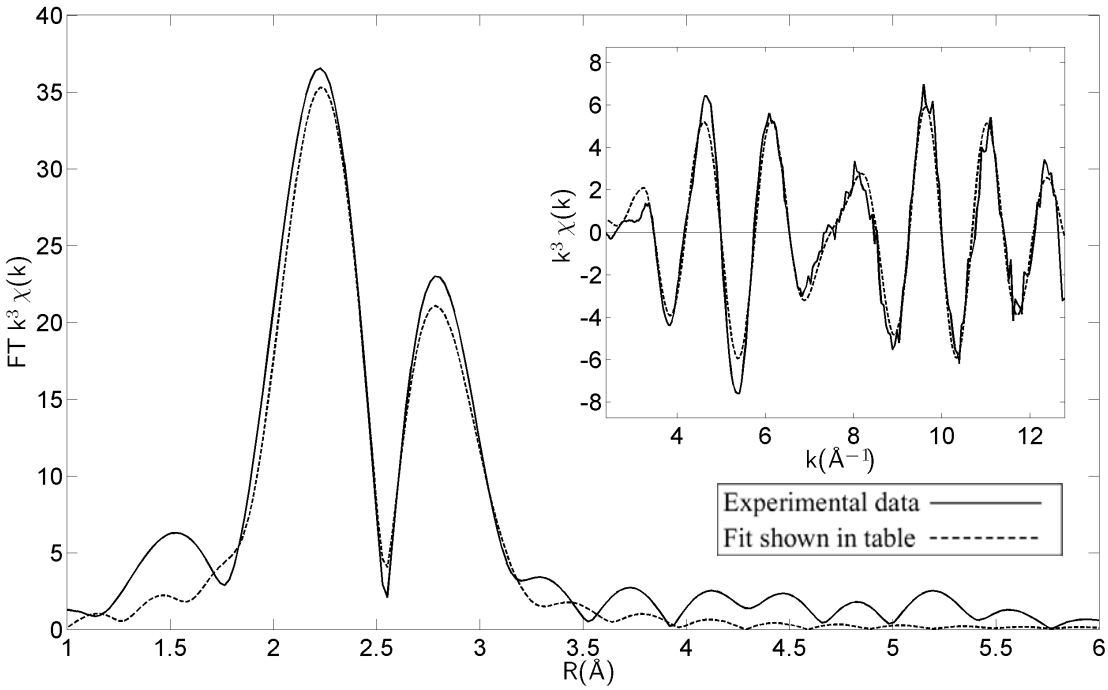

Scatterer	Distance (Å)	Debye-Waller (Å²)	-E_0 (eV)	F
3.0 S	2.27	0.010	6.03	0.411
2.0 Cu	2.72	0.011		

Figure 4.3. Cu K-edge EXAFS of C22,25A245Cys.

4.2.2 C22,25A245Sec

In the study of the CCS245Sec protein, the analysis of the Cu EXAFS was more complex, as it represents the average of the Cu binding to the D1 mononuclear and the D3 multinuclear site. With the C22,25A protein, a complete analysis of the D3 multinuclear site can be assessed from analysis of the Cu K-edge EXAFS in combination with the Se K-edge EXAFS data. At the Cu K-edge, the best fit (using Cu-Se = 2.38 ± 0.2 Å, and $2\sigma^2$(Cu-Cu) = 0.011 Å^2) gave 2.3 Cu-S at 2.24 Å (0.009 Å^2), 0.7 Cu-Se at 2.40 Å (0.006 Å^2), and 2.1 Cu-Cu at 2.70 (0.011 Å^2) (Figure 4.4). These parameters lead to consistency of metrical parameters at both Cu and Se absorption edges.

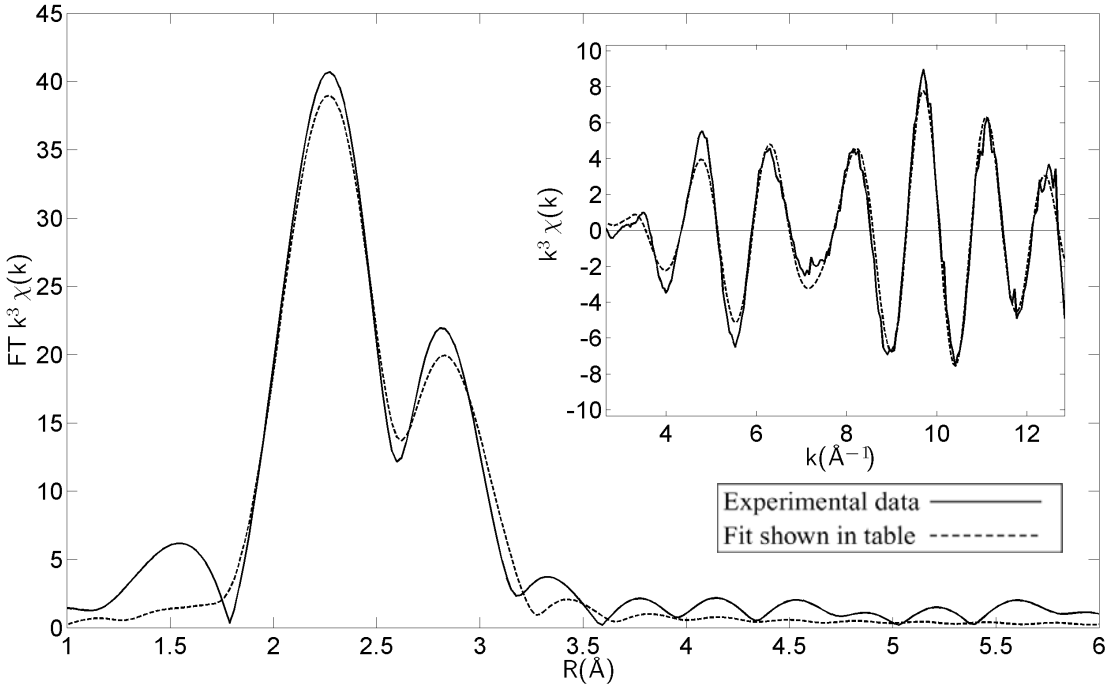

Scatterer	Distance (Å)	Debye-Waller (Å²)	-E_0 (eV)	F
2.3 S	2.24	0.009	3.89	0.369
2.1 Cu	2.70	0.011		
0.7 Se	2.40	0.006		

Figure 4.4. Cu K-edge EXAFS of C22,25A245Sec.

4.2.3 C22,25A245Sec copper titration

Due to the ability of the C22,25A245Sec mutant to bind more than 1 copper per protein, we decided to investigate the structure of the copper cluster using Cu-EXAFS when increasing equivalents of copper to protein are added. Although up to four coppers per protein were added to C22,25A245Sec, no more than 1.8 coppers were bound to the protein. When comparing the experimental data for each stoichiometric addition of copper, 2:1 and 3:1 Cu:protein additions appeared identical (Figure 4.5). Both of these additions had a final concentration of 1.8 Cu:protein, so this is not surprising. However, the 1:1 Cu:protein addition had a very different spectra, with a greater Cu and S contribution. It is unclear why this would be so, given that this protein only bound 1:1 Cu:protein.

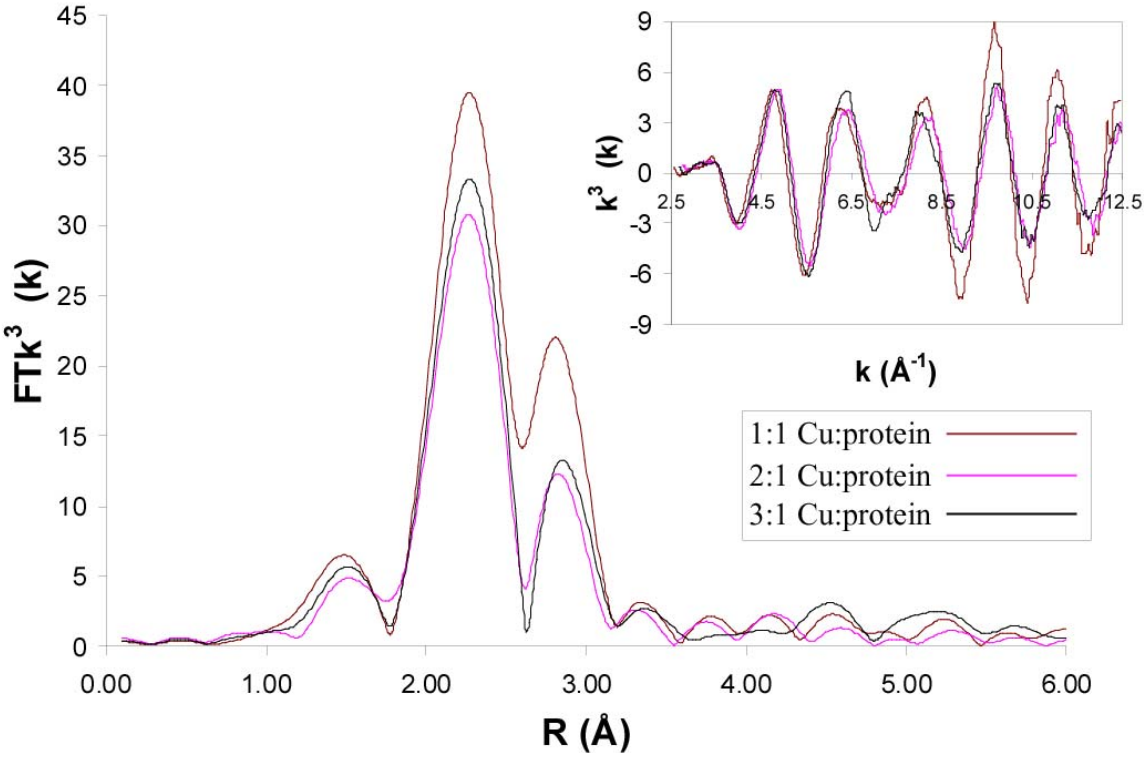

Figure 4.5. Cu K-edge EXAFS experimental data for C22,25A245Sec with different ratios of Cu:protein added.

4.3 Se-EXAFS on C22,25A245Cys and C22,25A245Sec

4.3.1 Apo C22,25A245Sec

As with CCS245Sec, with selenocysteine covalently attached to C22,25A245 as the C-terminal residue, it was possible to probe the speciation of the Se by Se K-edge EXAFS. The best fit was found to be a mixture of both Se-S (0.3) and Se-Se (0.7) with an F value of 0.328 (Figure 4.6). This shows that as isolated, the ligated protein appears to be oxidized, and exists as an equilibrium mixture of monomers with Se-S distances of 2.23 Å, and dimers with Se-Se distances of 2.32 Å. These results emphasized the need for reduction of the ligated proteins on the immobilized TCEP column prior to reconstitution

with Cu(I).

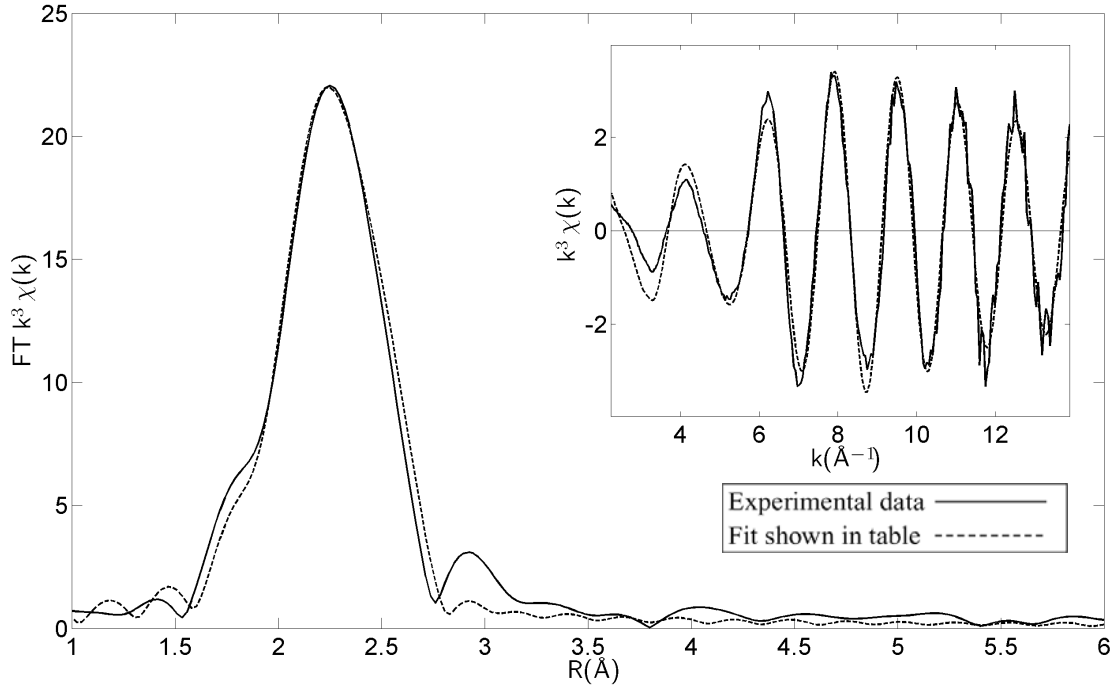

Scatterer	Distance (Å)	Debye-Waller (Å²)	-E_0 (eV)	F
1.0 C	2.00	0.006	7.32	0.328
0.7 Se	2.32	0.006		
0.3 S	2.23	0.006		

Figure 4.6. Se K-edge EXAFS of apo-C22,25A245Sec.

4.3.2 C22,25A245Sec

It was expected that the Se K-edge EXAFS of the C22,25A245Sec protein would be similar to that of the CCS245Sec protein, containing contributions from 1 Se-C and a number of Se-Cu interactions, depending on the cluster structural composition. Simulations were attempted with 1 Se-C and a varying number of Se-Cu interactions. A single Se-Cu gave a F value of 0.652 with Se-C and Se-Cu [R, ($2\sigma^2$)] of 2.01 Å (0.002 Å^2) and 2.38 Å (0.001 Å^2) respectively. In this fit, the EXAFS amplitude was not adequately fit even with the extremely low Se-Cu DW factor. A much improved fit, F= 0.275, was obtained with 1 Se-C and 2 Se-Cu with $R(2\sigma^2)_{Se\text{-}C}$ = 1.99 Å (0.005 Å^2) and $R(2\sigma^2)_{Se\text{-}Cu}$ = 2.38 Å (0.007 Å^2) (Figure 4.7). When the Se-Cu occupation number and DW were allowed to float freely the Se-Cu coordination number refined to 2.1 with

$2\sigma^2$=0.007 Å^2. These simulations lead to the conclusion that each Se is bound by 2 Cu atoms at 2.38 Å in the D3 cluster. The C22,25A245Sec protein Se K-edge EXAFS looks almost identical to that for the CCS245Sec protein.

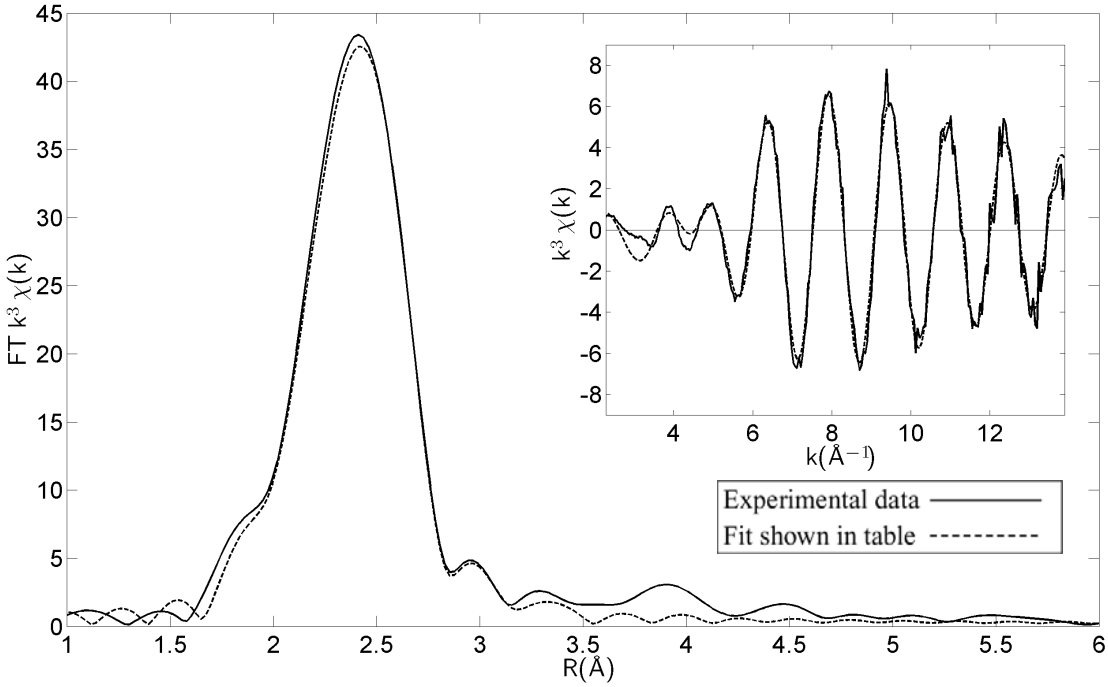

Scatterer	Distance (Å)	Debye-Waller (Å^2)	-E_0 (eV)	F
1.0 C	1.99	0.005	5.04	0.275
2.1 Cu	2.38	0.007		

Figure 4.7. Se K-edge EXAFS of C22,25A245Sec.

4.3.3 C22,25A245Sec copper titration

As seen in the Cu K-edge EXAFS, when copper was added stoichiometrically to C22,25245Sec, only a maximum of 1.8 Cu:protein were able to be bound by the protein. The 1:1 Cu:protein preparation appeared to have a greater contribution of Cu and S at the Cu edge. However, when comparing the Se K-edge EXAFS experimental data of the different Cu:protein preparations (Figure 4.8), the 1:1 Cu:protein addition has a lower copper contribution at the Se edge, whereas the 2:1 and 3:1 (both equivalent to 1.8:1 Cu:protein final concentration) have the expected 2 coppers seen at the Se edge when fit. This indicates a more complex Cu-Se cluster forming with greater additions of copper,

whereas with lower copper there is a greater Cu-S environment formed. Like the CCS245Sec copper titrations, the K-edge feature at ~4.5 $Å^{-1}$ appears to change between the lower Cu:protein and higher Cu:protein spectra. This could be due to increasing copper in the cluster or to Se-S interactions across the cluster.

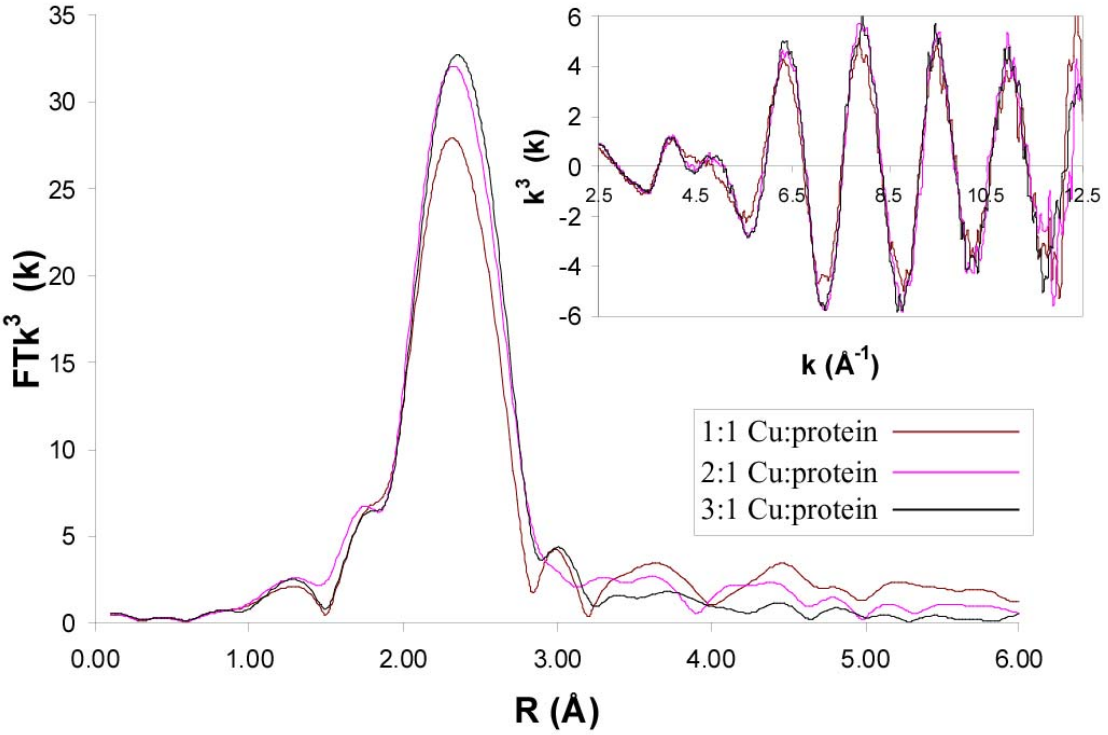

Figure 4.8. Se K-edge EXAFS experimental data of C22,25A245Sec with different ratios of Cu:protein added.

4.4 EXAFS of C22,25A245Sec in complex with SOD1

4.4.1 C22,25A245Sec with apo-SOD1 Cu EXAFS

Although transfer of copper was observed from CCS245Sec to SOD1, the presence of the D1 copper center makes analysis of the Cu-EXAFS more complex. By analyzing transfer from C22,25A245Sec to E,Zn-SOD1, the advantage of having only one copper center will be gained. Copper transfer from this protein can only occur from the D3 copper cluster where the spectroscopic probe, Se, is present. The procedure was identical to that

of the CCS245Sec transfer (Section 3.4.2). A mixture of fully metallated C22,25A245Sec and E,Zn-SOD1 was incubated at 37°C for 30 minutes, and both Cu- and Se-EXAFS were analyzed.

When C22,25A245Sec is mixed with apo-SOD1 in a ratio of 1:5, the contribution of a histidine shell at the Cu K-edge can be seen (Figure 4.9). Also, because the Cu-S and Cu-Se contribution is still observed, it can be assumed not all copper is transferred to apo-SOD1 from C22,25A245Sec. The best fit (using Cu-Se = 2.38 ± 0.3 Å, and $2\sigma^2$(Cu-Cu) = 0.011 Å^2) gave 1.0 Cu-His 1.92 Å (0.011 Å^2), 1.2 Cu-S at 2.19 Å (0.006 Å^2), 1.0 Cu-Se at 2.41 Å (0.006 Å^2), and 1.8 Cu-Cu at 2.68 (0.011 Å^2). As with CCS245Sec, complete transfer of copper from the D3-D3 cluster could not be achieved.

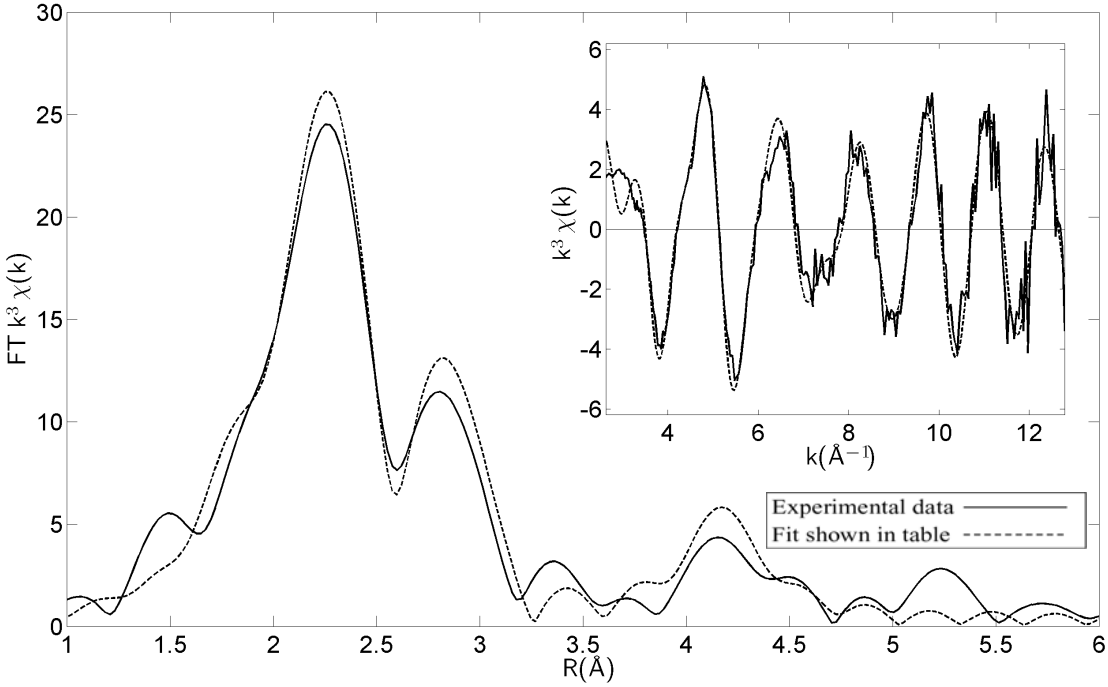

Scatterer	Distance (Å)	Debye-Waller (Å²)	-E_0 (eV)	F
1.0 N	1.92	0.011	0.009	0.503
1.0 C	2.91	0.010		
1.0 C	3.20	0.010		
1.0 N	4.17	0.019		
1.0 C	4.20	0.019		
1.2 S	2.19	0.006		
1.9 Cu	2.68	0.012		
1.0 Se	2.41	0.006		

Figure 4.9. Cu K-edge EXAFS of a mixture of C22,25A245Sec and E,Zn-SOD1.

4.4.2 C22,25A245Sec with apo-SOD1 Se EXAFS

Although copper is still present in C22,25A245Sec when it is mixed with apo-SOD1, there is much less copper in the D3 cluster when looking at Se K-edge EXAFS (Figure 4.10). The best fit gave 1.0 Se-C 1.987 Å (0.006 Å^2), 0.7 Se-Cu at 2.410 Å (0.006 Å^2), 0.5 Se-Se at 2.294 Å (0.006 Å^2), and 0.3 Se-S at 2.186 (0.006 Å^2). Se-Se and Se-S ratios are similar to that seen in apo-C22,25A245Sec (Figure 4.6). This fit appears to indicate that a diselenide forms when copper leaves the D3 cluster upon transfer to apo-SOD1. This diselenide must form between two molecules of C22,25A245Sec. Therefore, these data support a mixture of Cu-loaded and apo-C22,25A245Sec. If we consider that the ratio of Se-Cu before transfer is ~2, and after transfer 0.7, about 65% of the copper may have transferred to E,Zn-SOD1. Thus, the Cu-histidine coordination number should be ~2 (considering a three-coordinate SOD1 environment). It is unclear why only 1 Cu-histidine is observed at the Cu K-edge (Figure 4.9). Two Cu-histidine can be fit with an F value of 0.522 to the Cu EXAFS data, but only with a high DW (0.029 Å^2).

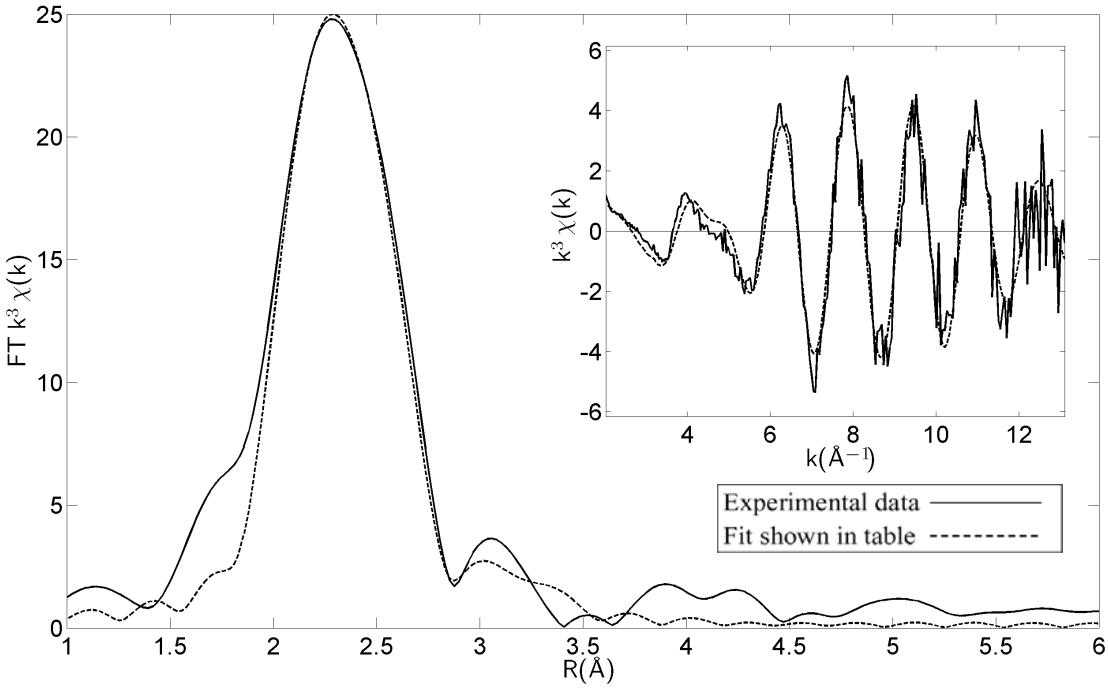

Scatterer	Distance (Å)	Debye-Waller (Å²)	-E_0 (eV)	F
1.0 C	1.99	0.006	4.27	0.873
0.3 S	2.19	0.006		
0.5 Se	2.29	0.006		
0.7 Cu	2.41	0.006		

Figure 4.10. Se K-edge EXAFS of a mixture of C22,25A245Sec and SOD1.

4.5 Conclusions

This chapter reports the semisynthesis of a selenocysteine derivative of the D1 double mutant C22,25A human copper chaperone for superoxide dismutase, substituted with Sec at the C-terminal Cys246 residue. The intein-mediated amino acid ligation resulted in high yield and generated the desired C22,25A245Sec protein of the expected mass. Measurements of C22,25A245Sec-induced SOD1 activation have shown that the CXU D3 sequence is both necessary and sufficient for E,Zn-SOD maturation.

Apo-C22,25A245Sec was found to be present in forms containing both Se-S and Se-Se cross links as in the CCS245Sec protein. The Se-S selenylsulfido form could represent either intramolecular crosslinking between C244 and U246 or intermolecular

dimerization. The Se-Se interaction identified in the Se K-edge EXAFS of the apo-CCS245Sec can only arise from an intermolecular diselenide formed via dimerization of the D3 polypeptide.

C22,25A245Sec binds up to 1.8 mole equivalents of Cu(I), as seen with the copper titration studies. The consistent increase in Cu:CCS monomer ratios above 1.0 suggests that the D3-D3 cluster has a nuclearity greater than 2. Cu and Se K-edge EXAFS have been analyzed to provide metrical details of the coordination environments of the Cu and Se atoms. Due to the necessity of Cu-Se and Se-Cu interactions determined from the Cu- and Se-datasets to have identical coordination numbers, bond-lengths and DW factors, these constraints should produce a more accurate picture of the multinuclear Cu(I) cluster, and the positions of the Se atoms (and hence, residue 246) within the cluster. The Se-Cu interaction extracted form the Se K-edge data shows 2.1 Se-Cu interactions at 2.38 Å, almost identical to the results found for the CCS245Sec protein (2 Se-Cu interactions at 2.41 Å). Therefore, each Se sees ~2 Cu atoms in its first shell, and therefore must occupy a bridging position in the cluster, confirming the results found in the study of the CCS245Sec protein. Previous work on the full-length C22,25A hCCS protein proposed that the D3-D3 cluster formed a Cu_4S_6 adamantane type structure, composed of three Cu_3S_3 hexagonal rings fused together (Stasser et al., 2007). In this structure, the Cu(I) centers are 3-coordinate and have three neighboring Cu(I) centers with a Cu-Cu separation of ~2.7 Å, with each Cu(I) ion bridged to its neighbor by a thiolate S. The C22,25A245Sec Cu K-edge EXAFS show only two neighboring Cu(I) centers at the Cu edge, with each copper seeing 2.1 Cu at 2.70 Å. This seems more consistent with the Cu_3S_4 trinuclear cluster. Furthermore, each copper sees a greater contribution from S than from Se. Due to the mutation of the D1 Cys residues, one would suspect an equal contribution of S and Se from the remaining D3 CXU present in the cluster formation. With this information, the formation of a dinuclear cluster in these constructs can be ruled out, favoring the trinuclear or tetranuclear structures as possible candidates (Figure 3.19). It would be beneficial to mutate the second Cys residue in the D3 copper-binding motif to a Sec in order to fully tease out the D3-D3 copper cluster. Also, a D3 UXU mutation would potentially eliminate any S contribution in the cluster if only the residues

from D3 are involved in the cluster.

Copper was shown to be successfully transferred to E, Zn-SOD1 from C22,25A245Sec based on the presence of a Cu-histidine contribution in the Cu and Se K-edge EXAFS analysis of the C22,25A245Sec/E,Zn-SOD1 mixture. Like CCS245Sec, complete transfer of copper from the semisynthetic protein to the E,Zn-SOD1 could not be achieved.

CHAPTER 5: STUDIES ON CCS243CACDGA, CCS243CAUDGA, CCS243CACA, CCS243CAUA, CCS243UACA, AND CCS243UAUA PROTEINS

5.1 Initial characterization of CCS243-CACDGA, CCS243-CAUDGA, CCS243-CACA, CCS243-CAUA, CCS243-UACA, and CCS243-UAUA

In the last two chapters, the characterization of CCS245Sec C22,25A245-Sec revealed that the D3-D3 copper cluster is a multinuclear cluster with greater than two coppers present containing both S and Se with the Se at residue 246 occupying a bridging position. This was made clear from the Se K-edge EXAFS data of CCS245Sec and the Cu K-edge data of C22,25A245Sec. However, the complete geometry of the cluster including the position of residue 244 remains unclear. This chapter describes the ligation of longer peptides to wild-type and D1 C22,25A mutants of a CCS243 truncation resulting in products where residues 244 and 246 of the D3 CXC motif have each been replaced with selenocysteine to help resolve the remaining ambiguity concerning the D3-D3 copper cluster structure. All of the peptide ligation constructs bind copper, are active, and provide further proof for the existence of a Cu_4S_6 adamantane-type species at the D3-D3 dimer interface of hCCS.

5.1.1 Semisynthesis

A C22,25A243 and a CCS243 ^{243}Ala truncation mutant, where the Ile243 was mutated to an Ala for more efficient ligation, was created by PCR amplification of full-length hCCS and C22,25A hCCS DNA. The 243 truncation polypeptide was then expressed in *E. coli* ER2566 and purified on a chitin column with intein cleavage by MESNA. Six synthetic peptides were prepared for ligation: -CACDGA, -CAUDGA, -CACA, -CAUA, -UACA, and –UAUA. Peptides were synthesized by Kevin Smith at the University of Illinois as part of a collaboration with Dr. Wilfred Van der Donk. Peptide ligation was performed in the same manner as for a single amino acid ligation and performed anaerobically (Section 3.1.1). As with Seleno-DL-cystine, peptides were first reduced with TCEP and then added 1:10 (protein:peptide) to the truncated protein. After 4 nights of anaerobic incubation, free peptides and TCEP were removed by dialysis. Successful ligation was confirmed by ICP analysis of zinc and selenium concentrations and by mass spectrometry analysis. Efficient ligation of peptide –CAUDGA (as determined by mass spectral analysis, insufficient copper-binding, and no SOD1-activation activity) was never achieved, and this ligation was abandoned due to the success of the –CAUA peptide.

5.1.2 Copper reconstitution

As with the previous single Sec ligation products, to circumvent the tendency towards oxidation, in peptides containing the Sec residue, it was necessary to reduce the diselenide with TCEP followed by rapid addition of the Cu(I) under anaerobic conditions. Using an immobilized TCEP reducing gel, protein was added to the TCEP-bound agarose in a column and left to reduce for one hour. After elution with two volumes of buffer, three mole-equivalents of $[Cu(I)(CH_3CN]_4^+$ in acetonitrile were immediately added to the protein. Reconstituted proteins were then dialyzed against decreasing amounts of acetonitrile in 50mM phosphate buffer in order to remove free copper and acetonitrile. Results of metal analysis by ICP-OES are shown in Table 5-1. All of the peptide ligation product proteins bound copper as seen previously, with D1 mutants binding less than or equal to 2.1 Cu/protein, and CCS243 ligations binding 2-3 Cu/protein.

Protein	[Cu] (μM)	[Zn] (μM)	[Se] (μM)	[Cu]/ protein
CCS243CACDGA	1120	670	-	1.7
CCS243CACA	1400	650	-	2.2
C22,25A243CACDGA	600	515	-	1.2
C22,25A243CACA	500	320	-	1.6
CCS243CAUA	1050	500	505	2.1
CCS243UACA	680	280	290	2.4
CCS243UAUA	1300	500	990	2.6
C22,25A243CAUA	600	500	510	1.2
C22,25A243UACA	490	350	360	1.4
C22,25A243UAUA	1160	540	1240	2.1

Table 5-1. Metal ICPOES analysis results of peptide ligation products. Error for [Cu] and [Zn] were always within ± 10, whereas for [Se] it was within ± 50 with 3 replicates.

5.1.3 Ligation Efficiency

Mass spectral data give an independent estimate of the efficiency of the ligation process (Table 5-2). All masses are very close to those expected with cleavage of the Met1 residue and the presence of disulfides, as seen previously with the single amino acid ligations. Clear mass spectral analysis data was not obtained for the –CACDGA ligation products due to rapid protein degradation, but based on successful copper-binding and SOD1-activation activity, analysis of this protein was continued. The presence of more than two disulfides suggests that at least one additional S-S or Se-S exists in the protein. Although a few of the mass spectral analyses results show an additional lower peak (Figures 5.1-5.8), none of these correspond with unligated protein (C22,25A243 *m/z* = 25589; CCS243 *m/z* = 25653). The identity of this peak is unknown.

Protein	Expected *m/z*	Met1 cleaved, 2 S-S *m/z*	Observed *m/z*
CCS243CACA	26001	25866	25863
C22,25A243CACA	25937	25802	25800
CCS243CAUA	26048	25913	25912
CCS243UACA	26048	25913	25907
CCS243UAUA	26095	25960	25960
C22,25A243CAUA	25984	25849	25851
C22,25A243UACA	25984	25849	25844
C22,25A243UAUA	26031	25896	25897

Table 5-2. Mass spectral analysis data for the peptide ligation products, including expected *m/z*, expected *m/z* for the Met1 cleaved protein with 2 disulfides, and the observed *m/z*.

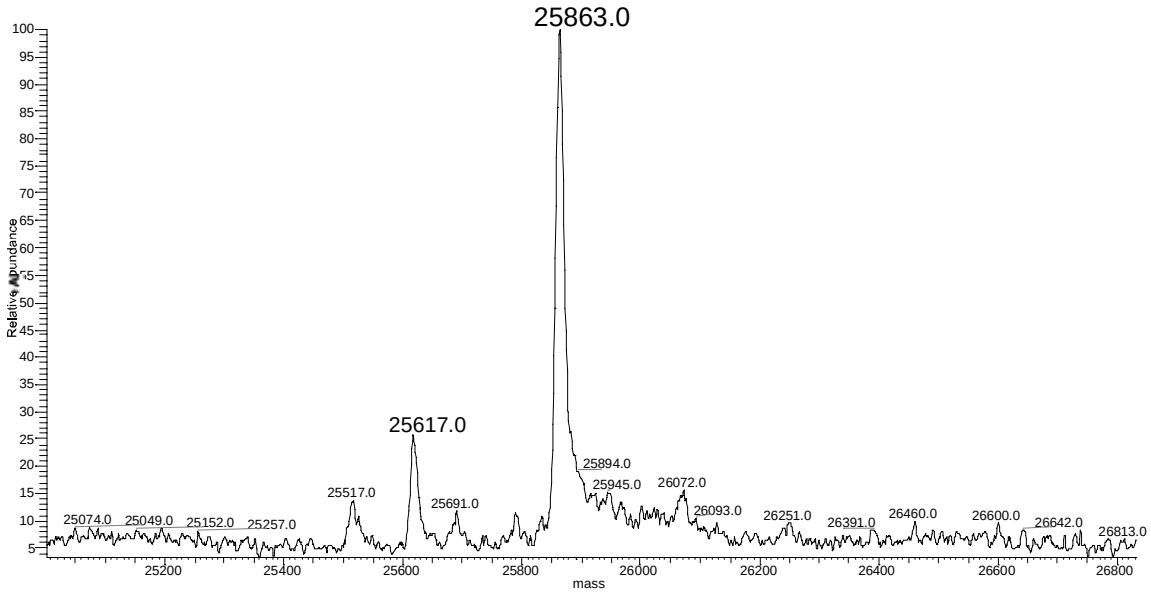

Figure 5.1. Mass spectral data for CCS243CACA.

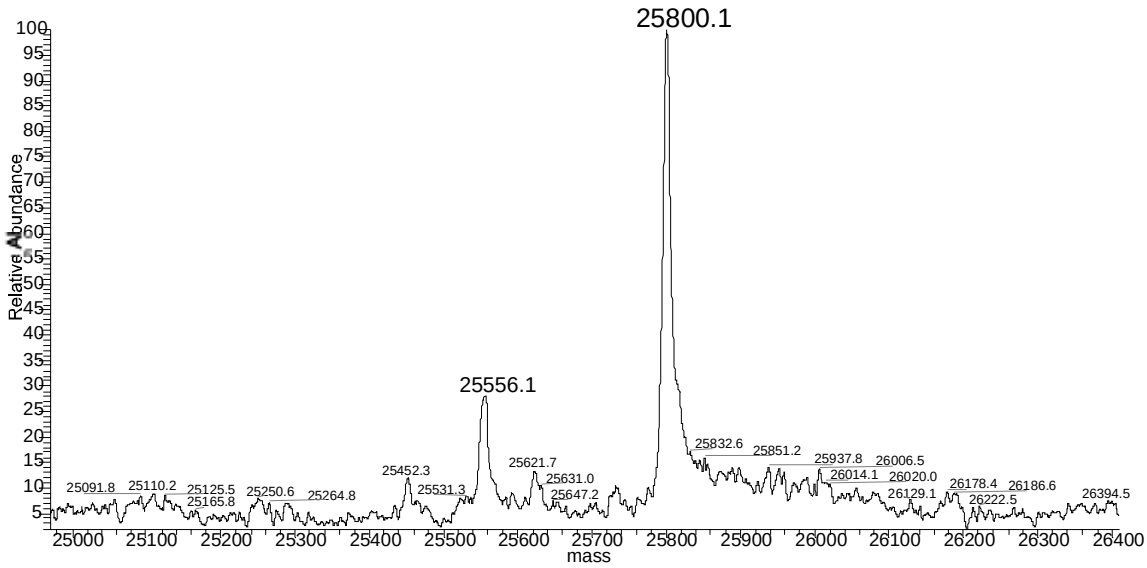

Figure 5.2. Mass spectral data for C22,25A243CACA.

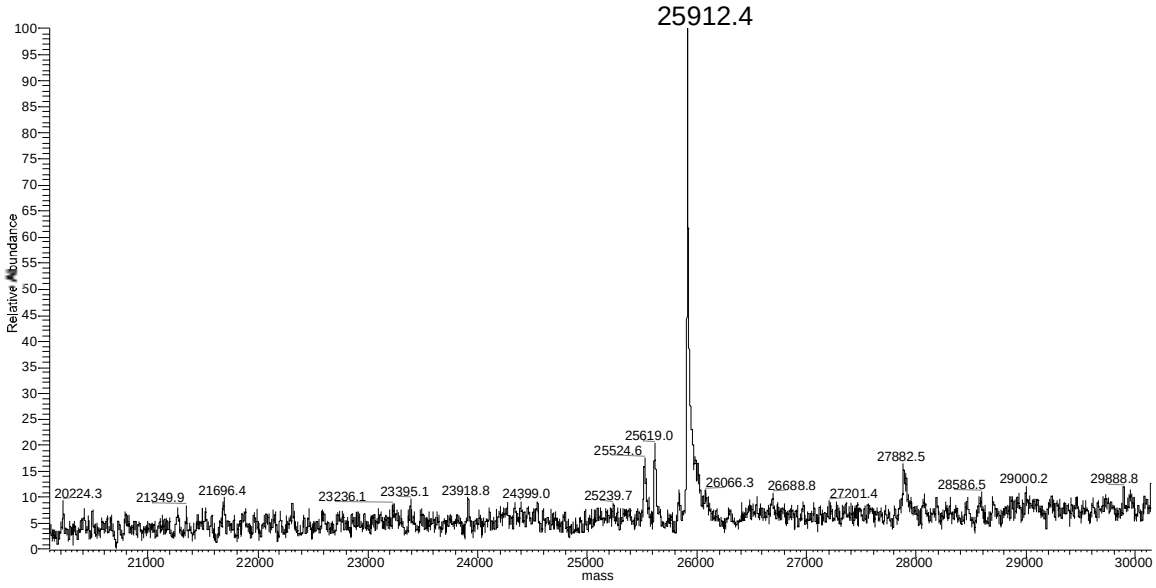

Figure 5.3. Mass spectral data for CCS243CAUA.

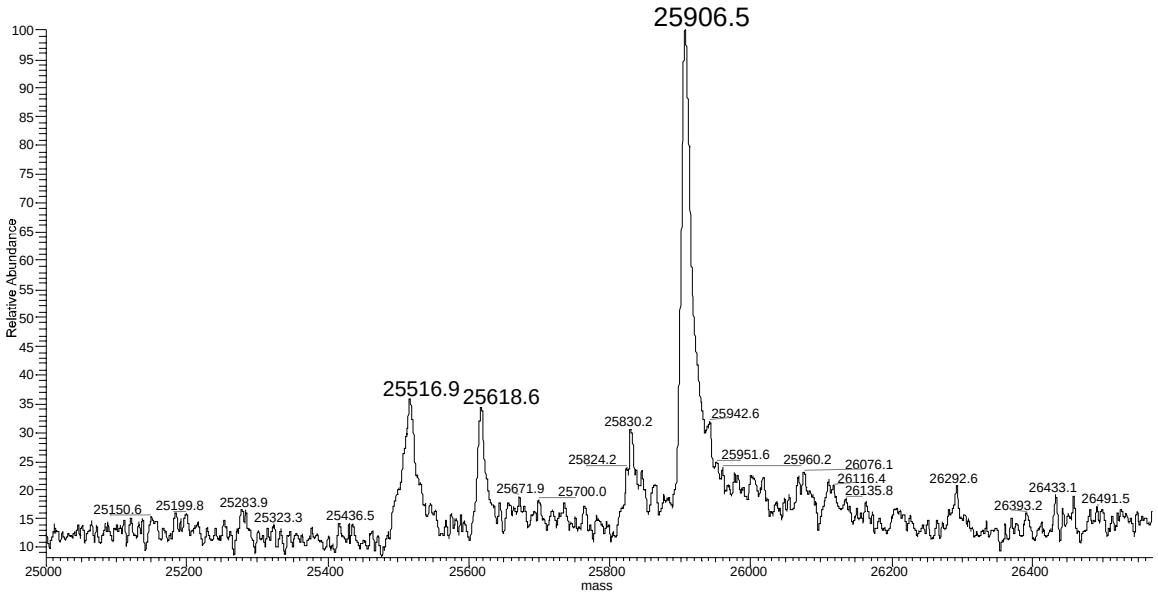

Figure 5.4. Mass spectral data for CCS243UACA.

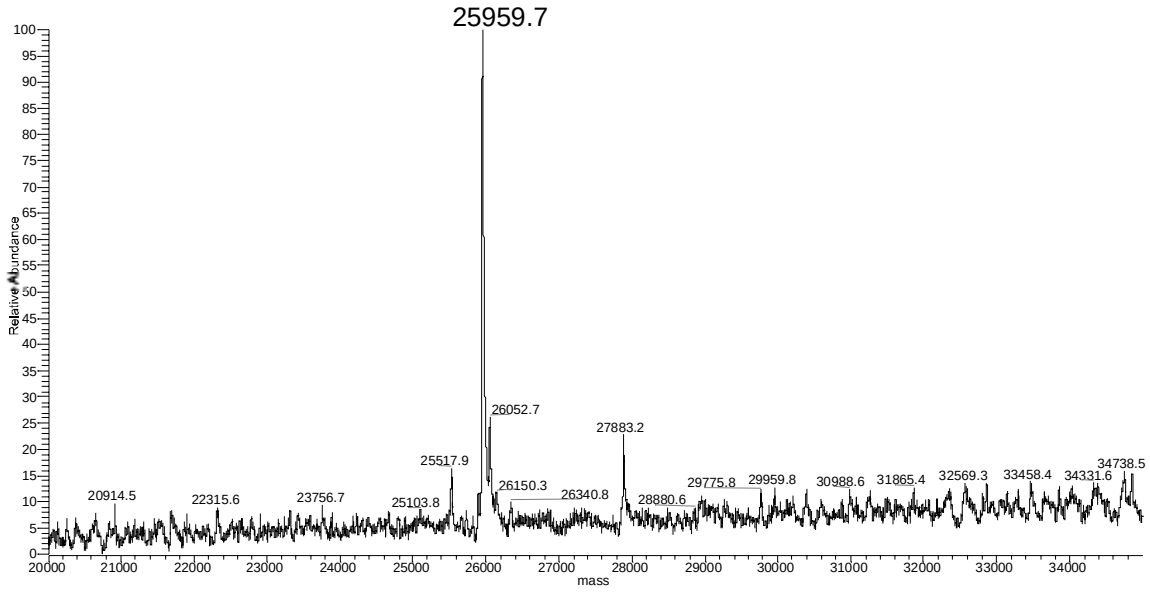

Figure 5.5. Mass spectral data for CCS243UAUA.

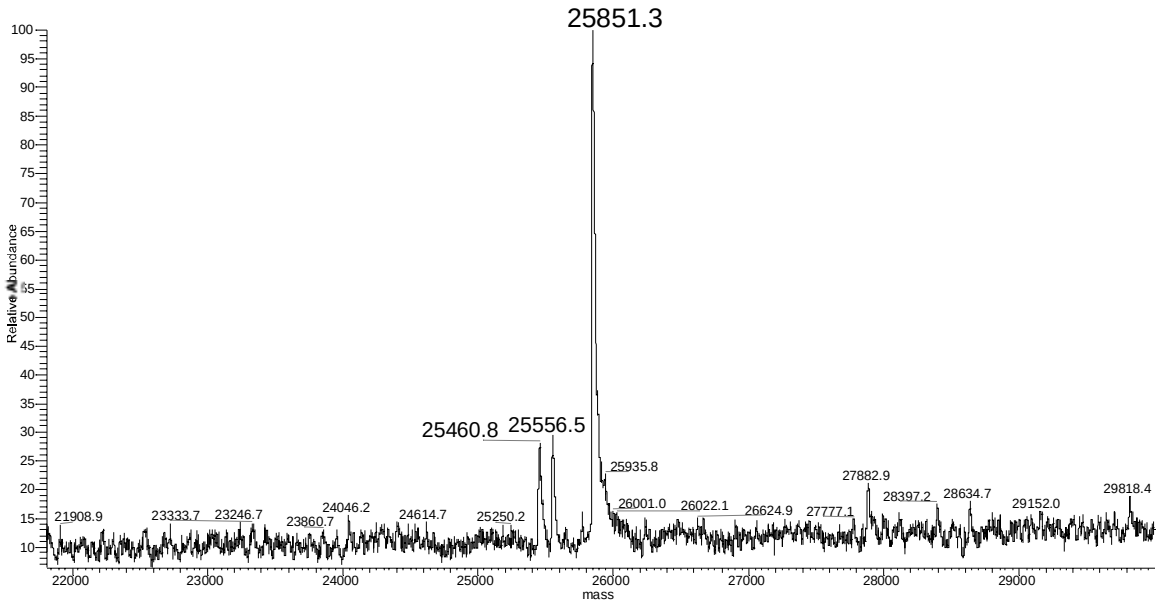

Figure 5.6. Mass spectral data for C22,25A243CAUA.

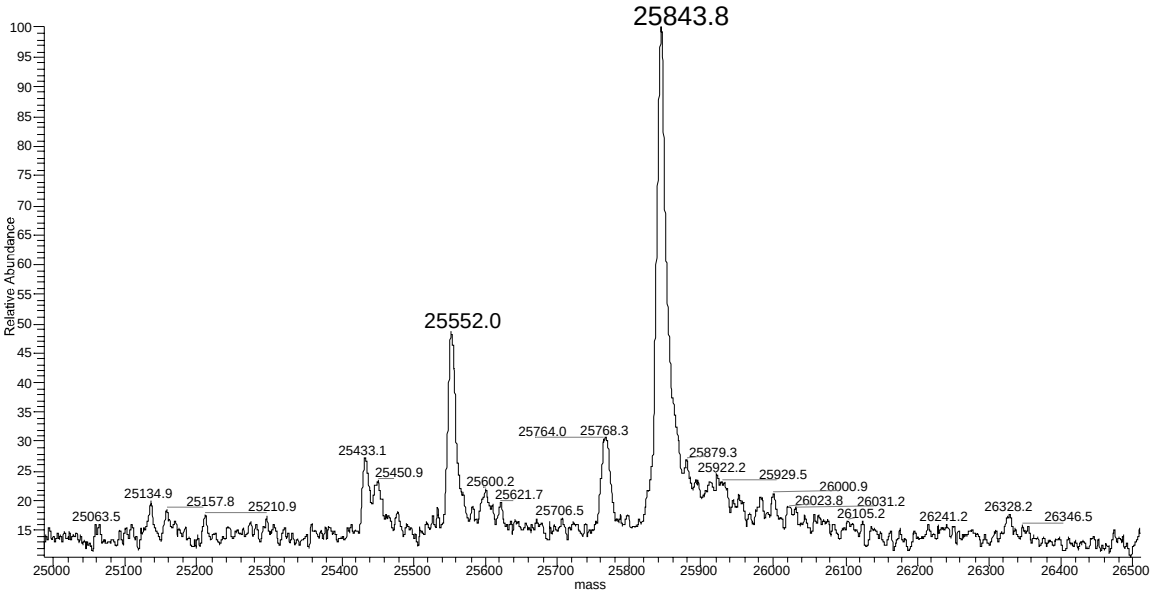

Figure 5.7. Mass spectral data for C22,25A243UACA.

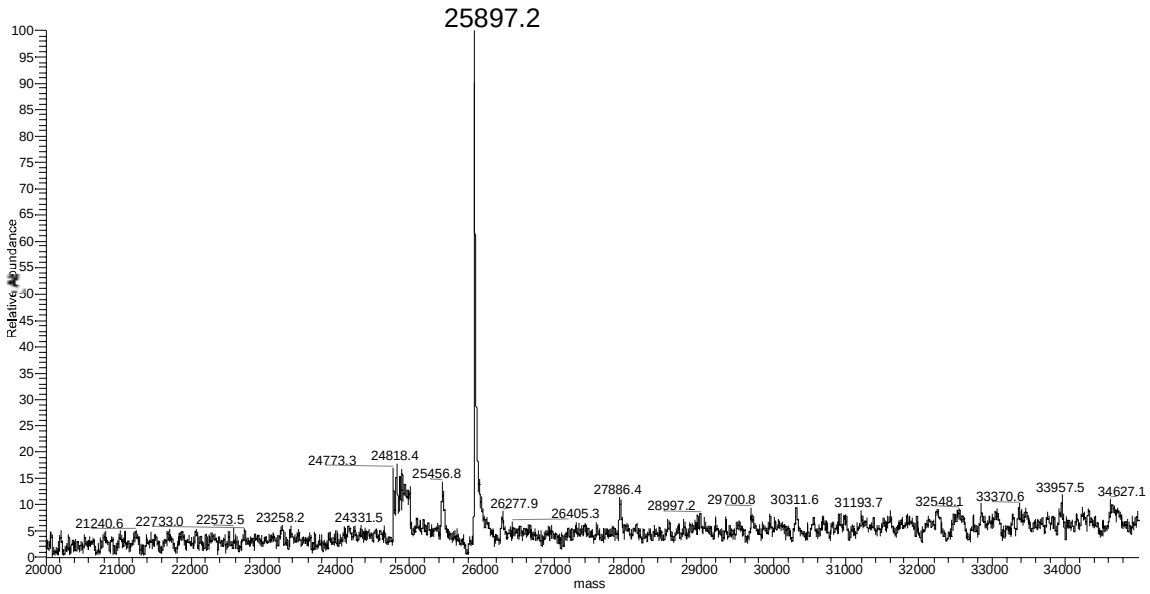

Figure 5.8. Mass spectral data for C22,25A243UAUA.

5.1.4 SOD-activation activity

All peptide ligation constructs were assayed for activity by measuring their ability to transfer copper with a 30 minute incubation time to apo-E-ZnSOD1 at a ratio of 1:1 hCCS:SOD1 (Table 5-3). The lowest activity observed was that of the CCS243CACA product, retaining 64% of its activity compared to CCS246, whereas the highest activities were near that of wild-type hCCS. Unlike the C22,25A245Sec and CCS245Sec proteins, the Sec-containing peptide ligations did not have decreased activity compared to wild-type hCCS and CCS246. The substitution of Se for S appeared to have no affect on the SOD1 maturation activity.

Protein	Activity (units)
Cu,Zn-SOD1	2000
hCCS	1500
CCS246	1282
CCS243CACDGA	1163 ± 80
CCS243CACA	821 ± 120
C22,25A243CACDGA	943 ± 100
C22,25A243CACA	1121 ± 70
CCS243CAUA	1479 ± 200
CCS243UACA	1397 ± 170
CCS243UAUA	1334 ± 190
C22,25A243CAUA	1048 ± 116
C22,25A243UACA	972 ± 90
C22,25A243UAUA	1266 ± 112

Table 5-3. SOD1-activation activity assays for peptide ligation proteins.

5.2 Cu-EXAFS

5.2.1 CCS243CACDGA

Cu K-edge EXAFS of the CCS243CACDGA protein are shown in Figure 5.9. As expected, the CCS243CACDGA protein Cu edge is similar to the CCS245Cys semisynthetic protein and to the previously reported XAS of the wild-type protein (Stasser et al., 2007). Two shells of scatterers are observed at ~2.2 and 2.7 Å, corresponding to Cu-S and Cu-Cu respectively. Curve fitting analysis leads to a best fit with 2.8 Cu-S interactions (R, $2\sigma^2$) at 2.26 Å (0.010 $Å^2$) and 1.2 Cu-Cu at 2.71 Å (0.013 $Å^2$).

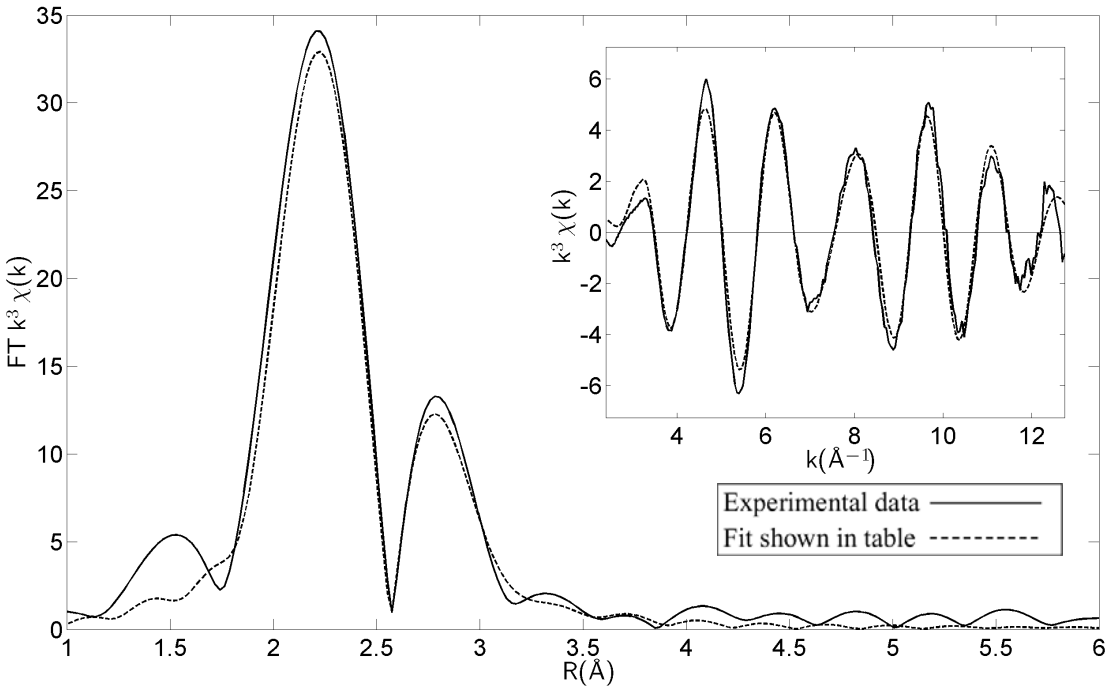

Scatterer	Distance (Å)	Debye-Waller (Å²)	-E_0 (eV)	F
2.8 S	2.26	0.010	5.95	0.323
1.2 Cu	2.71	0.013		

Figure 5.9. Cu K-edge EXAFS of CCS243CACDGA.

5.2.2 CCS243CACA

Cu K-edge EXAFS of the CCS243CACA protein are shown in Figure 5.10. Curve fitting analysis leads to a best fit with 2.8 Cu-S interactions (R, $2\sigma^2$) at 2.25 Å (0.011 Å^2) and 1.2 Cu-Cu at 2.72 Å (0.020 Å^2). The high DW value of the Cu-Cu shell indicates that there is less Cu signal present as compared to the CCS243CACDGA protein. This is consistent with the EXAFS analysis of the CCS246 protein. It is unclear why there would be less of a Cu-Cu interaction in these proteins.

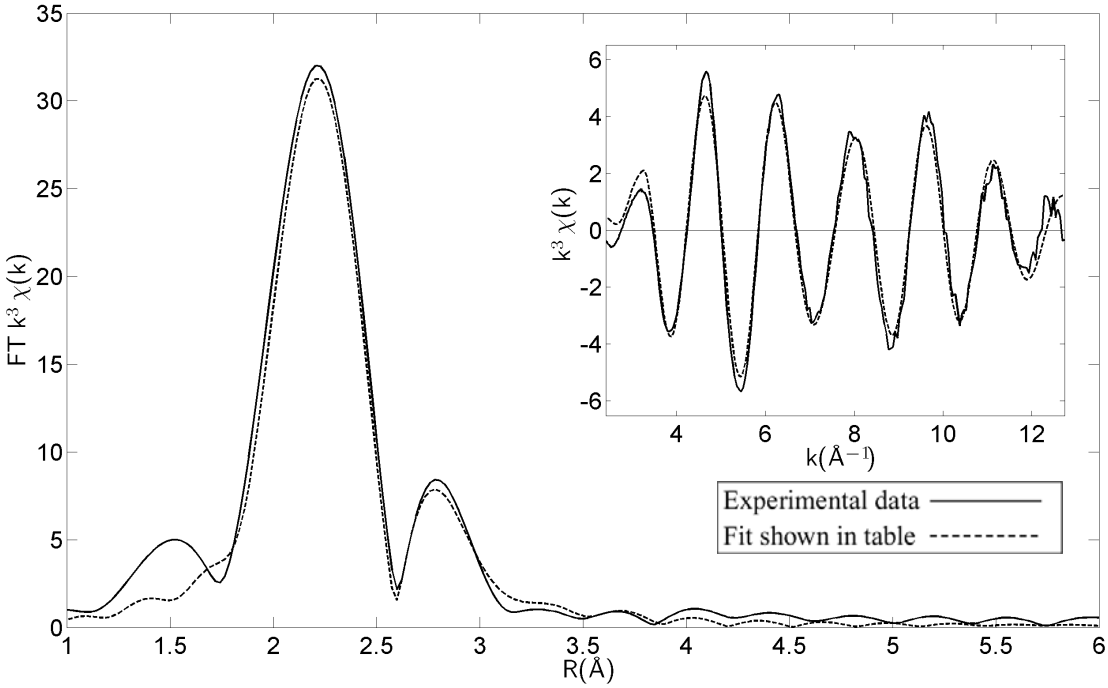

Scatterer	Distance (Å)	Debye-Waller (Å²)	-E_0 (eV)	F
2.8 S	2.25	0.011	5.67	0.283
1.2 Cu	2.72	0.020		

Figure 5.10. Cu K-edge EXAFS of CCS243CACA.

5.2.3 C22,25A243CACDGA

Cu K-edge EXAFS of the C22,25A243CACDGA protein are shown in Figure 5.11. As expected, the Cu K-edge EXAFS of the C22,25A243CACDGA protein is very similar to those of the C22,25A245Cys ligation and to the previously reported XAS of the full-length C22,25A protein (Stasser et al., 2007) with two shells of scatterers observed at ~2.2 and 2.7 Å, corresponding to Cu-S and Cu-Cu respectively. Curve fitting analysis leads to a best fit with 2.6 Cu-S interactions (R, $2\sigma^2$) at 2.27 Å (0.007 Å^2) and 2.8 Cu-Cu at 2.72 Å (0.013 Å^2). This is consistant with data for the full-length C22,25A mutant, where up to 2.8 Cu were fit (Stasser, 2007).

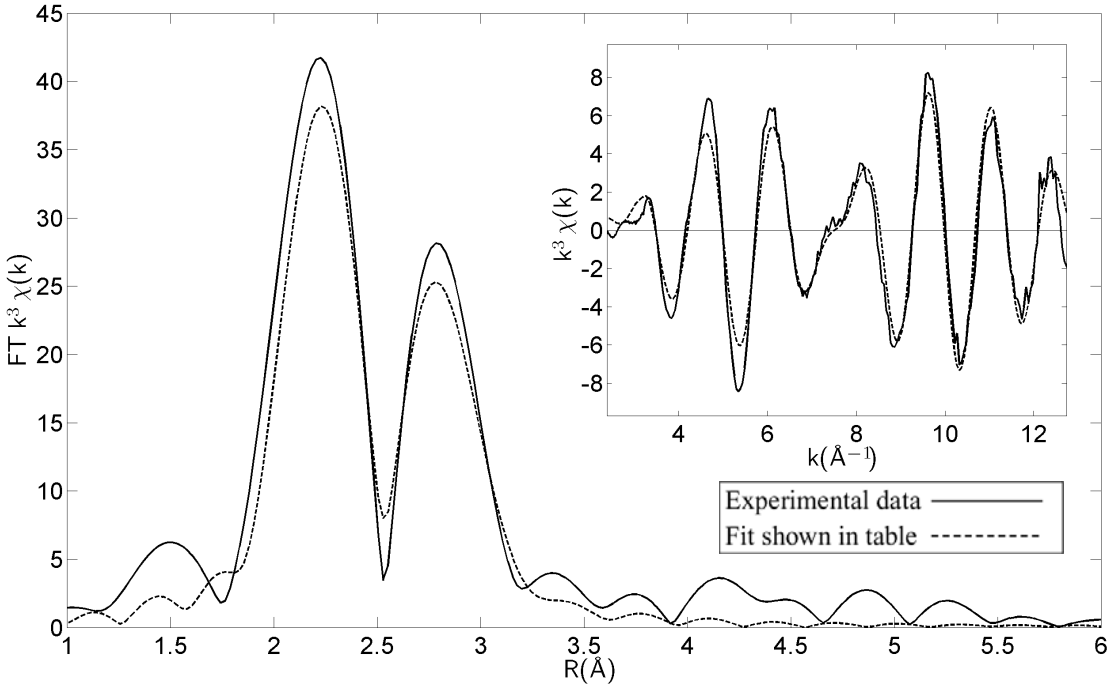

Scatterer	Distance (Å)	Debye-Waller (Å²)	-E_0 (eV)	F
2.7 S	2.27	0.007	6.28	0.429
2.8 Cu	2.72	0.013		

Figure 5.11. Cu K-edge EXAFS of C22,25A243CACDGA.

5.2.4 C22,25A243CACA

Cu K-edge EXAFS of the C22,25A243CACA protein are shown in Figure 5.12. Not surprisingly, the Cu edge of the C22,25A243CACA protein is very similar to the –CACDGA ligation. Two shells of scatterers are observed at ~2.2 and 2.7 Å, corresponding to Cu-S and Cu-Cu respectively. Curve fitting analysis leads to a best fit with 2.7 Cu-S interactions (R, $2\sigma^2$) at 2.26 Å (0.008 $Å^2$) and 2 Cu-Cu at 2.71 Å (0.013 $Å^2$).

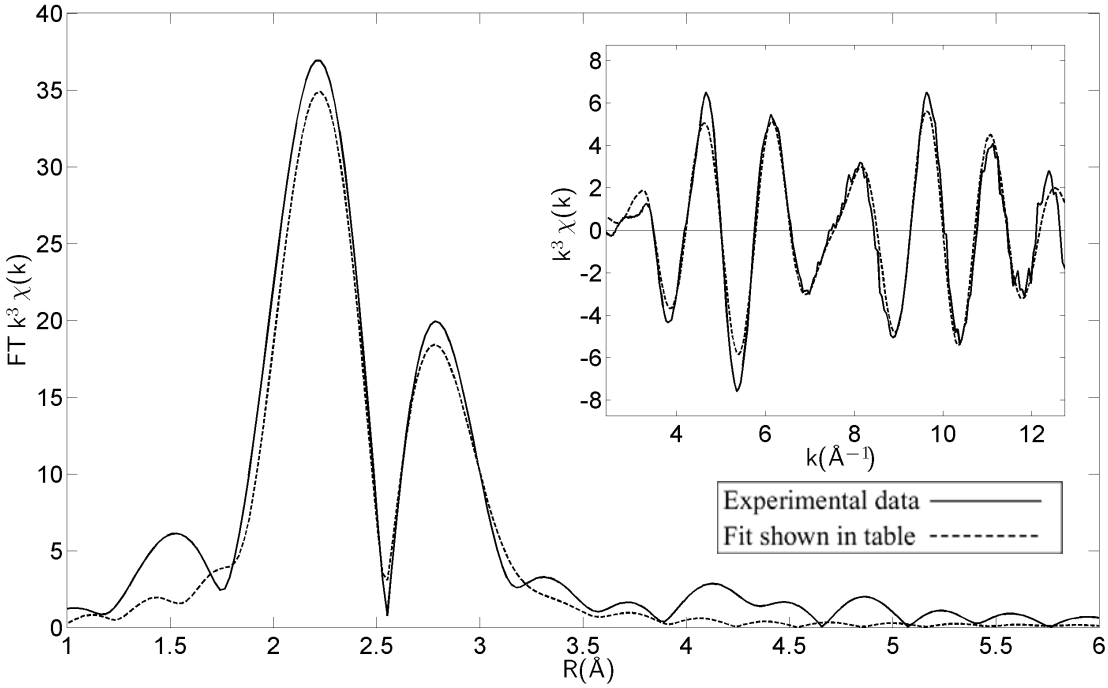

Scatterer	Distance (Å)	Debye-Waller (Å²)	-E_0 (eV)	F
2.7 S	2.26	0.008	5.69	0.404
2.0 Cu	2.71	0.013		

Figure 5.12. Cu K-edge EXAFS of C22,25A243CACA.

5.2.5 CCS243CAUA

Like the CCS245Sec protein, the analysis of the CCS243CAUA protein Cu K-edge EXAFS represents the average of the Cu binding to the D1 mononuclear and the D3 multinuclear site. The best fit gave 2.0 Cu-S at 2.22 Å (0.007 Å^2), 0.8 Cu-Se at 2.45 Å (0.011 Å^2), and 1.2 Cu-Cu at 2.68 (0.011 Å^2), but this fit is not consistent with the Se absorption edge parameters. Using Cu-Se = 2.38 ± 0.2 Å ($2\sigma^2$(Cu-Se) = 0.007 Å^2) and $2\sigma^2$(Cu-Cu) = 0.012 Å^2, the best fit (F = 0.536) shows 1.2 Cu at 2.63 Å, 2.0 S at 2.20 Å (DW = 0.012 Å^2), and 0.8 Se at 2.38 Å (Figure 5.13). These parameters lead to consistency of metrical parameters at both Cu and Se absorption edges. This is similar to that seen for the CCS245Sec protein, as expected.

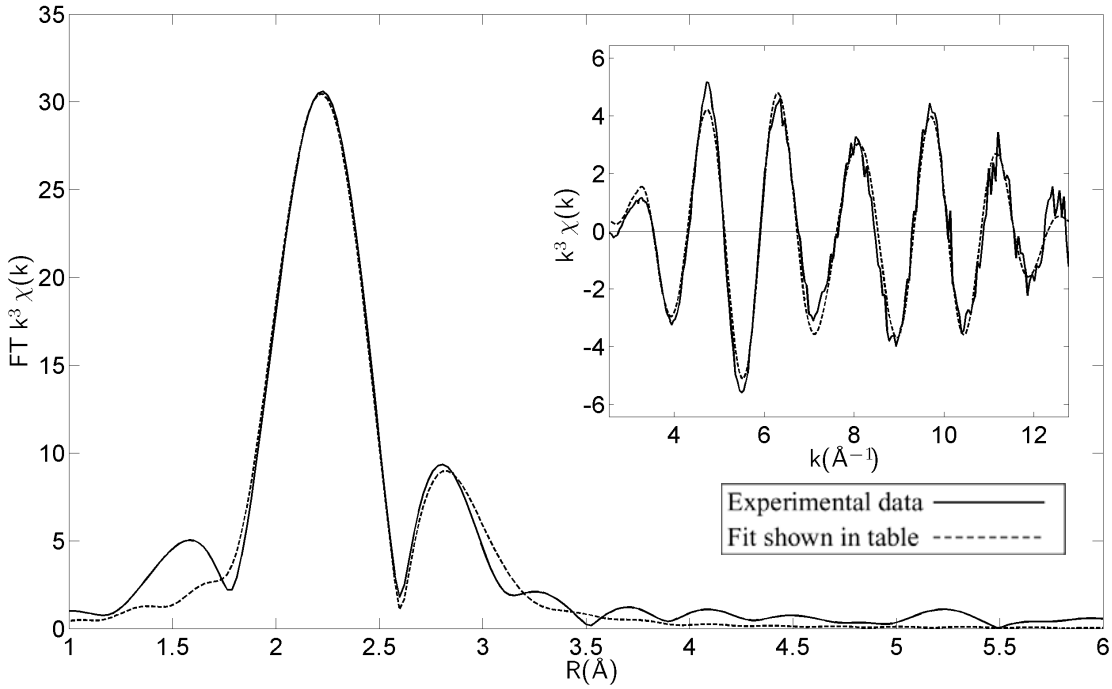

Scatterer	Distance (Å)	Debye-Waller (Å²)	-E_0 (eV)	F
2.0 S	2.20	0.012	2.91	0.536
0.8 Se	2.38	0.007		
1.2 Cu	2.63	0.012		

Figure 5.13. Cu K-edge EXAFS of CCS243CAUA.

5.2.6 CCS243UACA

The best fit gave 2.0 Cu-S at 2.20 Å (0.014 Å^2), 0.8 Cu-Se at 2.39 Å (0.008 Å^2), and 1.2 Cu-Cu at 2.59 (0.014 Å^2) (Figure 5.14). These parameters lead to consistency of metrical parameters at both Cu and Se absorption edges. This is very similar to the spectra seen for CCS243CAUA, indicating that the presence of the Sec at residue 244 or 246 does not significantly change the structure of the copper environment.

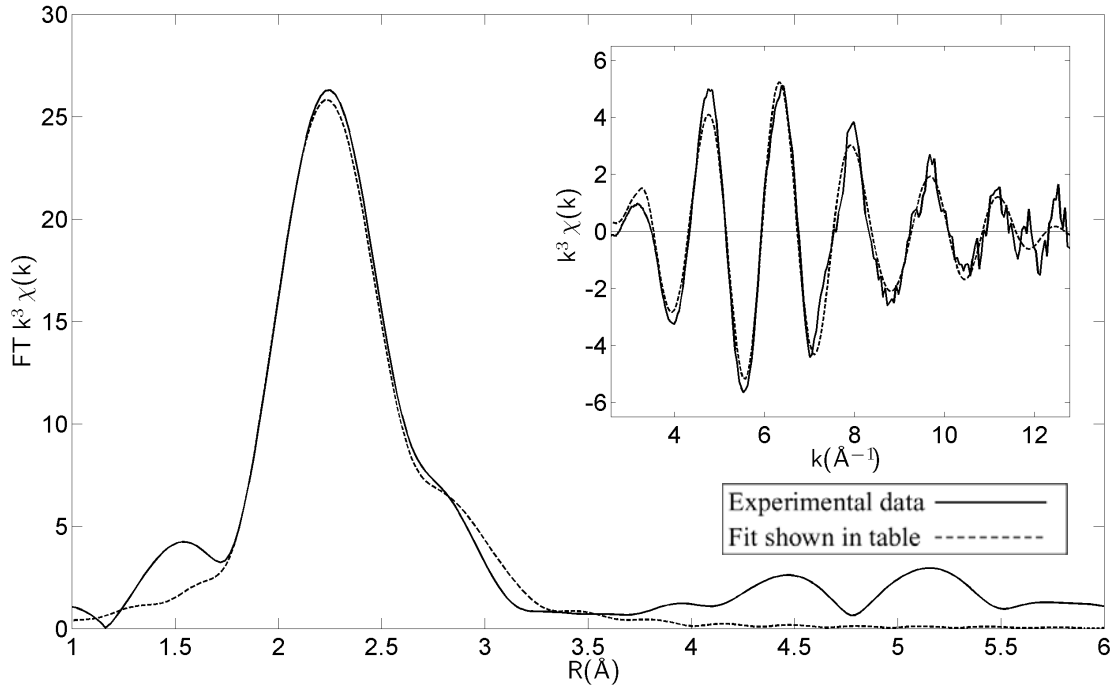

Scatterer	Distance (Å)	Debye-Waller (Å²)	-E_0 (eV)	F
2.0 S	2.20	0.014	-0.978	0.576
0.8 Se	2.39	0.008		
1.2 Cu	2.59	0.014		

Figure 5.14. Cu K-edge EXAFS of CCS243UACA.

5.2.7 CCS243UAUA

The best fit gave 2.0 Cu-S at 2.21 Å (0.008 Å^2), 0.8 Cu-Se at 2.39 Å (0.008 Å^2), and 1.2 Cu-Cu at 2.70 (0.016 Å^2) (Figure 5.15). These parameters lead to consistency of metrical parameters at both Cu and Se absorption edges. This is very similar to the spectra seen for the other CCS243 ligations, indicating that the presence of the Sec at both residues 244 or 246 does not significantly change the structure of the copper environment. Interestingly, the contribution from S also does not decrease. Since both Cys residues of the CXC motif in D3 have been mutated to Sec residues, one would expect a loss of sulfur at the Cu K-edge if only the D3 Cu-binding motif residues were involved in the D3-D3 copper cluster. Furthermore, a greater contribution of Cu-Se would be expected. With the presence of the D1 Cu-binding site, further analysis of the D3-D3 interaction at the Cu K-edge is hindered.

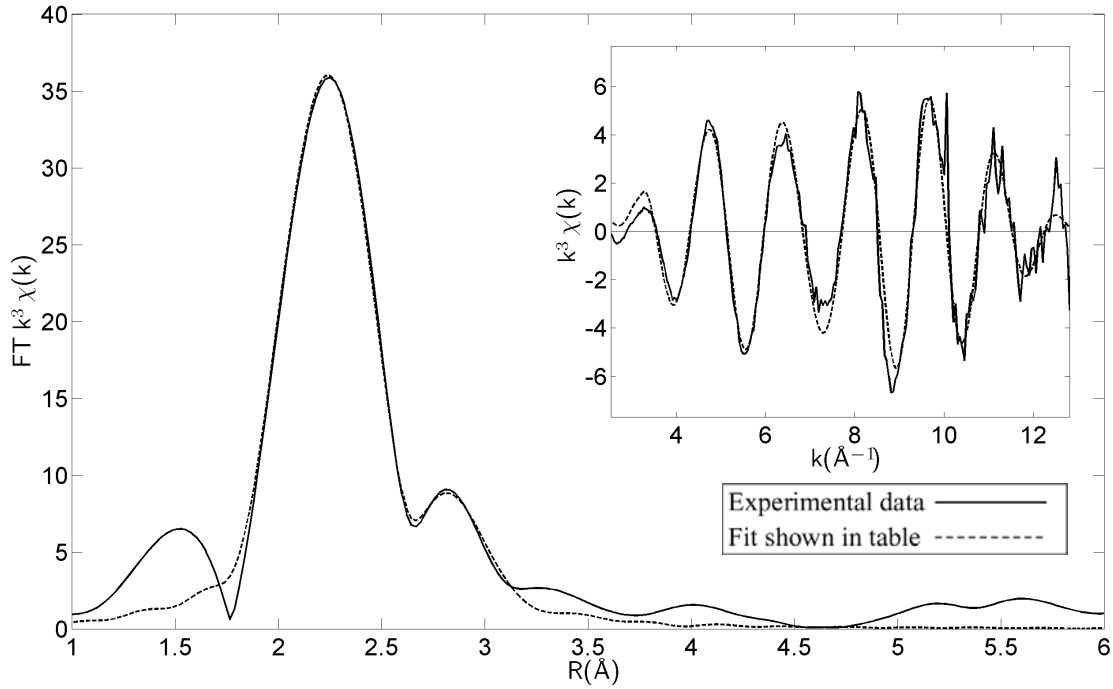

Scatterer	Distance (Å)	Debye-Waller (Å²)	-E_0 (eV)	F
2.0 S	2.21	0.008	2.53	0.581
0.8 Se	2.39	0.008		
1.2 Cu	2.70	0.016		

Figure 5.15. Cu K-edge EXAFS of CCS243UAUA.

5.2.8 C22,25A243CAUA

Unlike the CCS243 peptide ligations, the analysis of the C22,25A243 ligations Cu K-edge EXAFS represents only the Cu binding to the D3 multinuclear site. For C22,25A243CAUA, the best fit gave 2.0 Cu-S at 2.24 Å (0.006 Å^2), 1.0 Cu-Se at 2.41 Å (0.013 Å^2), and 2.0 Cu-Cu at 2.71 (0.010 Å^2) (Figure 5.16), but this fit is not consistent with the Se absorption edge parameters. Using Cu-Se = 2.38 ± 0.2 Å ($2\sigma^2$(Cu-Se) = 0.007 Å^2), the best fit (F = 0.314) shows 2.0 Cu at 2.71 Å (DW = 0.013 Å^2), 2.3 S at 2.25 Å (DW = 0.009 Å^2), and 0.7 Se at 2.38 Å. These parameters lead to consistency of metrical parameters at both Cu and Se absorption edges. This fit is also very similar to that of the C22,25A245Sec protein, as expected.

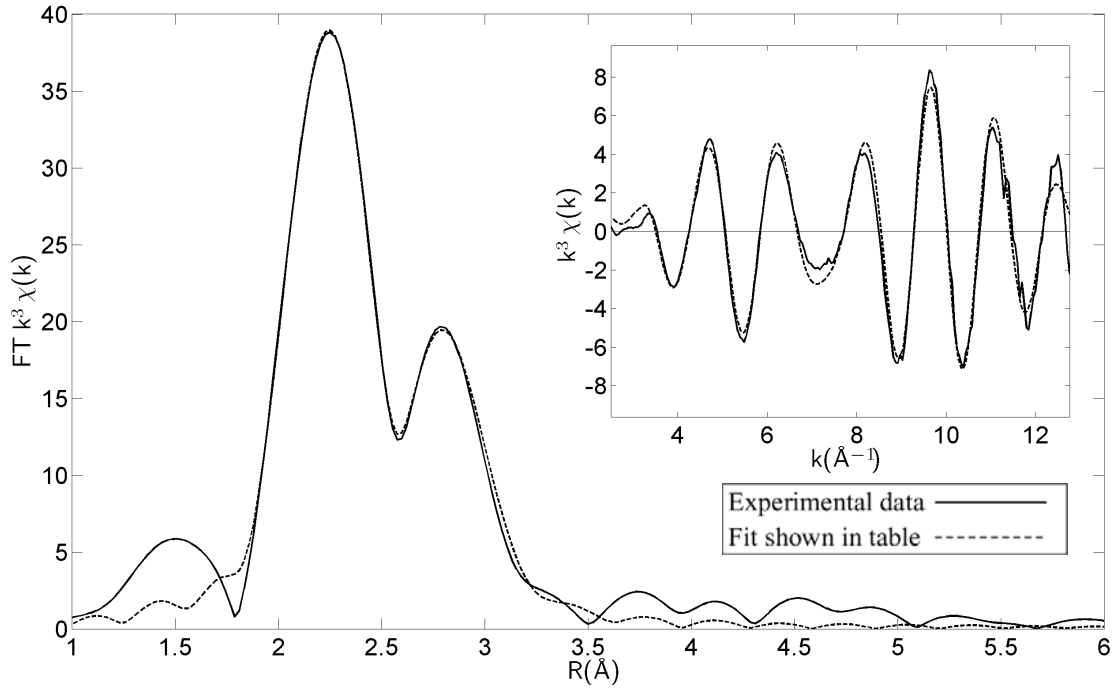

Scatterer	Distance (Å)	Debye-Waller (Å²)	-E_0 (eV)	F
2.0 S	2.24	0.006	3.88	0.272
1.0 Se	2.41	0.013		
2.0 Cu	2.71	0.010		

Figure 5.16. Cu K-edge EXAFS of C22,25A243CAUA.

5.2.9 C22,25A243UACA

Analysis of the C22,25A243UACA construct was almost identical to that of the C22,25A243CAUA construct. For C22,25A243UACA, the best fit gave 2.0 Cu-S at 2.23 Å (0.008 Å^2), 1.0 Cu-Se at 2.41 Å (0.009 Å^2), and 2.0 Cu-Cu at 2.71 (0.010 Å^2) (Figure 5.17), but this fit is inconsistent with the Se absorption edge parameters. Using Cu-Se = 2.38 ± 0.2 Å ($2\sigma^2$(Cu-Se) = 0.008 Å^2), the best fit (F = 0.265) shows 2.0 Cu-Cu at 2.70 Å ($2\sigma^2$(Cu-Cu) = 0.012 Å^2), 2.0 Cu-S at 2.23 Å ($2\sigma^2$(Cu-S) = 0.010 Å^2), and 1.0 Cu-Se at 2.40 Å. These parameters lead to consistency of metrical parameters at both Cu and Se absorption edges. The similarity of this fit to C22,25A243CAUA indicates that residue 244 and 246 each have the same copper environment.

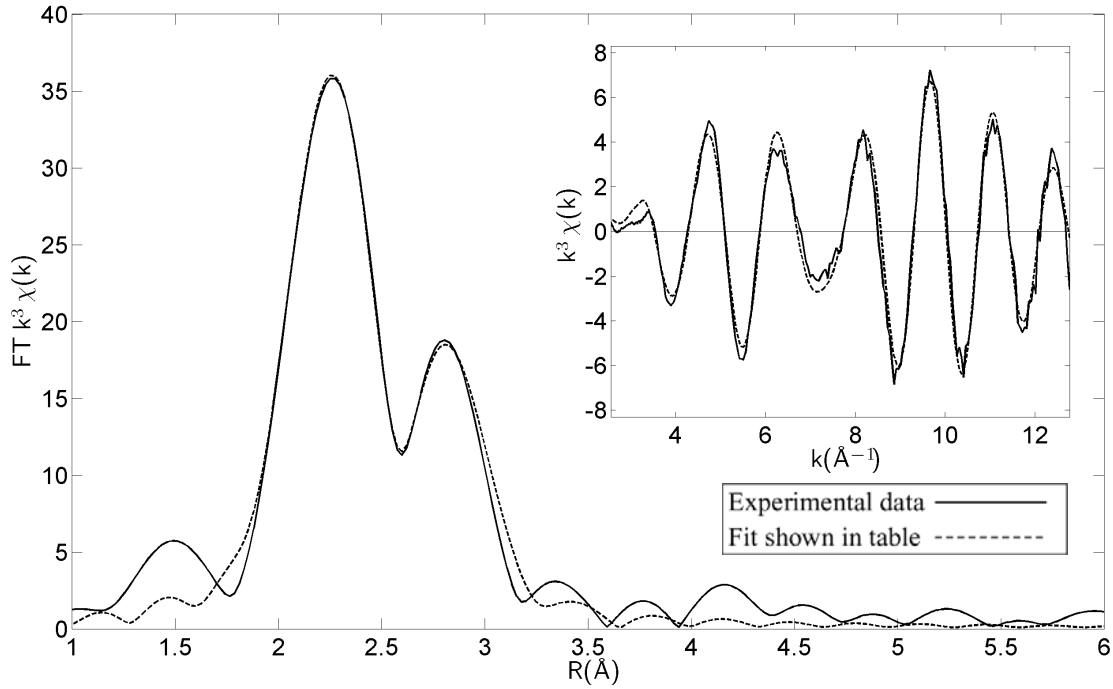

Scatterer	Distance (Å)	Debye-Waller (Å²)	-E_0 (eV)	F
2.0 S	2.23	0.008	2.83	0.249
1.0 Se	2.41	0.009		
2.0 Cu	2.70	0.010		

Figure 5.17. Cu K-edge EXAFS of C22,25A243UACA.

5.2.10 C22,25A243UAUA

Cu K-edge EXAFS of the C22,25A243UAUA construct showed both Cu-Se and Cu-S interactions. The best fit gave 1.0 Cu-S at 2.17 Å (0.002 Å^2), 2.0 Cu-Se at 2.39 Å (0.007 Å^2), and 2.0 Cu-Cu at 2.67 (0.010 Å^2) (Figure 5.18). Unlike the CCS243UAUA construct spectra, the C22,25A243UAUA spectra differ significantly from the –CAUA or –UACA ligation proteins. There is a much more significant contribution from Cu-Se. Furthermore, a Cu-S signal remains, indicating the presence of S in the D3-D3 copper cluster, even though both of the Cu-binding Cys residues in the CXC motif have been mutated to Sec residues. This indicates that residues outside of the D1 and the D3 motif must be involved in Cu-binding.

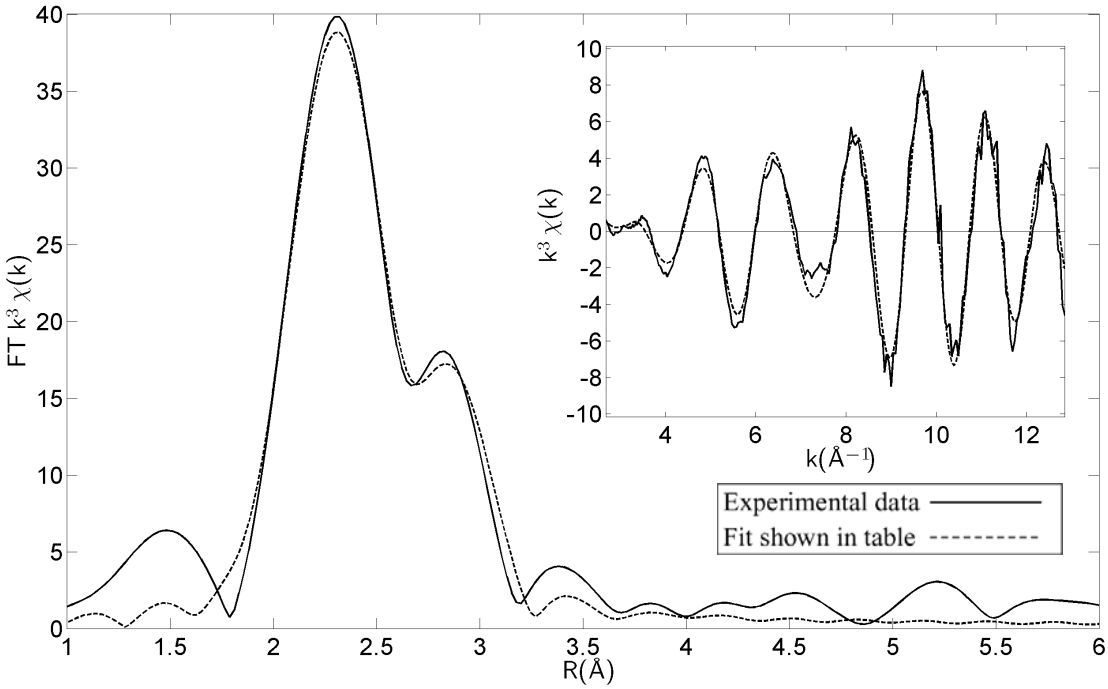

Scatterer	Distance (Å)	Debye-Waller (Å²)	-E_0 (eV)	F
1.0 S	2.17	0.002	-1.63	0.402
2.0 Se	2.39	0.007		
2.0 Cu	2.67	0.010		

Figure 5.18. Cu K-edge EXAFS of C22,25A243UAUA.

5.3 Se-EXAFS

5.3.1 CCS243CAUA

As with CCS245Sec and C22,25A245Sec, with selenocysteine covalently attached to the CCS243 ligation constructs, it was possible to probe the speciation of the Se by Se K-edge EXAFS. The –CAUA ligations were examined before copper addition to compare to the previous apo Sec-ligated proteins. For the ApoCCS243CAUA protein, the best fit of the Se K-edge EXAFS was found to be a mixture of both Se-S (0.5) and Se-Se (0.5) with an F value of 0.479 (Figure 5.19). This shows that as isolated, the ligated protein appears to be oxidized, and exists as an equilibrium mixture of monomers with Se-S distances of 2.15 Å, and dimers with Se-Se distances of 2.32 Å.

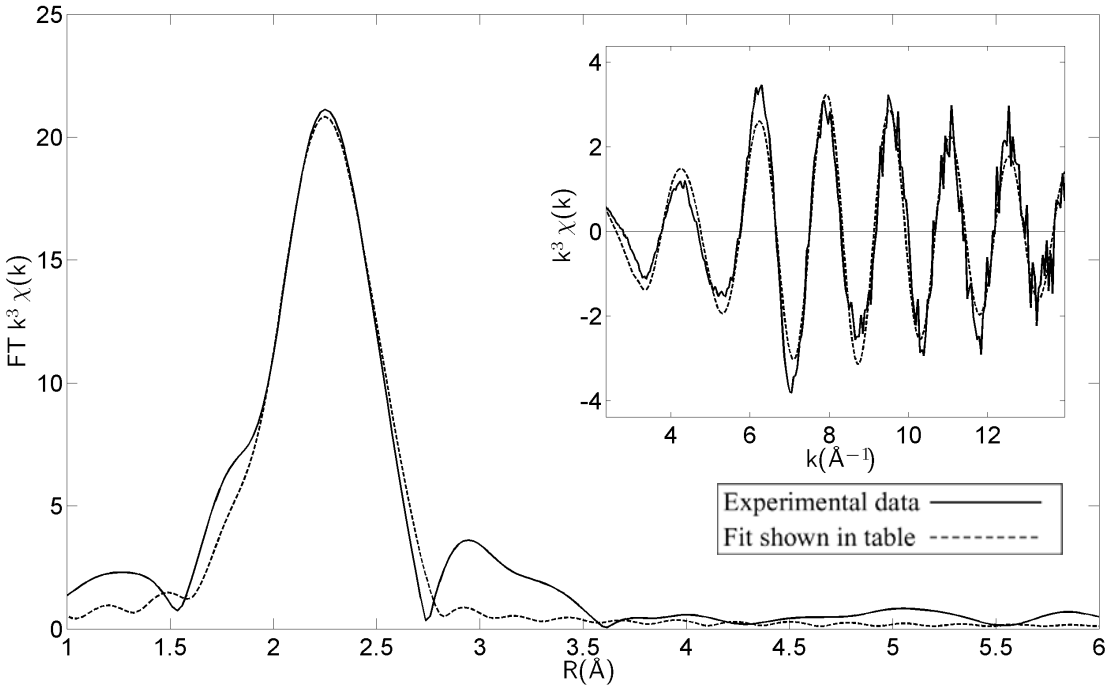

Scatterer	Distance (Å)	Debye-Waller (Å²)	-E_0 (eV)	F
1.0 C	2.01	0.015	4.72	0.479
0.5 S	2.15	0.008		
0.5 Se	2.32	0.004		

Figure 5.19. Se K-edge EXAFS of ApoCCS243CAUA.

It was expected that the Se K-edge EXAFS of the reconstituted CCS243CAUA protein would be similar to that of the CCS245Sec protein, containing contributions from 1 Se-C and two Se-Cu interactions. The best fit, F= 0..838, was obtained with 1 Se-C and 2 Se-Cu with $R(2\sigma^2)_{Se\text{-}C}$ = 2.03 Å (0.012 Å^2) and $R(2\sigma^2)_{Se\text{-}Cu}$ = 2.38 Å (Figure 5.20). Therefore, each Se is bound by 2 Cu atoms at 2.38 Å in the D3 cluster as with the CCS245Sec and C22,25A245Sec proteins. The CCS243CAUA provided an adequate control to ensure the consistency of the replacement of Cys246 residue with Sec by intein-mediated peptide ligation.

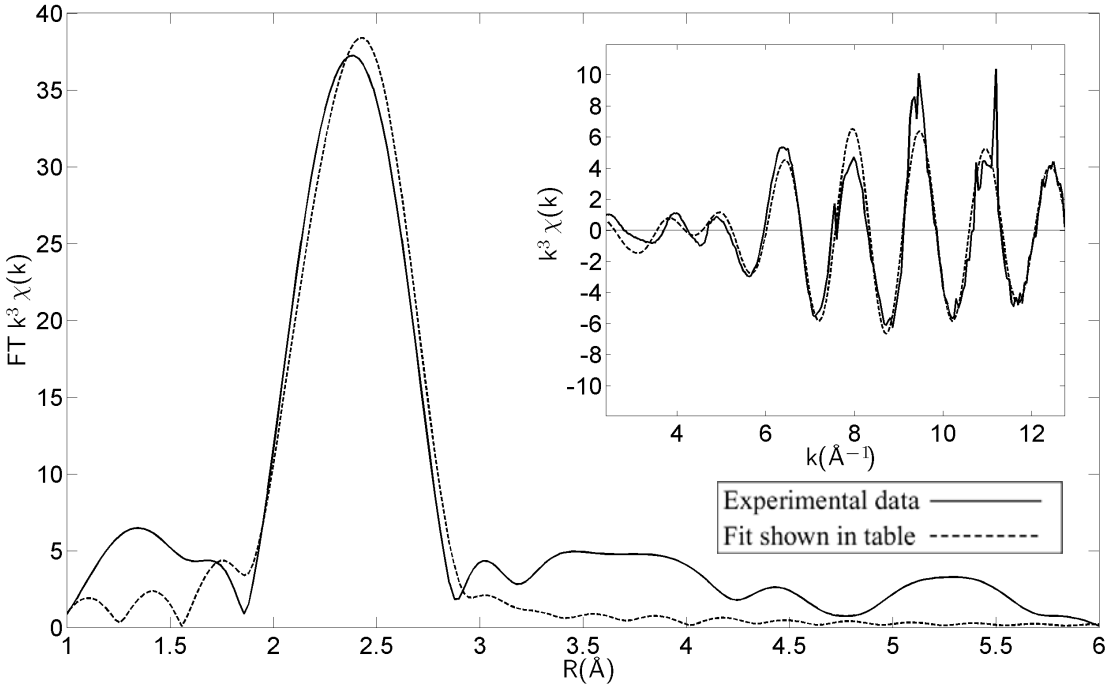

Scatterer	Distance (Å)	Debye-Waller (Å²)	-E_0 (eV)	F
1.0 C	2.03	0.012	3.84	0.838
2.0 Cu	2.38	0.007		

Figure 5.20. Se K-edge EXAFS of CCS243CAUA.

5.3.2 CCS243UACA

Due to the similarity at the Cu K-edge, it was expected that the Se K-edge EXAFS of the CCS243UACA protein would be similar to that of the –CAUA ligation construct with contributions from 1 Se-C and two Se-Cu. Surprisingly, the best fit was obtained with 1 Se-C with $R(2\sigma^2)_{Se\text{-}C}$ = 1.98 Å (0.002 Å^2), 0.5 Se-S with $R(2\sigma^2)_{Se\text{-}S}$ = 2.17 Å (0.003 Å^2), and 1.1 Se-Cu with $R(2\sigma^2)_{Se\text{-}Cu}$ = 2.38 Å (0.008 Å^2) (Figure 5.21). This fit indicates that some of the selenium is in the Se-S form. This could indicate insufficient copper loading, and subsequent oxidation of the free selenocysteine. Although Se-S is seen at the Se K-edge, at the Cu K-edge, the spectra look as expected for the fully Cu-loaded form. If binding at the D3 site is limited due to oxidized Se, it would be expected that there would be more D1 Cu-S signal present overall at the Cu K-edge. It is unclear why there is a discrepancy between the two edges.

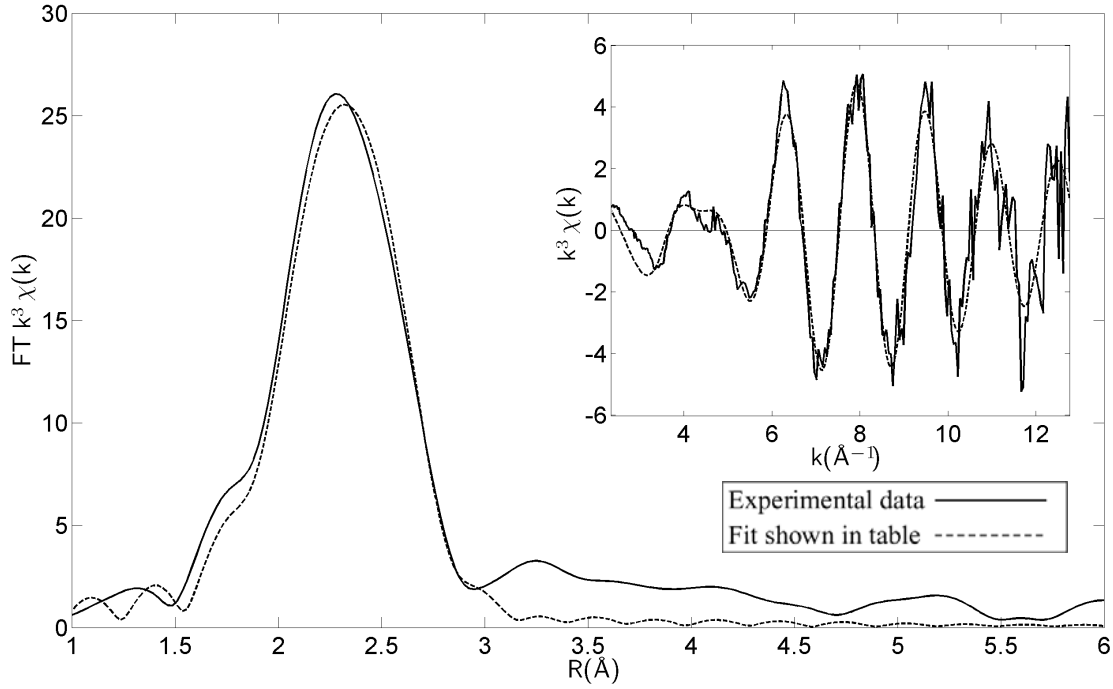

Scatterer	Distance (Å)	Debye-Waller (Å²)	-E_0 (eV)	F
1.0 C	1.98	0.012	3.72	1.00
1.1 Cu	2.38	0.008		
0.5 S	2.17	0.003		

Figure 5.21. Se K-edge EXAFS of CCS243UACA.

5.3.3 CCS243UAUA

If both residues 244 and 246 of the CXC motif have the same environment when copper is bound, it would be expected that the Se K-edge EXAFS of the CCS243UAUA construct would be identical to that of the single Sec substitution proteins with respect to the amount of copper seen. This was found to be true with the best fit showing contributions from 1 Se-C with $R(2\sigma^2)_{Se\text{-}C}$ = 2.01 Å (0.006 Å^2) and 2.0 Se-Cu with $R(2\sigma^2)_{Se\text{-}Cu}$ = 2.39 Å (0.008 Å^2) (Figure 5.22).

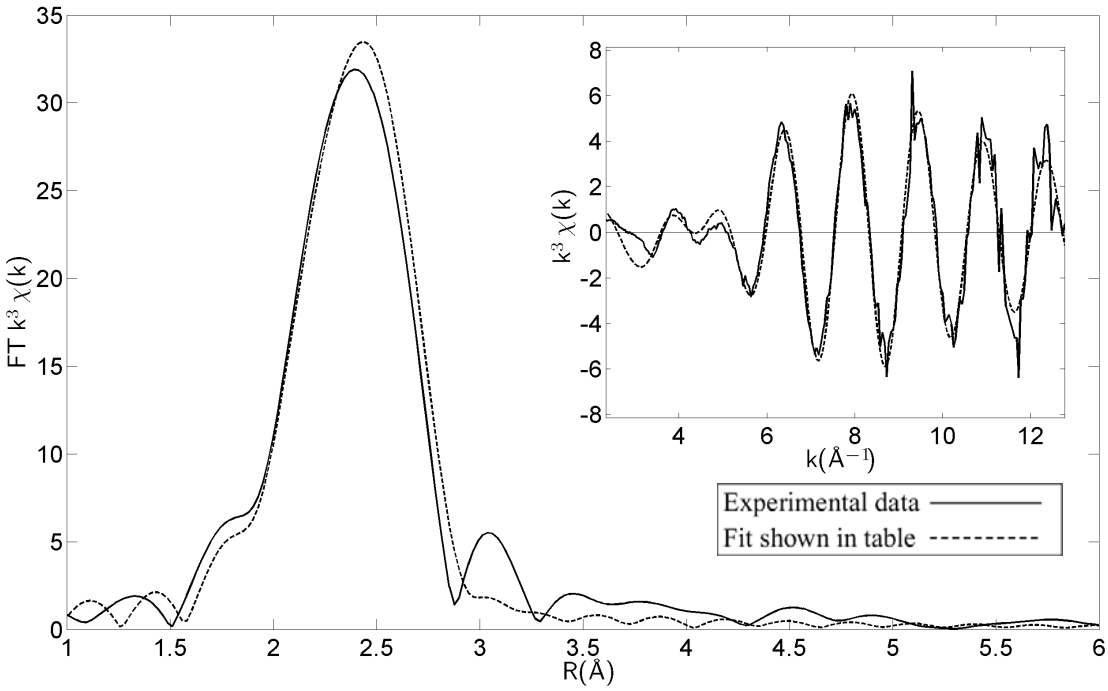

Scatterer	Distance (Å)	Debye-Waller (Å²)	-E_0 (eV)	F
1.0 C	2.01	0.006	5.15	0.586
2.0 Cu	2.39	0.008		

Figure 5.22. Se K-edge EXAFS of CCS243UAUA.

5.3.4 C22,25A243CAUA

As with the CCS243CAUA protein, the C22,25A243CAUA protein was examined before copper addition to compare to the previous apo Sec-ligated proteins. For the ApoC22,25A243CAUA protein, the best fit of the Se K-edge EXAFS was found to be a mixture of both Se-S (0.5) and Se-Se (0.5) with an F value of 0.310 (Figure 5.23). This shows that as isolated, the ligated protein appears to be oxidized, and exists as an equilibrium mixture of monomers with Se-S distances of 2.17 Å, and dimers with Se-Se distances of 2.31 Å.

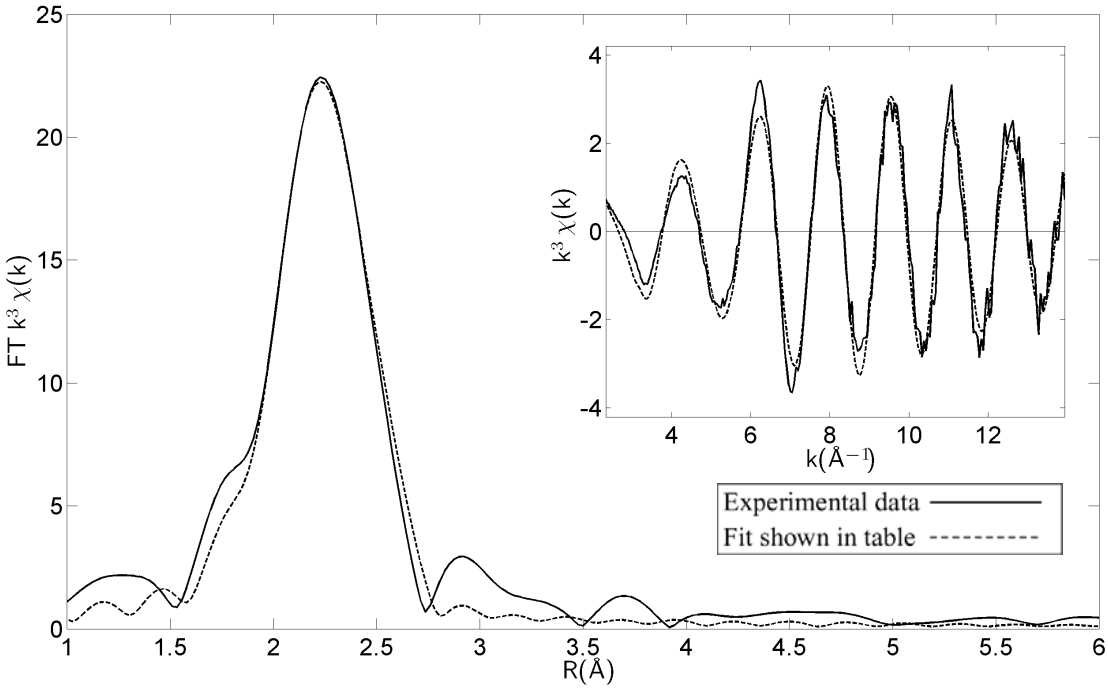

Scatterer	Distance (Å)	Debye-Waller (Å²)	-E_0 (eV)	F
1.0 C	1.99	0.012	4.97	0.310
0.5 S	2.17	0.007		
0.5 Se	2.31	0.004		

Figure 5.23. Se K-edge EXAFS of ApoC22,25A243CAUA.

It was expected that the Se K-edge EXAFS of the reconstituted C22,25ACAUA protein would be similar to that of the C22,25A245Sec protein, containing contributions from one Se-C and two Se-Cu interactions. The best fit, F= 0.287, was obtained with 1 Se-C and 2 Se-Cu with $R(2\sigma^2)_{Se\text{-}C}$ = 1.98 Å (0.007 Å^2) and $R(2\sigma^2)_{Se\text{-}Cu}$ = 2.38 Å (0.007 Å^2) (Figure 5.24). Therefore, each Se is bound by 2 Cu atoms at 2.38 Å in the D3 cluster, as observed for the CCS245Sec, C22,25A245Sec, and CCS243CAUA proteins.

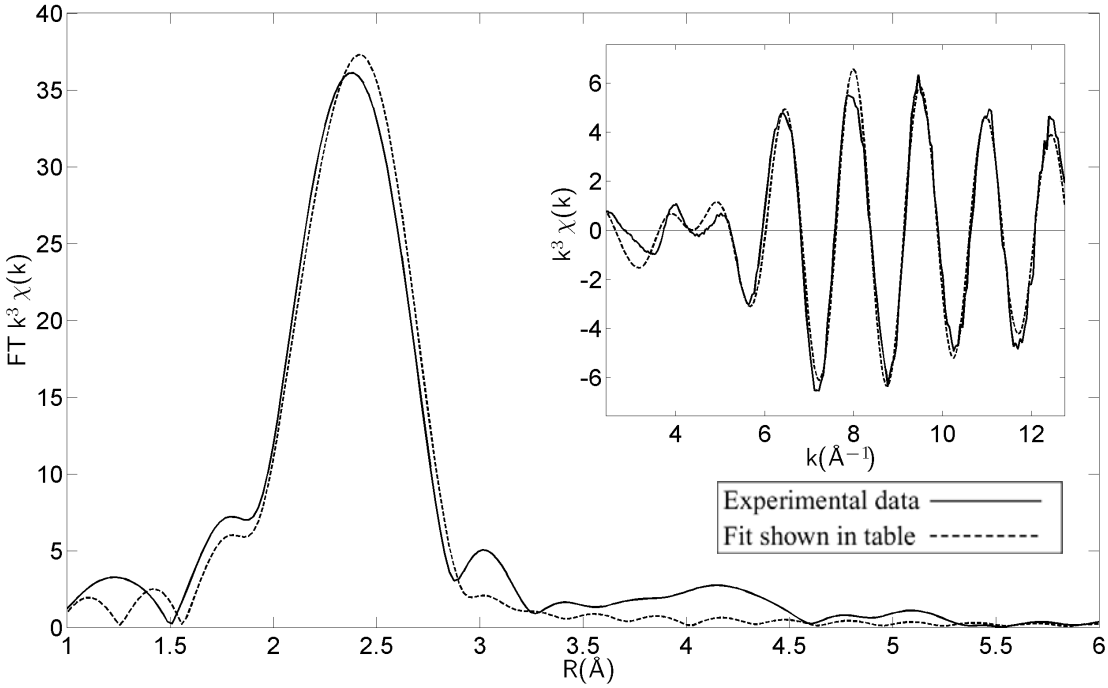

Scatterer	Distance (Å)	Debye-Waller (Å²)	-E_0 (eV)	F
1.0 C	1.98	0.007	3.58	0.287
2.0 Cu	2.38	0.007		

Figure 5.24. Se K-edge EXAFS of C22,25A243CAUA.

5.3.5 C22,25A243UACA

Due to the similarity at the Cu K-edge, it was expected that the Se K-edge EXAFS of the CCS243UACA protein would be similar to that of the –CAUA ligation construct with contributions from one Se-C and two Se-Cu. The best fit was obtained with 1 Se-C and 2 Se-Cu with $R(2\sigma^2)_{Se\text{-}C}$ = 2.00 Å (0.007 Å^2) and $R(2\sigma^2)_{Se\text{-}Cu}$ = 2.38 Å (0.008 Å^2) (Figure 5.25).

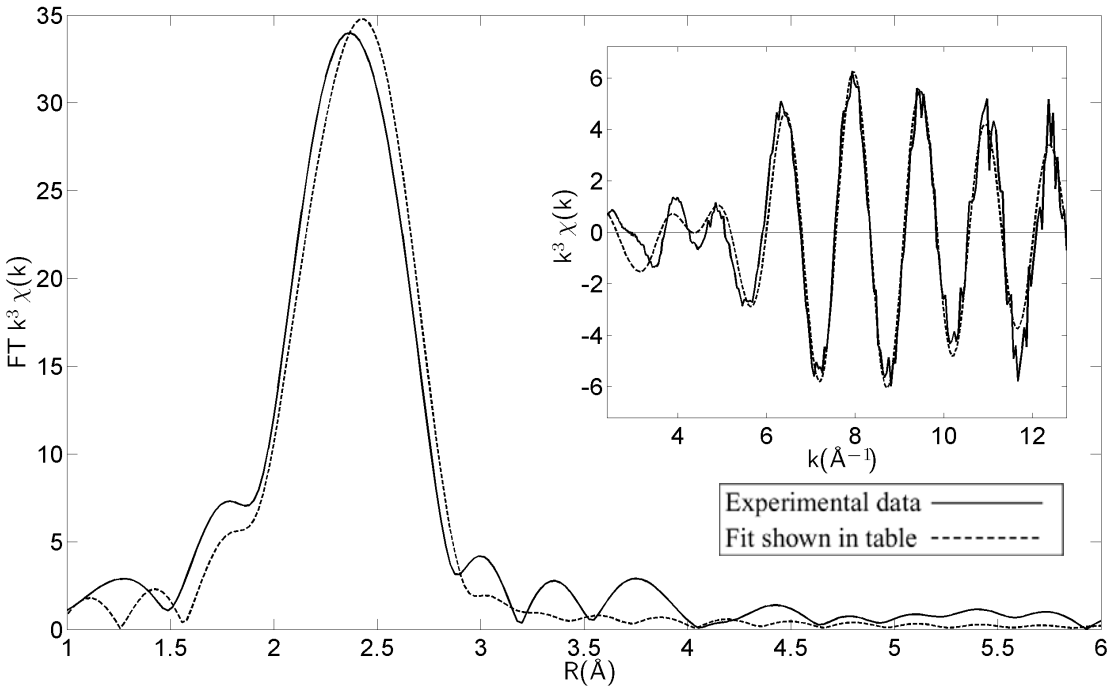

Scatterer	Distance (Å)	Debye-Waller (Å²)	-E_0 (eV)	F
1.0 C	2.00	0.007	4.10	0.523
2.0 Cu	2.38	0.008		

Figure 5.25. Se K-edge EXAFS of C22,25A243UACA.

5.3.6 C22,25A243UAUA

Like the CCS243UAUA construct, it would be expected that C22,25A243UAUA would have a similar Se environment to the single Sec substitutions if residues 244 and 246 have a similar environment. The best fit of the Se K-edge EXAFS shows contributions from 1 Se-C with $R(2\sigma^2)_{Se\text{-}C}$ = 2.01 Å (0.006 Å^2) and 2.0 Se-Cu with $R(2\sigma^2)_{Se\text{-}Cu}$ = 2.39 Å (0.007 Å^2), almost an identical fit to that seen for the single Sec substitutions (Figure 5.26).

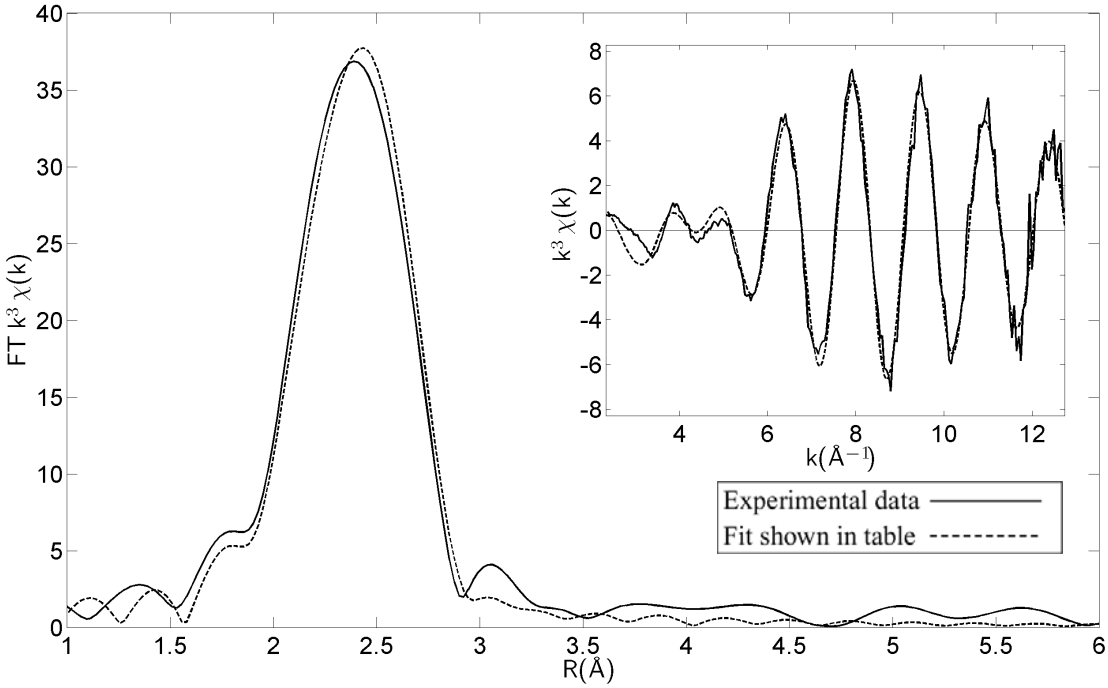

Scatterer	Distance (Å)	Debye-Waller (Å²)	-E_0 (eV)	F
1.0 C	2.01	0.006	5.09	0.338
2.0 Cu	2.39	0.007		

Figure 5.26. Se K-edge EXAFS of C22,25A243UAUA.

5.4 Conclusions

This chapter reports the successful ligation of peptides to a truncation of hCCS and to the D1 double mutant hCCS at amino acid 243. Ligation was attempted with two 6-residue peptides, but only successful with one, -CACDGA. Successful ligation of this peptide was confirmed with copper-binding, SOD1-activation assays, and Cu K-edge EXAFS, whereas mass spectral data was unclear. To further probe the D3-D3 copper cluster, four 4-residue peptides, -CAUA, -UACA, -UAUA, and –CACA (as a control), were successfully ligated, making eight constructs total. Mass spectral data, SOD1-activation assays, and copper-binding data all confirmed ligation. The intein-mediated amino acid ligation resulted in high yield and generated the desired CCS243X and C22,25A243X (X=peptide) protein of the expected mass.

As in the previous studies of apo-CCS245Sec and apo-C22,25A245Sec, apo-CCS243 and apo-C22,25A243CAUA were found to be present in forms containing both Se-S and Se-Se crosslinks. The Se-S selenylsulfido form could represent either intramolecular crosslinking between C244 and U246 or intermolecular dimerization. The Se-Se interaction identified in the Se K-edge EXAFS of the apo-CCS245Sec can only arise from an intermolecular diselenide formed via dimerization of the D3 polypeptide.

The C22,25A243 semisynthetic constructs bind between 1-2 Cu(I), with the –UAUA ligation construct binding 2.1 Cu/protein. As with the C22,25A245Sec and –Cys proteins, the consistent increase in Cu:CCS monomer ratios above 1.0 suggests that the D3-D3 cluster has a nuclearity greater than 2. The CCS243 constructs bind between 2-3 Cu(I), as with the CCS245 ligation constructs. Cu and Se K-edge EXAFS have been analyzed to provide metrical details of the coordination environments of the Cu and Se atoms (Table 5-4 -Table 5-7). The Se K-edge EXAFS of all of the constructs is almost identical with each Se edge environment containing 1 C and 2 Cu, except for the anomalous CCS243UACA construct. The peptide ligations again confirm that each Se sees ~2 Cu atoms in its first shell, and therefore must occupy a bridging position in the cluster, and that residues 244 and 246 are in analogous positions. The Cu EXAFS data for the ligations provides the strongest clue as to the structure of the D3-D3 copper cluster. The –CAUA and –UACA ligations both are similar to the single amino acid ligations, whereas the C22,25A243UAUA constructs provide the most compelling evidence for the existence of a Cu_4S_6 cluster as opposed to a trinuclear cluster (Figure 3.19). At the Cu edge, the C22,25A243UAUA protein has a contribution of 2 Cu-Se at 2.39 Å, as expected with two Sec residues present at the D3 Cu-binding site. In addition, there is 1 Cu-S at a distance of 2.17 Å. Because both the D1 and the D3 copper binding Cys residues have been mutated to Ala or Sec respectively, this contribution would only be seen if S was also a part of the D3-D3 copper cluster. Since both of the Sec residues are also involved as seen by the Se edge data, the structure must be a more complex Cu_4S_6 adamantane-like cluster as opposed to the Cu_3S_4 trinuclear cluster (Figure 5.27). This is also consistent with the number of Cu-S and Cu-Se interactions seen at the Cu edge for all of the peptide ligation variants.

When examining the Cu-Cu interactions in the C22,25A243UAUA protein Cu EXAFS, one would expect a contribution of 3 Cu-Cu at approximately 2.70 Å if the Cu_4S_6 cluster is present. A previous study of a synthetic Cu_4S_6 cluster showed that Cu EXAFS show 3 Cu-Cu interactions at approximately 2.70 Å with a DW value of 0.015 $Å^2$ and 3 Cu-S interactions at approximately 2.20 Å (Pickering et al. 1993). As described in Section 5.2.10, the DW value for the 2 Cu-Cu interactions of the C22,25A243UAUA fit (Figure 5.18) was set at 0.010 $Å^2$. If we increase this value to 0.015 $Å^2$, a contribution of 3 Cu-Cu can be defined with an overall F value of 0.391, a lower F value than the fit with 2 Cu-Cu at a DW of 0.010 $Å^2$ of 0.402. The change in modeled DW and accompanying change in the modeled Cu-Cu contribution can be applied to all of the peptide Cu EXAFS data, illustrating that indeed the Cu_4S_6 is a possible model for the D3-D3 copper cluster geometry. When refining for F as a function of the number of copper scatterers and DW in the C22,25A243UAUA Cu-EXAFS data (Figure 5.28), where the Cu-Cu metal-ligand distance and the number of Cu-S and Cu-Se are kept constant, we can see that DW and the number of copper scatterers affect one another, with the lowest F values forming a "trough". This is because the number of copper scatterers affects the amplitude of the Cu EXAFS wave, whereas the DW parameter attenuates the amplitude as k increases. Thus, knowledge of the copper stoichiometry and previous studies of reasonable DW values must be taken into consideration when examining possible fits for Cu EXAFS experimental data. It can be seen, however, that a value of 3 Cu-Cu scatterers at a DW of 0.015 $Å^2$ gives a lower F value than 2 Cu-Cu scatterers at a DW of 0.010 $Å^2$ (Figure 5.28), again showing that the Cu_4S_6 is the best model for the D3-D3 copper cluster.

Other Cys residues are present in the protein, most notably in the SOD1-like D2 domain, which is thought to form the dimerization site for apo-hCCS (Stasser et al., 2007). These include Cys141 and its disulfide partner Cys227. Recently, the Blackburn lab has constructed a Cys141Ala mutant of hCCS, and this contained no D3 copper cluster (Personal communication with Gnana Sutha Siluvai). Thus, Cys141 could provide the extra sulfur atoms required for the adamantine-like tetranuclear copper cluster.

Protein	Scatterer	Distance (Å)	Debye-Waller ($Å^2$)	$-E_0$ (eV)	F
CCS243CACDGA	2.8 S	2.26	0.01	5.95	0.323
	1.2 Cu	2.71	0.013		
CCS243CACA	2.8 S	2.25	0.011	5.67	0.283
	1.2 Cu	2.72	0.02		
CCS243CAUA	2.0 S	2.2	0.012	2.91	0.536
	0.8 Se	2.38	0.007		
	1.2 Cu	2.63	0.012		
CCS243UACA	2.0 S	2.2	0.014	-0.978	0.576
	0.8 Se	2.39	0.008		
	1.2 Cu	2.59	0.014		
CCS243UAUA	2.0 S	2.21	0.008	2.53	0.581
	0.8 Se	2.39	0.008		
	1.2 Cu	2.7	0.016		

Table 5-4. Master table of CCS243X Cu-EXAFS parameters.

Protein	Scatterer	Distance (Å)	Debye-Waller ($Å^2$)	$-E_0$ (eV)	F
C22,25A243CACDGA	2.7 S	2.27	0.007	6.28	0.429
	2.8 Cu	2.72	0.013		
C22,25A243CACA	2.7 S	2.26	0.008	5.69	0.404
	2.0 Cu	2.71	0.013		
C22,25A243CAUA	2.0 S	2.24	0.006	3.88	0.272
	1.0 Se	2.41	0.013		
	2.0 Cu	2.71	0.01		
C22,25A243UACA	2.0 S	2.23	0.008	2.83	0.249
	1.0 Se	2.41	0.009		
	2.0 Cu	2.7	0.01		
C22,25A243UAUA	1.0 S	2.17	0.002	-1.63	0.402
	2.0 Se	2.39	0.007		
	2.0 Cu	2.67	0.01		

Table 5-5. Master table of C22,25A243X Cu-EXAFS parameters.

Protein	Scatterer	Distance (Å)	Debye-Waller ($Å^2$)	$-E_0$ (eV)	F
ApoCCS243CAUA	1.0 C	2.01	0.015	4.72	0.479
	0.5 S	2.15	0.008		
	0.5 Se	2.32	0.004		
CCS243CAUA	1.0 C	2.03	0.012	3.84	0.838
	2.0 Cu	2.38	0.007		
CCS243UACA	1.0 C	1.98	0.012	3.72	1
	1.1 Cu	2.38	0.008		
	0.5 S	2.17	0.003		
CCS243UAUA	1.0 C	2.01	0.006	5.15	0.586
	2.0 Cu	2.39	0.008		

Table 5-6. Master table of CCS243X Se-EXAFS data.

Protein	Scatterer	Distance (Å)	Debye-Waller ($Å^2$)	$-E_0$ (eV)	F
ApoC22,25A243CAUA	1.0 C	1.99	0.012	4.97	0.31
	0.5 S	2.17	0.007		
	0.5 Se	2.31	0.004		
C22,25A243CAUA	1.0 C	1.98	0.007	3.58	0.287
	2.0 Cu	2.38	0.007		
C22,25A243UACA	1.0 C	2	0.007	4.1	0.523
	2.0 Cu	2.38	0.008		
C22,25A243UAUA	1.0 C	2.01	0.006	5.09	0.338
	2.0 Cu	2.39	0.007		

Table 5-7. Master table of C22,25A243X Se-EXAFS data.

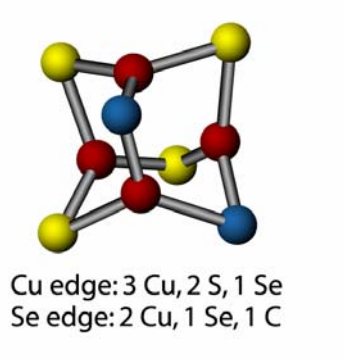

Figure 5.27. Cu_4S_6 tetranuclear cluster composed of three fused Cu_3S_3 hexagonal rings with two Se residues in blue, Cu in red, and S in yellow.

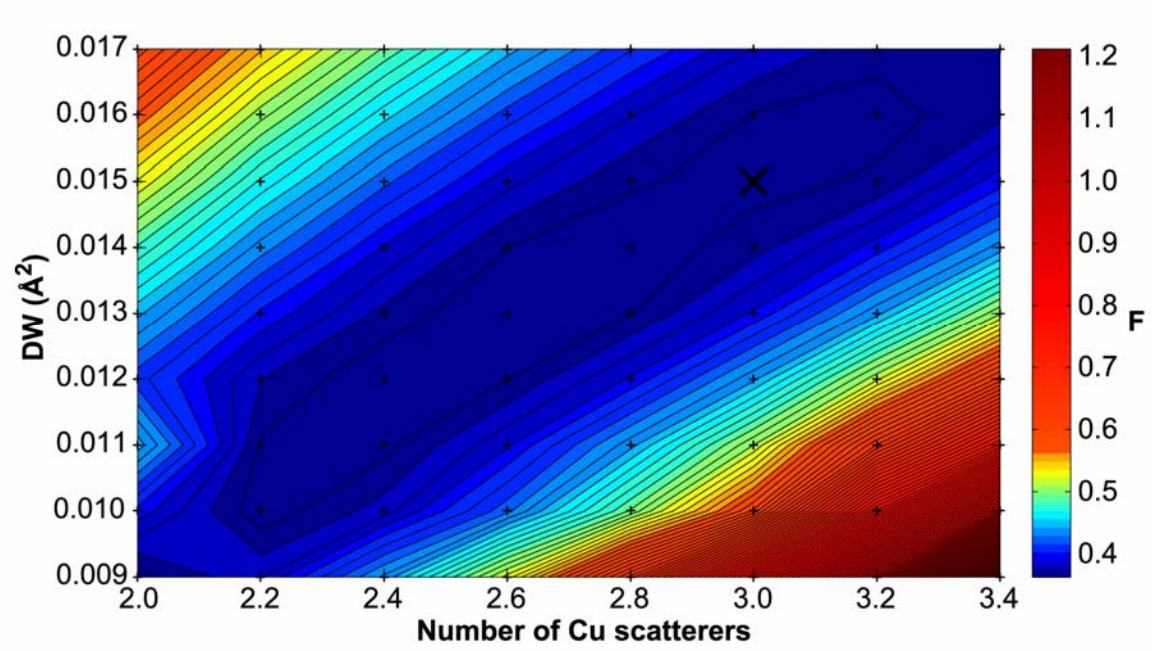

Figure 5.28. Contour plot of F as a function of the number of copper scatterers and DW in the C22,25A243UAUA Cu-EXAFS data.

CHAPTER 6: CONCLUSIONS AND FUTURE STUDIES

At the beginning of this project, the structure of the copper cluster in D3 of hCCS was unknown. Three possible candidates for the cluster structure include a bis-cysteine bridged dinuclear cluster, a trinuclear cluster based on a Cu_3S_3 hexagonal ring with one additional bridging cysteine, and a Cu_4S_6 tetranuclear cluster composed of three fused Cu_3S_3 hexagonal rings (Figure 3.19). This thesis describes the creation of a variety of hCCS selenocysteine-containing constructs using intein-mediated peptide ligation in order to investigate the D3-D3 copper cluster in detail. Ligation of a single amino acid, a 4-residue peptide, or 6-residue peptide were all shown to be successful with a high yield. Examination of apo-proteins by Se K-edge EXAFS illustrated the need for reduction of the D3 residues with TCEP before Cu binding. Cu binding was shown to be equivalent to full-length hCCS. Furthermore, all of the ligation variants were shown to be able to activate E,Zn-SOD1, including truncation variants that ended at residue 246 ending with the D3 CXC Cu-binding motif.

Copper transfer to E,Zn-SOD1 from CCS245Sec and C22,25A245Sec was monitored by Cu and Se EXAFS. Transfer from wild-type hCCS appeared to cause the D3 copper cluster to disappear, whereas a cluster was still present in both CCS245Sec and C22,25A245Sec. Furthermore, SOD1 could not be completely purified from the CCS245Sec/SOD1 mixture. This may indicate a stronger CCS245Sec/SOD1 complex

compared to that of hCCS/SOD, resulting in more complex EXAFS spectra at the Cu K-edge and the appearance of an intact Cu cluster at the Se edge.

Cu edge and Se edge data of the CCS245Sec variant provided the first clues as to the structure of the copper cluster. In this construct, the Se-Cu interaction extracted from the Se K-edge data shows 2 Se-Cu interactions at 2.41 Å. Fits using lower Se-Cu coordination numbers produce higher least squares residuals, and more importantly, lead to parameters which lead to unacceptable fits to the Cu-edge data. Therefore, each Se sees 2 Cu atoms in its first shell, and therefore must occupy a bridging position in the cluster. A dinuclear cluster with two bridging Se atoms would require each Cu to be coordinated to 2 Se and 1 S (Figure 3.19). Attempts to fit the Cu K-edge data to this model, using the Cu-Se distances and DW factors extracted from the Se edge were routinely unsuccessful, leading to inconsistent analyses at the Cu and Se K-edge respectively. However, when higher cluster nuclearity was introduced, the Cu and Se K-edge data could be simulated with parameters which were consistent at both edges. In the CCS245Sec construct, the presence of Cu(I) bound in D1 still contributed to the Cu K-edge data, introducing some ambiguity into the fitting results.

The use of D1 C22,25A mutants at the CXXC Cu(I) binding helped resolve the ambiguity concerning the Cu-edge data of the CCS245Sec protein. The C22,25A245Sec Cu K-edge EXAFS showed two neighboring Cu(I) centers at the Cu edge, with each copper seeing 2.1 Cu at 2.70 Å. Due to the higher nuclearity, the structure of the Cu cluster must not fit the dinuclear model. Furthermore, each copper sees a greater contribution from S than from Se. Due to the mutation of the D1 Cys residues, one would suspect an equal contribution of S and Se from the remaining D3 CXU present in the cluster formation. With this information, the formation of a dinuclear cluster in these constructs can be ruled out, favoring the trinuclear or tetranuclear structures as possible candidates (Figure 3.19).

In order to investigate these two possibilities, it was beneficial to mutate the second Cys residue in the D3 copper-binding motif to a Sec in order to fully tease out the D3-D3 copper cluster. To further probe the D3-D3 copper cluster, one 6-residue and four 4-residue peptides, -CACDGA, -CAUA, -UACA, -UAUA, and –CACA (where –CACDGA and –CACA were used as controls), were successfully ligated, making ten constructs total. The Se K-edge EXAFS of all of the constructs was almost identical with each Se edge environment containing 1 C and 2 Cu (Table 5-6; Table 5-7). The peptide ligations again confirm that each Se sees ~2 Cu atoms in its first shell, and therefore must occupy a bridging position in the cluster, and, more importantly, that both the Sec244 and Sec246 residues of the D3 Cu-binding motif occupy a bridging position within the cluster. The Cu edge data for the ligations provided the strongest clue as to the structure of the D3-D3 copper cluster (Table 5-4; Table 5-5). The –CAUA and –UACA ligations both are similar to the single amino acid ligations, whereas the –UAUA constructs provide the most compelling evidence for the existence of a Cu_4S_6 cluster as opposed to a trinuclear cluster. At the Cu K-edge, the C22,25A243UAUA protein has a contribution of 1 Cu-S at a distance of 2.19 Å. Because both the D1 and the D3 copper binding Cys residues have been mutated to Ala or Sec respectively, this contribution would only be seen if S was also a part of the D3-D3 copper cluster. Since both of the Sec residues are also involved as seen by the Se edge data, the structure must be a more complex Cu_4S_6 adamantane-like cluster as opposed to the Cu_3S_4 trinuclear cluster (Figure 3.19). With this final information, the formation of a dinuclear or a trinuclear cluster in these constructs can be ruled out, favoring the tetranuclear structure.

A possible mechanism including the Cu_4S_6 copper cluster is shown (Figure 6.1). If the mechanism were to follow the left-hand path of the figure, the D3-D3 copper cluster could remain intact upon copper transfer with the formation of a dimer of dimers of hCCS and SOD1. By following the right-hand path of the mechanism, the copper cluster would have to disassemble in order to form a heterodimer with one monomer of hCCS and SOD1. It is unclear if the hCCS D3 copper-binding site would contain copper once transfer to SOD1 was complete.

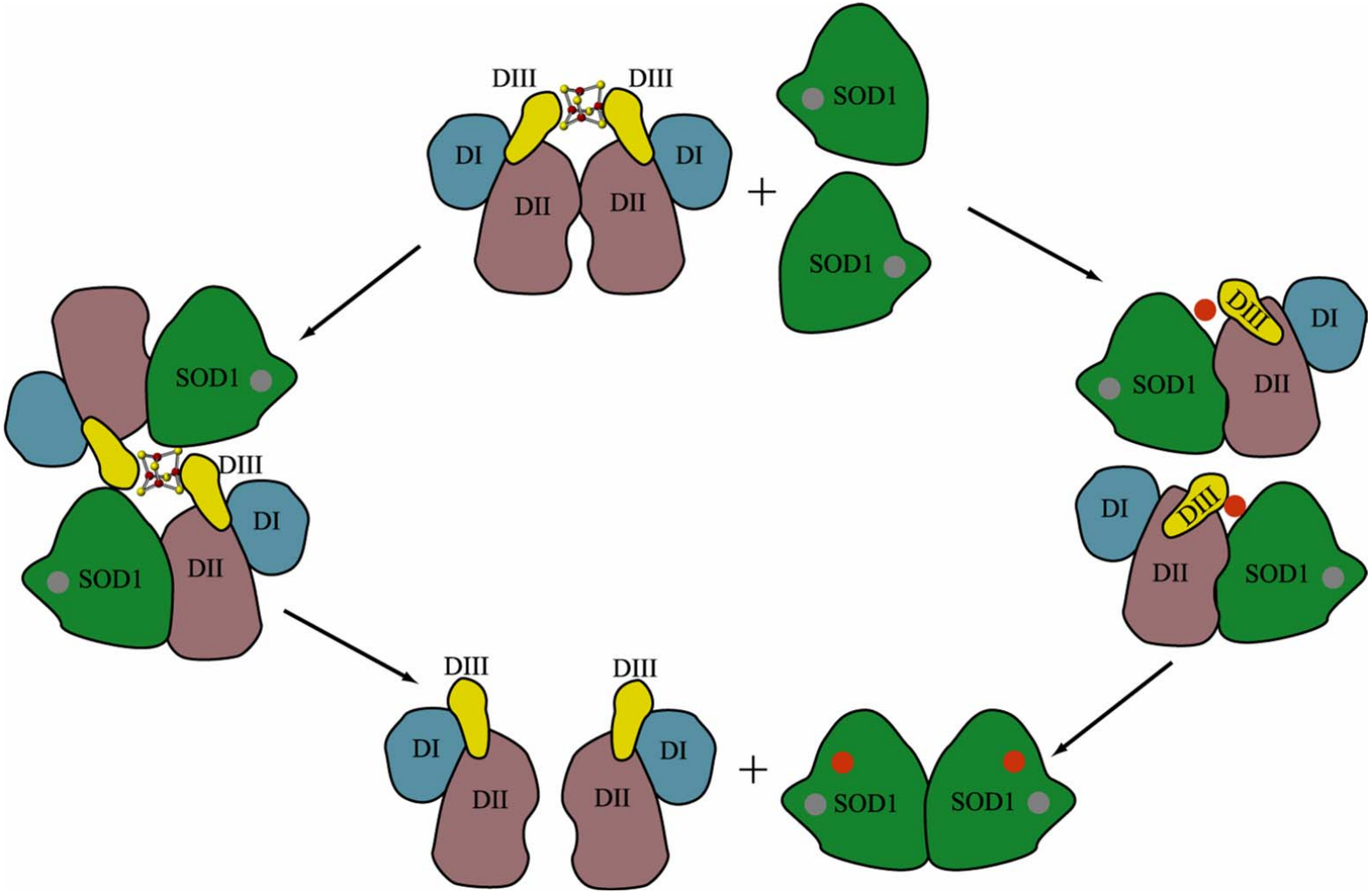

Figure 6.1. Possible mechanism for transfer to SOD1 from hCCS including the Cu_4S_6 D3-D3 copper cluster.

Other Cys residues are present in the protein, most notably in the SOD1-like D2 domain, which is thought to form the dimerization site for apo-hCCS (Stasser et al., 2007) (Figure 6.2). It is conceivable that these residues might be involved in the formation of the copper cluster at the D3-D3 interface. Furthermore, copper transfer experiments from selenocysteine variants of hCCS to E,Zn-SOD1 monitored with Cu and Se EXAFS always showed copper still present at the Se edge even when transfer appeared successful by Cu-histidine signal at the Cu edge. This would be possible if only one copper transferred from the tetranuclear cluster, specifically the copper bound to the additional S atoms from residues in another part of the CCS protein.

```
  1 MASDSGNQGTLCTLEFAVQMTCQSCVDAVR 30
 31 KSLQGVAGVQDVEVHLEDQMVLVHTTLPSQ 60
 61 EVQALLEGTGRQAVLKGMGSGQLQNLGAAV 90
 91 AILGGPGTVQGVVRFLQLTPERCLIEGTID 120
121 GLEPGLHGLHVHQYGDLTNNCNSCGNHFNP 150
151 DGASHGGPQDSDRHRGDLGNVRADADGRAI 180
181 FRMEDEQLKVWDVIGRSLIIDEGEDDLGRG 210
211 GHPLSKITGNSGERLACGIIARSAGLFQNP 240
241 KQICSCDGLTIWEERGRPIAGKGRKESA
```

Figure 6.2. hCCS sequence. Cys residues in copper-binding motifs are in red, all others are in green.

Mutation of Cys residues in D2 of hCCS in conjunction with selenocysteine incorporation would provide greater insight into the structure of the D3-D3 copper cluster, as there are still questions about the structure. In D2, these include Cys113, Cys144, Cys141 and its disulfide partner Cys227, which form a homologous disulfide to that found in SOD1 (Lamb et al. 2000; Rae et al. 2001). Intriguingly, the homologous cysteine in SOD1, Cys57, to the hCCS Cys141 was found to form a disulfide with Cys229 from yCCS in the yCCS-ySOD1 crystal structure (Lamb et al. 2001) (Figure). It is conceivable that Cys141 of hCCS provides the extra Cys ligand in the Cu_4S_6 D3-D3

copper cluster, and upon binding to SOD1 for copper transfer, is replaced by the SOD1 Cys57 to facilitate copper transfer from the cluster to the SOD1 metal-binding site. Recently, the Blackburn lab has constructed a Cys141Ala mutant of hCCS, and this contained no D3 copper cluster (Personal communication from Gnana Sutha Siluvai). Thus, Cys141 could provide the extra sulfur atoms required for the adamantine-like tetranuclear copper cluster. Is the Cu-S contribution from D2 Cys residues? If so, are these residues required for successful copper transfer from hCCS to SOD1? If apo-hCCS forms a dimer at a D2-D2 interface, how does the mutation of Cys residues in this domain affect this dimer as copper is added to the protein? If involved in copper binding at the D3-D3 interface, it is conceivable that these Cys residues are required for separation of the apo-hCCS homodimer upon Cu reconstitution.

Furthermore, another method of creating an internal selenocysteine probe without truncating hCCS may provide useful information about the copper cluster structure. For example, Cys244 and Cys246 could be mutated to Met residues. Protocols have been developed and applied in the production of selenomethionine labeled proteins using the conditional Met auxotroph *E. coli* B834 (Hadener et al., 1993; Pieper et al., 1997; Sreenath et al., 2005). Thus, Se would still be present at all Met residues without truncation and subsequent amino acid ligation. To avoid incorporation in other Met residues within the protein, these could be mutated as well. The full-length protein would be more similar to wild-type hCCS as compared to the truncation mutants and may provide a more analogous model of copper binding and activation of SOD1.

BIBLIOGRAPHY

Abajian, C., and Rosenzweig, A. C. (2006). Crystal structure of yeast Sco1. *J Biol Inorg Chem* **11,** 459-66.

Abajian, C., Yatsunyk, L. A., Ramirez, B. E., and Rosenzweig, A. C. (2004). Yeast cox17 solution structure and Copper(I) binding. *J Biol Chem* **279,** 53584-92.

Aller, S. G., and Unger, V. M. (2006). Projection structure of the human copper transporter CTR1 at 6-A resolution reveals a compact trimer with a novel channel-like architecture. *Proc Natl Acad Sci U S A* **103,** 3627-32.

Anastassopoulou, I., Banci, L., Bertini, I., Cantini, F., Katsari, E., and Rosato, A. (2004). Solution structure of the apo and copper(I)-loaded human metallochaperone HAH1. *Biochemistry* **43,** 13046-53.

Andrews, G. K. (2000). Regulation of metallothionein gene expression by oxidative stress and metal ions. *Biochem Pharmacol* **59,** 95-104.

Angeletti, B., Waldron, K. J., Freeman, K. B., Bawagan, H., Hussain, I., Miller, C. C., Lau, K. F., Tennant, M. E., Dennison, C., Robinson, N. J., and Dingwall, C.

(2005). BACE1 cytoplasmic domain interacts with the copper chaperone for superoxide dismutase-1 and binds copper. *J Biol Chem* **280,** 17930-7.

Arnesano, F., Banci, L., Bertini, I., and Martinelli, M. (2005). Ortholog search of proteins involved in copper delivery to cytochrome C oxidase and functional analysis of paralogs and gene neighbors by genomic context. *J Proteome Res* **4,** 63-70.

Aschner, M. (1996). The functional significance of brain metallothioneins. *Faseb J* **10,** 1129-36.

Aschner, M., Syversen, T., Souza, D. O., and Rocha, J. B. (2006). Metallothioneins: mercury species-specific induction and their potential role in attenuating neurotoxicity. *Exp Biol Med (Maywood)* **231,** 1468-73.

Askwith, C. C., and Kaplan, J. (1998). Site-directed mutagenesis of the yeast multicopper oxidase Fet3p. *J Biol Chem* **273,** 22415-9.

Auf der Maur, A., Belser, T., Wang, Y., Gunes, C., Lichtlen, P., Georgiev, O., and Schaffner, W. (2000). Characterization of the mouse gene for the heavy metal-responsive transcription factor MTF-1. *Cell Stress Chaperones* **5,** 196-206.

Balatri, E., Banci, L., Bertini, I., Cantini, F., and Ciofi-Baffoni, S. (2003). Solution structure of Sco1: a thioredoxin-like protein Involved in cytochrome c oxidase assembly. *Structure* **11,** 1431-43.

Banci, L., Bertini, I., Calderone, V., Ciofi-Baffoni, S., Mangani, S., Martinelli, M., Palumaa, P., and Wang, S. (2006). A hint for the function of human Sco1 from different structures. *Proc Natl Acad Sci U S A* **103,** 8595-600.

Banci, L., Bertini, I., Cantini, F., Ciofi-Baffoni, S., Gonnelli, L., and Mangani, S. (2004). Solution structure of Cox11, a novel type of beta-immunoglobulin-like fold

involved in CuB site formation of cytochrome c oxidase. *J Biol Chem* **279,** 34833-9.

Banci, L., Bertini, I., Cantini, F., D'Onofrio, M., and Viezzoli, M. S. (2002a). Structure and dynamics of copper-free SOD: The protein before binding copper. *Protein Sci* **11,** 2479-92.

Banci, L., Bertini, I., Cramaro, F., Del Conte, R., and Viezzoli, M. S. (2002b). The solution structure of reduced dimeric copper zinc superoxide dismutase. The structural effects of dimerization. *Eur J Biochem* **269,** 1905-15.

Bartnikas, T. B., and Gitlin, J. D. (2003). Mechanisms of biosynthesis of mammalian copper/zinc superoxide dismutase. *J Biol Chem* **278,** 33602-8.

Beaudoin, J., and Labbe, S. (2001). The fission yeast copper-sensing transcription factor Cuf1 regulates the copper transporter gene expression through an Ace1/Amt1-like recognition sequence. *J Biol Chem* **276,** 15472-80.

Beaudoin, J., Mercier, A., Langlois, R., and Labbe, S. (2003). The Schizosaccharomyces pombe Cuf1 is composed of functional modules from two distinct classes of copper metalloregulatory transcription factors. *J Biol Chem* **278,** 14565-77.

Beckman, J. S., Esetvez, A. G., Barbeito, L., and Crow, J. P. (2002). CCS knockout mice establish an alternative source of copper for SOD in ALS. *Free Radic Biol Med* **33,** 1433-5.

Beers, J., Glerum, D. M., and Tzagoloff, A. (1997). Purification, characterization, and localization of yeast Cox17p, a mitochondrial copper shuttle. *J Biol Chem* **272,** 33191-6.

Beers, J., Glerum, D. M., and Tzagoloff, A. (2002). Purification and characterization of yeast Sco1p, a mitochondrial copper protein. *J Biol Chem* **277,** 22185-90.

Bellemare, D. R., Sanschagrin, M., Beaudoin, J., and Labbe, S. (2001). A novel copper-regulated promoter system for expression of heterologous proteins in Schizosaccharomyces pombe. *Gene* **273,** 191-8.

Bellemare, D. R., Shaner, L., Morano, K. A., Beaudoin, J., Langlois, R., and Labbe, S. (2002). Ctr6, a vacuolar membrane copper transporter in Schizosaccharomyces pombe. *J Biol Chem* **277,** 46676-86.

Bertinato, J., Iskandar, M., and L'Abbe, M. R. (2003). Copper deficiency induces the upregulation of the copper chaperone for Cu/Zn superoxide dismutase in weanling male rats. *J Nutr* **133,** 28-31.

Bertinato, J., and L'Abbe, M. R. (2003). Copper modulates the degradation of copper chaperone for Cu,Zn superoxide dismutase by the 26 S proteosome. *J Biol Chem* **278,** 35071-8.

Binsted, N., and Hasnain, S. S. (1996). State-of-the-Art Analysis of Whole X-ray Absorption Spectra. *J Synchrotron Radiat* **3,** 185-96.

Blackburn, N. J., Hasnain, S. S., Diakun, G. P., Knowles, P. F., Binsted, N., and Garner, C. D. (1983). An extended X-ray-absorption-fine-structure study of the copper and zinc sites of freeze-dried bovine superoxide dismutase. *Biochem J* **213,** 765-8.

Boden, N., Holmes, M. C., and Knowles, P. F. (1979). Properties of the cupric sites in bovine superoxide dismutase studied by nuclear-magnetic-relaxation measurements. *Biochem J* **177,** 303-9.

Borghouts, C., Scheckhuber, C. Q., Stephan, O., and Osiewacz, H. D. (2002). Copper homeostasis and aging in the fungal model system Podospora anserina: differential expression of PaCtr3 encoding a copper transporter. *Int J Biochem Cell Biol* **34,** 1355-71.

Bremner, I. (1991). Metallothionein and copper metabolism in liver. *Methods Enzymol* **205,** 584-91.

Britton, R. S. (1996). Metal-induced hepatotoxicity. *Semin Liver Dis* **16,** 3-12.

Brown, K. R., Keller, G. L., Pickering, I. J., Harris, H. H., George, G. N., and Winge, D. R. (2002). Structures of the cuprous-thiolate clusters of the Mac1 and Ace1 transcriptional activators. *Biochemistry* **41,** 6469-76.

Brown, N. M., Torres, A. S., Doan, P. E., and O'Halloran, T. V. (2004). Oxygen and the copper chaperone CCS regulate posttranslational activation of Cu,Zn superoxide dismutase. *Proc Natl Acad Sci U S A* **101,** 5518-23.

Buchwald, P., Krummeck, G., and Rodel, G. (1991). Immunological identification of yeast SCO1 protein as a component of the inner mitochondrial membrane. *Mol Gen Genet* **229,** 413-20.

Bull, P. C., Thomas, G. R., Rommens, J. M., Forbes, J. R., and Cox, D. W. (1993). The Wilson disease gene is a putative copper transporting P-type ATPase similar to the Menkes gene. *Nat Genet* **5,** 327-37.

Carr, H. S., George, G. N., and Winge, D. R. (2002). Yeast Cox11, a protein essential for cytochrome c oxidase assembly, is a Cu(I)-binding protein. *J Biol Chem* **277,** 31237-42.

Carr, H. S., and Winge, D. R. (2003). Assembly of cytochrome c oxidase within the mitochondrion. *Acc Chem Res* **36,** 309-16.

Carroll, M. C., Girouard, J. B., Ulloa, J. L., Subramaniam, J. R., Wong, P. C., Valentine, J. S., and Culotta, V. C. (2004). Mechanisms for activating Cu- and Zn-containing superoxide dismutase in the absence of the CCS Cu chaperone. *Proc Natl Acad Sci U S A* **101,** 5964-9.

Carroll, M. C., Outten, C. E., Proescher, J. B., Rosenfeld, L., Watson, W. H., Whitson, L. J., Hart, P. J., Jensen, L. T., and Cizewski Culotta, V. (2006). The effects of glutaredoxin and copper activation pathways on the disulfide and stability of Cu,Zn superoxide dismutase. *J Biol Chem* **281,** 28648-56.

Carter, P. (1987). Improved oligonucleotide-directed mutagenesis using M13 vectors. *Methods Enzymol* **154,** 382-403.

Caruano-Yzermans, A. L., Bartnikas, T. B., and Gitlin, J. D. (2006). Mechanisms of the copper-dependent turnover of the copper chaperone for superoxide dismutase. *J Biol Chem* **281,** 13581-7.

Casareno, R. L., Waggoner, D., and Gitlin, J. D. (1998). The copper chaperone CCS directly interacts with copper/zinc superoxide dismutase. *J Biol Chem* **273,** 23625-8.

Cater, M. A., Forbes, J., La Fontaine, S., Cox, D., and Mercer, J. F. (2004). Intracellular trafficking of the human Wilson protein: the role of the six N-terminal metal-binding sites. *Biochem J* **380,** 805-13.

Chelly, J., Tumer, Z., Tonnesen, T., Petterson, A., Ishikawa-Brush, Y., Tommerup, N., Horn, N., and Monaco, A. P. (1993). Isolation of a candidate gene for Menkes disease that encodes a potential heavy metal binding protein. *Nat Genet* **3,** 14-9.

Chinenov, Y. V. (2000). Cytochrome c oxidase assembly factors with a thioredoxin fold are conserved among prokaryotes and eukaryotes. *J Mol Med* **78,** 239-42.

Chong, S., Mersha, F. B., Comb, D. G., Scott, M. E., Landry, D., Vence, L. M., Perler, F. B., Benner, J., Kucera, R. B., Hirvonen, C. A., Pelletier, J. J., Paulus, H., and Xu, M. Q. (1997). Single-column purification of free recombinant proteins using a self-cleavable affinity tag derived from a protein splicing element. *Gene* **192,** 271-81.

Cobine, P. A., Ojeda, L. D., Rigby, K. M., and Winge, D. R. (2004). Yeast contain a non-proteinaceous pool of copper in the mitochondrial matrix. *J Biol Chem* **279,** 14447-55.

Corson, L. B., Strain, J. J., Culotta, V. C., and Cleveland, D. W. (1998). Chaperone-facilitated copper binding is a property common to several classes of familial amyotrophic lateral sclerosis-linked superoxide dismutase mutants. *Proc Natl Acad Sci U S A* **95,** 6361-6.

Culotta, V. C., and Gitlin, J. D. (2001). The disorders of copper transport. *In* "The metabolic and molecular bases of inherited disease." (D. Valle, Ed.), pp. 3105-3126. McGraw-Hill, New York.

Culotta, V. C., Howard, W. R., and Liu, X. F. (1994). CRS5 encodes a metallothionein-like protein in Saccharomyces cerevisiae. *J Biol Chem* **269,** 25295-302.

Culotta, V. C., Joh, H. D., Lin, S. J., Slekar, K. H., and Strain, J. (1995). A physiological role for Saccharomyces cerevisiae copper/zinc superoxide dismutase in copper buffering. *J Biol Chem* **270,** 29991-7.

Dancis, A., Haile, D., Yuan, D. S., and Klausner, R. D. (1994a). The Saccharomyces cerevisiae copper transport protein (Ctr1p). Biochemical characterization, regulation by copper, and physiologic role in copper uptake. *J Biol Chem* **269,** 25660-7.

Dancis, A., Yuan, D. S., Haile, D., Askwith, C., Eide, D., Moehle, C., Kaplan, J., and Klausner, R. D. (1994b). Molecular characterization of a copper transport protein in S. cerevisiae: an unexpected role for copper in iron transport. *Cell* **76,** 393-402.

David, R., Richter, M. P., and Beck-Sickinger, A. G. (2004). Expressed protein ligation. Method and applications. *Eur J Biochem* **271,** 663-77.

De Silva, D. M., Askwith, C. C., Eide, D., and Kaplan, J. (1995). The FET3 gene product required for high affinity iron transport in yeast is a cell surface ferroxidase. *J Biol Chem* **270,** 1098-101.

Dickinson, E. K., Adams, D. L., Schon, E. A., and Glerum, D. M. (2000). A human SCO2 mutation helps define the role of Sco1p in the cytochrome oxidase assembly pathway. *J Biol Chem* **275,** 26780-5.

Duquesne, A. E., Ruijter, M., Brouwer, J., Drijfhout, J. W., Nabuurs, S. B., Spronk, C. A., Vuister, G. W., Ubbink, M., and Canters, G. W. (2005). Solution Structure of the Second PDZ Domain of the Neuronal Adaptor X11alpha and its Interaction with the C-terminal Peptide of the Human Copper Chaperone for Superoxide Dismutase. *J Biomol NMR* **32,** 209-18.

Durnam, D. M., and Palmiter, R. D. (1987). Analysis of the detoxification of heavy metal ions by mouse metallothionein. *Experientia Suppl* **52,** 457-63.

Egli, D., Selvaraj, A., Yepiskoposyan, H., Zhang, B., Hafen, E., Georgiev, O., and Schaffner, W. (2003). Knockout of 'metal-responsive transcription factor' MTF-1

in Drosophila by homologous recombination reveals its central role in heavy metal homeostasis. *Embo J* **22,** 100-8.

Egli, D., Yepiskoposyan, H., Selvaraj, A., Balamurugan, K., Rajaram, R., Simons, A., Multhaup, G., Mettler, S., Vardanyan, A., Georgiev, O., and Schaffner, W. (2006). A family knockout of all four Drosophila metallothioneins reveals a central role in copper homeostasis and detoxification. *Mol Cell Biol* **26,** 2286-96.

Eisses, J. F., and Kaplan, J. H. (2005). The mechanism of copper uptake mediated by human CTR1: a mutational analysis. *J Biol Chem* **280,** 37159-68.

Eisses, J. F., Stasser, J. P., Ralle, M., Kaplan, J. H., and Blackburn, N. J. (2000). Domains I and III of the human copper chaperone for superoxide dismutase interact via a cysteine-bridged Dicopper(I) cluster. *Biochemistry* **39,** 7337-42.

Endo, T., Fujii, T., Sato, K., Taniguchi, N., and Fujii, J. (2000). A pivotal role of Zn-binding residues in the function of the copper chaperone for SOD1. *Biochem Biophys Res Commun* **276,** 999-1004.

Evans, T. C., Jr., and Xu, M. Q. (1999). Intein-mediated protein ligation: harnessing nature's escape artists. *Biopolymers* **51,** 333-42.

Feng, W., Cai, J., Pierce, W. M., Franklin, R. B., Maret, W., Benz, F. W., and Kang, Y. J. (2005). Metallothionein transfers zinc to mitochondrial aconitase through a direct interaction in mouse hearts. *Biochem Biophys Res Commun* **332,** 853-8.

Ferguson-Miller, S., and Babcock, G. T. (1996). Heme/Copper Terminal Oxidases. *Chem Rev* **96,** 2889-2908.

Fridovich, I. (1995). Superoxide radical and superoxide dismutases. *Annu Rev Biochem* **64,** 97-112.

Furukawa, Y., Torres, A. S., and O'Halloran, T. V. (2004). Oxygen-induced maturation of SOD1: a key role for disulfide formation by the copper chaperone CCS. *Embo J* **23,** 2872-81.

Garcia, S., Prado, M., Degano, R., and Dominguez, A. (2002). A copper-responsive transcription factor, CRF1, mediates copper and cadmium resistance in Yarrowia lipolytica. *J Biol Chem* **277,** 37359-68.

George, G. N. (2001). EXAFSPAK.

Giedroc, D. P., Chen, X., and Apuy, J. L. (2001). Metal response element (MRE)-binding transcription factor-1 (MTF-1): structure, function, and regulation. *Antioxid Redox Signal* **3,** 577-96.

Glerum, D. M., Shtanko, A., and Tzagoloff, A. (1996a). Characterization of COX17, a yeast gene involved in copper metabolism and assembly of cytochrome oxidase. *J Biol Chem* **271,** 14504-9.

Glerum, D. M., Shtanko, A., and Tzagoloff, A. (1996b). SCO1 and SCO2 act as high copy suppressors of a mitochondrial copper recruitment defect in Saccharomyces cerevisiae. *J Biol Chem* **271,** 20531-5.

Gralla, E. B., Thiele, D. J., Silar, P., and Valentine, J. S. (1991). ACE1, a copper-dependent transcription factor, activates expression of the yeast copper, zinc superoxide dismutase gene. *Proc Natl Acad Sci U S A* **88,** 8558-62.

Guo, Y., Smith, K., Lee, J., Thiele, D. J., and Petris, M. J. (2004). Identification of methionine-rich clusters that regulate copper-stimulated endocytosis of the human Ctr1 copper transporter. *J Biol Chem* **279,** 17428-33.

Gurman, S. J. (1995). Interpretation of EXAFS Data. *J Synchrotron Radiat* **2,** 56-63.

Hadener, A., Matzinger, P. K., Malashkevich, V. N., Louie, G. V., Wood, S. P., Oliver, P., Alefounder, P. R., Pitt, A. R., Abell, C., and Battersby, A. R. (1993). Purification, characterization, crystallisation and X-ray analysis of selenomethionine-labelled hydroxymethylbilane synthase from Escherichia coli. *Eur J Biochem* **211,** 615-24.

Halliwell, B., and Gutteridge, J. M. (1984). Oxygen toxicity, oxygen radicals, transition metals and disease. *Biochem J* **219,** 1-14.

Hamer, D. H., Thiele, D. J., and Lemontt, J. E. (1985). Function and autoregulation of yeast copperthionein. *Science* **228,** 685-90.

Hart, P. J., Balbirnie, M. M., Ogihara, N. L., Nersissian, A. M., Weiss, M. S., Valentine, J. S., and Eisenberg, D. (1999). A structure-based mechanism for copper-zinc superoxide dismutase. *Biochemistry* **38,** 2167-78.

Hassett, R., and Kosman, D. J. (1995). Evidence for Cu(II) reduction as a component of copper uptake by Saccharomyces cerevisiae. *J Biol Chem* **270,** 128-34.

Heaton, D., Nittis, T., Srinivasan, C., and Winge, D. R. (2000). Mutational analysis of the mitochondrial copper metallochaperone Cox17. *J Biol Chem* **275,** 37582-7.

Heaton, D. N., George, G. N., Garrison, G., and Winge, D. R. (2001). The mitochondrial copper metallochaperone Cox17 exists as an oligomeric, polycopper complex. *Biochemistry* **40,** 743-51.

Heuchel, R., Radtke, F., Georgiev, O., Stark, G., Aguet, M., and Schaffner, W. (1994). The transcription factor MTF-1 is essential for basal and heavy metal-induced metallothionein gene expression. *Embo J* **13,** 2870-5.

Himelblau, E., Mira, H., Lin, S. J., Culotta, V. C., Penarrubia, L., and Amasino, R. M. (1998). Identification of a functional homolog of the yeast copper homeostasis gene ATX1 from Arabidopsis. *Plant Physiol* **117,** 1227-34.

Hiser, L., Di Valentin, M., Hamer, A. G., and Hosler, J. P. (2000). Cox11p is required for stable formation of the Cu(B) and magnesium centers of cytochrome c oxidase. *J Biol Chem* **275,** 619-23.

Hofmann, R. M., and Muir, T. W. (2002). Recent advances in the application of expressed protein ligation to protein engineering. *Curr Opin Biotechnol* **13,** 297-303.

Horng, Y. C., Cobine, P. A., Maxfield, A. B., Carr, H. S., and Winge, D. R. (2004). Specific copper transfer from the Cox17 metallochaperone to both Sco1 and Cox11 in the assembly of yeast cytochrome C oxidase. *J Biol Chem* **279,** 35334-40.

Horng, Y. C., Leary, S. C., Cobine, P. A., Young, F. B., George, G. N., Shoubridge, E. A., and Winge, D. R. (2005). Human Sco1 and Sco2 function as copper-binding proteins. *J Biol Chem* **280,** 34113-22.

Huster, D., Hoppert, M., Lutsenko, S., Zinke, J., Lehmann, C., Mossner, J., Berr, F., and Caca, K. (2003). Defective cellular localization of mutant ATP7B in Wilson's disease patients and hepatoma cell lines. *Gastroenterology* **124,** 335-45.

Jensen, L. T., and Culotta, V. C. (2005). Activation of CuZn superoxide dismutases from Caenorhabditis elegans does not require the copper chaperone CCS. *J Biol Chem* **280,** 41373-9.

Jensen, L. T., Howard, W. R., Strain, J. J., Winge, D. R., and Culotta, V. C. (1996). Enhanced effectiveness of copper ion buffering by CUP1 metallothionein compared with CRS5 metallothionein in Saccharomyces cerevisiae. *J Biol Chem* **271,** 18514-9.

Jensen, L. T., Posewitz, M. C., Srinivasan, C., and Winge, D. R. (1998). Mapping of the DNA binding domain of the copper-responsive transcription factor Mac1 from Saccharomyces cerevisiae. *J Biol Chem* **273,** 23805-11.

Jiang, J., Nadas, I. A., Kim, M. A., and Franz, K. J. (2005). A Mets motif peptide found in copper transport proteins selectively binds Cu(I) with methionine-only coordination. *Inorg Chem* **44,** 9787-94.

Joshi, A., Serpe, M., and Kosman, D. J. (1999). Evidence for (Mac1p)2.DNA ternary complex formation in Mac1p-dependent transactivation at the CTR1 promoter. *J Biol Chem* **274,** 218-26.

Kagi, J. H. (1991). Overview of metallothionein. *Methods Enzymol* **205,** 613-26.

Kato, S., Sumi-Akamaru, H., Fujimura, H., Sakoda, S., Kato, M., Hirano, A., Takikawa, M., and Ohama, E. (2001). Copper chaperone for superoxide dismutase co-aggregates with superoxide dismutase 1 (SOD1) in neuronal Lewy body-like hyaline inclusions: an immunohistochemical study on familial amyotrophic lateral sclerosis with SOD1 gene mutation. *Acta Neuropathol (Berl)* **102,** 233-8.

Keller, G., Bird, A., and Winge, D. R. (2005). Independent metalloregulation of Ace1 and Mac1 in Saccharomyces cerevisiae. *Eukaryot Cell* **4,** 1863-71.

Kelner, G. S., Lee, M., Clark, M. E., Maciejewski, D., McGrath, D., Rabizadeh, S., Lyons, T., Bredesen, D., Jenner, P., and Maki, R. A. (2000). The copper transport protein Atox1 promotes neuronal survival. *J Biol Chem* **275,** 580-4.

Kille, P., Hemmings, A., and Lunney, E. A. (1994). Memories of metallothionein. *Biochim Biophys Acta* **1205,** 151-61.

Klomp, L. W., Lin, S. J., Yuan, D. S., Klausner, R. D., Culotta, V. C., and Gitlin, J. D. (1997). Identification and functional expression of HAH1, a novel human gene involved in copper homeostasis. *J Biol Chem* **272,** 9221-6.

Koningsberger, D. C., and Prins, R. (1988). "X-ray absorption : principles, applications, techniques of EXAFS, SEXAFS, and XANES." Wiley, New York.

Kosman, D. J. (2002). FET3P, ceruloplasmin, and the role of copper in iron metabolism. *Adv Protein Chem* **60,** 221-69.

Kosman, D. J. (2003). Molecular mechanisms of iron uptake in fungi. *Mol Microbiol* **47,** 1185-97.

Labbe, S., Pena, M. M., Fernandes, A. R., and Thiele, D. J. (1999). A copper-sensing transcription factor regulates iron uptake genes in Schizosaccharomyces pombe. *J Biol Chem* **274,** 36252-60.

Labbe, S., Zhu, Z., and Thiele, D. J. (1997). Copper-specific transcriptional repression of yeast genes encoding critical components in the copper transport pathway. *J Biol Chem* **272,** 15951-8.

Lamb, A. L., Torres, A. S., O'Halloran, T. V., and Rosenzweig, A. C. (2001). Heterodimeric structure of superoxide dismutase in complex with its metallochaperone. *Nat Struct Biol* **8,** 751-5.

Lamb, A. L., Wernimont, A. K., Pufahl, R. A., Culotta, V. C., O'Halloran, T. V., and Rosenzweig, A. C. (1999). Crystal structure of the copper chaperone for superoxide dismutase. *Nat Struct Biol* **6,** 724-9.

Lamb, A. L., Wernimont, A. K., Pufahl, R. A., O'Halloran, T. V., and Rosenzweig, A. C. (2000). Crystal structure of the second domain of the human copper chaperone for superoxide dismutase. *Biochemistry* **39,** 1589-95.

Lastowski-Perry, D., Otto, E., and Maroni, G. (1985). Nucleotide sequence and expression of a Drosophila metallothionein. *J Biol Chem* **260,** 1527-30.

Leary, S. C., Cobine, P. A., Kaufman, B. A., Guercin, G. H., Mattman, A., Palaty, J., Lockitch, G., Winge, D. R., Rustin, P., Horvath, R., and Shoubridge, E. A. (2007). The human cytochrome c oxidase assembly factors SCO1 and SCO2 have regulatory roles in the maintenance of cellular copper homeostasis. *Cell Metab* **5,** 9-20.

Lee, D. Y., Brewer, G. J., and Wang, Y. X. (1989). Treatment of Wilson's disease with zinc. VII. Protection of the liver from copper toxicity by zinc-induced metallothionein in a rat model. *J Lab Clin Med* **114,** 639-45.

Lee, J., Pena, M. M., Nose, Y., and Thiele, D. J. (2002). Biochemical characterization of the human copper transporter Ctr1. *J Biol Chem* **277,** 4380-7.

Lichtlen, P., and Schaffner, W. (2001). Putting its fingers on stressful situations: the heavy metal-regulatory transcription factor MTF-1. *Bioessays* **23,** 1010-7.

Lim, C. M., Cater, M. A., Mercer, J. F., and La Fontaine, S. (2006). Copper-dependent interaction of glutaredoxin with the N termini of the copper-ATPases (ATP7A and ATP7B) defective in Menkes and Wilson diseases. *Biochem Biophys Res Commun* **348,** 428-36.

Lin, S. J., Pufahl, R. A., Dancis, A., O'Halloran, T. V., and Culotta, V. C. (1997). A role for the Saccharomyces cerevisiae ATX1 gene in copper trafficking and iron transport. *J Biol Chem* **272,** 9215-20.

Liu, S. X., Fabisiak, J. P., Tyurin, V. A., Borisenko, G. G., Pitt, B. R., Lazo, J. S., and Kagan, V. E. (2000). Reconstitution of apo-superoxide dismutase by nitric oxide-induced copper transfer from metallothioneins. *Chem Res Toxicol* **13,** 922-31.

Lode, A., Kuschel, M., Paret, C., and Rodel, G. (2000). Mitochondrial copper metabolism in yeast: interaction between Sco1p and Cox2p. *FEBS Lett* **485,** 19-24.

Maroni, G., Otto, E., and Lastowski-Perry, D. (1986). Molecular and cytogenetic characterization of a metallothionein gene of Drosophila. *Genetics* **112,** 493-504.

Mattatall, N. R., Jazairi, J., and Hill, B. C. (2000). Characterization of YpmQ, an accessory protein required for the expression of cytochrome c oxidase in Bacillus subtilis. *J Biol Chem* **275,** 28802-9.

Maxfield, A. B., Heaton, D. N., and Winge, D. R. (2004). Cox17 is functional when tethered to the mitochondrial inner membrane. *J Biol Chem* **279,** 5072-80.

McCord, J. M. and I. Fridovich (1968). The reduction of cytochrome *c* by milk xanthine oxidase. *J Biol Chem* **243**(21): 5753-60.

McCord, J. M. and I. Fridovich (1969). Superoxide dismutase. An enzymic function for erythrocuprein (hemocuprein). *J Biol Chem* **244**(22): 6049-55.

McLoughlin, D. M., Standen, C. L., Lau, K. F., Ackerley, S., Bartnikas, T. P., Gitlin, J. D., and Miller, C. C. (2001). The neuronal adaptor protein X11alpha interacts

with the copper chaperone for SOD1 and regulates SOD1 activity. *J Biol Chem* **276,** 9303-7.

Mercer, J. F., Livingston, J., Hall, B., Paynter, J. A., Begy, C., Chandrasekharappa, S., Lockhart, P., Grimes, A., Bhave, M., Siemieniak, D., and et al. (1993). Isolation of a partial candidate gene for Menkes disease by positional cloning. *Nat Genet* **3,** 20-5.

Muir, T. W. (2003). Semisynthesis of proteins by expressed protein ligation. *Annu Rev Biochem* **72,** 249-89.

Muir, T. W., Sondhi, D., and Cole, P. A. (1998). Expressed protein ligation: a general method for protein engineering. *Proc Natl Acad Sci U S A* **95,** 6705-10.

Muramatsu, Y., Yamada, T., Moralejo, D. H., Suzuki, Y., and Matsumoto, K. (1998). Fetal copper uptake and a homolog (Atp7b) of the Wilson's disease gene in rats. *Res Commun Mol Pathol Pharmacol* **101,** 225-31.

Nittis, T., George, G. N., and Winge, D. R. (2001). Yeast Sco1, a protein essential for cytochrome c oxidase function is a Cu(I)-binding protein. *J Biol Chem* **276,** 42520-6.

Nose, Y., Rees, E. M., and Thiele, D. J. (2006). Structure of the Ctr1 copper trans'PORE'ter reveals novel architecture. *Trends Biochem Sci* **31,** 604-7.

Ogra, Y., Aoyama, M., and Suzuki, K. T. (2006). Protective role of metallothionein against copper depletion. *Arch Biochem Biophys* **451,** 112-8.

Okado-Matsumoto, A., Myint, T., Fujii, J., and Taniguchi, N. (2000). Gain in functions of mutant Cu,Zn-superoxide dismutases as a causative factor in familial

amyotrophic lateral sclerosis: less reactive oxidant formation but high spontaneous aggregation and precipitation. *Free Radic Res* **33,** 65-73.

Ooi, C. E., Rabinovich, E., Dancis, A., Bonifacino, J. S., and Klausner, R. D. (1996). Copper-dependent degradation of the Saccharomyces cerevisiae plasma membrane copper transporter Ctr1p in the apparent absence of endocytosis. *Embo J* **15,** 3515-23.

Palmiter, R. D. (1998). The elusive function of metallothioneins. *Proc Natl Acad Sci U S A* **95,** 8428-30.

Pena, M. M., Lee, J., and Thiele, D. J. (1999). A delicate balance: homeostatic control of copper uptake and distribution. *J Nutr* **129,** 1251-60.

Petris, M. J. (2004). The SLC31 (Ctr) copper transporter family. *Pflugers Arch* **447,** 752-5.

Petris, M. J., Mercer, J. F., Culvenor, J. G., Lockhart, P., Gleeson, P. A., and Camakaris, J. (1996). Ligand-regulated transport of the Menkes copper P-type ATPase efflux pump from the Golgi apparatus to the plasma membrane: a novel mechanism of regulated trafficking. *Embo J* **15,** 6084-95.

Petris, M. J., Smith, K., Lee, J., and Thiele, D. J. (2003). Copper-stimulated endocytosis and degradation of the human copper transporter, hCtr1. *J Biol Chem* **278,** 9639-46.

Pickering, I. J., George, G. N., Dameron, C. T., Kurz, B., Winge, D. R., and Dance, I. G. (1993) X-ray absorption spectroscopy of cuprous-thiolate clusters in proteins and model systems, *J. Am. Chem. Soc*. **115**, 9498-9505.

Pieper, M., Betz, M., Budisa, N., Gomis-Ruth, F. X., Bode, W., and Tschesche, H. (1997). Expression, purification, characterization, and X-ray analysis of selenomethionine 215 variant of leukocyte collagenase. *J Protein Chem* **16,** 637-50.

Prohaska, J. R., Broderius, M., and Brokate, B. (2003). Metallochaperone for Cu,Zn-superoxide dismutase (CCS) protein but not mRNA is higher in organs from copper-deficient mice and rats. *Arch Biochem Biophys* **417,** 227-34.

Puig, S., Lee, J., Lau, M., and Thiele, D. J. (2002). Biochemical and genetic analyses of yeast and human high affinity copper transporters suggest a conserved mechanism for copper uptake. *J Biol Chem* **277,** 26021-30.

Punter, F. A., and Glerum, D. M. (2003). Mutagenesis reveals a specific role for Cox17p in copper transport to cytochrome oxidase. *J Biol Chem* **278,** 30875-80.

Rae, T. D., Schmidt, P. J., Pufahl, R. A., Culotta, V. C., and O'Halloran, T. V. (1999). Undetectable intracellular free copper: the requirement of a copper chaperone for superoxide dismutase. *Science* **284,** 805-8.

Rae, T. D., Torres, A. S., Pufahl, R. A., and O'Halloran, T. V. (2001). Mechanism of Cu,Zn-superoxide dismutase activation by the human metallochaperone hCCS. *J Biol Chem* **276,** 5166-76.

Ralle, M., Berry, S. M., Nilges, M. J., Gieselman, M. D., van der Donk, W. A., Lu, Y., and Blackburn, N. J. (2004). The selenocysteine-substituted blue copper center: spectroscopic investigations of Cys112SeCys Pseudomonas aeruginosa azurin. *J Am Chem Soc* **126,** 7244-56.

Ralle, M., Lutsenko, S., and Blackburn, N. J. (2003). X-ray absorption spectroscopy of the copper chaperone HAH1 reveals a linear two-coordinate Cu(I) center capable

of adduct formation with exogenous thiols and phosphines. *J Biol Chem* **278,** 23163-70.

Ralle, M., Verkhovskaya, M. L., Morgan, J. E., Verkhovsky, M. I., Wikstrom, M., and Blackburn, N. J. (1999). Coordination of CuB in reduced and CO-liganded states of cytochrome bo3 from Escherichia coli. Is chloride ion a cofactor? *Biochemistry* **38,** 7185-94.

Rentzsch, A., Krummeck-Weiss, G., Hofer, A., Bartuschka, A., Ostermann, K., and Rodel, G. (1999). Mitochondrial copper metabolism in yeast: mutational analysis of Sco1p involved in the biogenesis of cytochrome c oxidase. *Curr Genet* **35,** 103-8.

Richardson, J., Thomas, K. A., Rubin, B. H., and Richardson, D. C. (1975). Crystal structure of bovine Cu,Zn superoxide dismutase at 3 A resolution: chain tracing and metal ligands. *Proc Natl Acad Sci U S A* **72,** 1349-53.

Rosen, D. R., Siddique, T., Patterson, D., Figlewicz, D. A., Sapp, P., Hentati, A., Donaldson, D., Goto, J., O'Regan, J. P., Deng, H. X., and et al. (1993). Mutations in Cu/Zn superoxide dismutase gene are associated with familial amyotrophic lateral sclerosis. *Nature* **362,** 59-62.

Rothstein, J. D., Dykes-Hoberg, M., Corson, L. B., Becker, M., Cleveland, D. W., Price, D. L., Culotta, V. C., and Wong, P. C. (1999). The copper chaperone CCS is abundant in neurons and astrocytes in human and rodent brain. *J Neurochem* **72,** 422-9.

Ruzsa, S. M., and Scandalios, J. G. (2003). Altered Cu metabolism and differential transcription of Cu/ZnSod genes in a Cu/ZnSOD-deficient mutant of maize: evidence for a Cu-responsive transcription factor. *Biochemistry* **42,** 1508-16.

Schmidt, P. J., Kunst, C., and Culotta, V. C. (2000). Copper activation of superoxide dismutase 1 (SOD1) in vivo. Role for protein-protein interactions with the copper chaperone for SOD1. *J Biol Chem* **275,** 33771-6.

Schmidt, P. J., Ramos-Gomez, M., and Culotta, V. C. (1999). A gain of superoxide dismutase (SOD) activity obtained with CCS, the copper metallochaperone for SOD1. *J Biol Chem* **274,** 36952-6.

Serpe, M., Joshi, A., and Kosman, D. J. (1999). Structure-function analysis of the protein-binding domains of Mac1p, a copper-dependent transcriptional activator of copper uptake in Saccharomyces cerevisiae. *J Biol Chem* **274,** 29211-9.

Severinov, K., and Muir, T. W. (1998). Expressed protein ligation, a novel method for studying protein-protein interactions in transcription. *J Biol Chem* **273,** 16205-9.

Shi, X., Stoj, C., Romeo, A., Kosman, D. J., and Zhu, Z. (2003). Fre1p Cu2+ reduction and Fet3p Cu1+ oxidation modulate copper toxicity in Saccharomyces cerevisiae. *J Biol Chem* **278,** 50309-15.

Shiraishi, M., Utsumi, K., Morimoto, S., Joja, I., Iida, S., Takeda, Y., and Aono, K. (1982). Inhibition of nitroblue tetrazolium reduction by metallothionein. *Physiol Chem Phys* **14,** 533-7.

Silar, P., and Wegnez, M. (1990). Expression of the Drosophila melanogaster metallothionein genes in yeast. *FEBS Lett* **269,** 273-6.

Son, M., Cloyd, C. D., Rothstein, J. D., Rajendran, B., and Elliott, J. L. (2003). Aggregate formation in Cu,Zn superoxide dismutase-related proteins. *J Biol Chem* **278,** 14331-6.

Sreenath, H. K., Bingman, C. A., Buchan, B. W., Seder, K. D., Burns, B. T., Geetha, H. V., Jeon, W. B., Vojtik, F. C., Aceti, D. J., Frederick, R. O., Phillips, G. N., Jr., and Fox, B. G. (2005). Protocols for production of selenomethionine-labeled proteins in 2-L polyethylene terephthalate bottles using auto-induction medium. *Protein Expr Purif* **40,** 256-67.

Stasser, J. P., Eisses, J. F., Barry, A. N., Kaplan, J. H., and Blackburn, N. J. (2005). Cysteine-to-serine mutants of the human copper chaperone for superoxide dismutase reveal a copper cluster at a domain III dimer interface. *Biochemistry* **44,** 3143-52.

Stasser, J. P., Siluvai Pitchai, G., Barry, A. N., and Blackburn, N. J. (2007). A Multinuclear Copper (I) Cluster Forms the Dimerization Interface in Copper-loaded Human Copper Chaperone for Superoxide Dismutase. *Biochemistry* **In publication**.

Stearman, R., Yuan, D. S., Yamaguchi-Iwai, Y., Klausner, R. D., and Dancis, A. (1996). A permease-oxidase complex involved in high-affinity iron uptake in yeast. *Science* **271,** 1552-7.

Strange, R. W., Antonyuk, S., Hough, M. A., Doucette, P. A., Rodriguez, J. A., Hart, P. J., Hayward, L. J., Valentine, J. S., and Hasnain, S. S. (2003). The structure of holo and metal-deficient wild-type human Cu, Zn superoxide dismutase and its relevance to familial amyotrophic lateral sclerosis. *J Mol Biol* **328,** 877-91.

Subramaniam, J. R., Lyons, W. E., Liu, J., Bartnikas, T. B., Rothstein, J., Price, D. L., Cleveland, D. W., Gitlin, J. D., and Wong, P. C. (2002). Mutant SOD1 causes motor neuron disease independent of copper chaperone-mediated copper loading. *Nat Neurosci* **5,** 301-7.

Suzuki, T., Yamanaka, H., Nakajima, K., Kanatani, K., Suzuki, K., Kimura, M., Nakazawa, Y., and Otaki, N. (1993). Induction of metallothionein by CdCl2 administration in rat prostate. *Prostate* **22,** 163-70.

Szczypka, M. S., Zhu, Z., Silar, P., and Thiele, D. J. (1997). Saccharomyces cerevisiae mutants altered in vacuole function are defective in copper detoxification and iron-responsive gene transcription. *Yeast* **13,** 1423-35.

Taanman, J. W., and Capaldi, R. A. (1992). Purification of yeast cytochrome c oxidase with a subunit composition resembling the mammalian enzyme. *J Biol Chem* **267,** 22481-5.

Tanzi, R. E., Petrukhin, K., Chernov, I., Pellequer, J. L., Wasco, W., Ross, B., Romano, D. M., Parano, E., Pavone, L., Brzustowicz, L. M., and et al. (1993). The Wilson disease gene is a copper transporting ATPase with homology to the Menkes disease gene. *Nat Genet* **5,** 344-50.

Telenti, A., Southworth, M., Alcaide, F., Daugelat, S., Jacobs, W. R., Jr., and Perler, F. B. (1997). The Mycobacterium xenopi GyrA protein splicing element: characterization of a minimal intein. *J Bacteriol* **179,** 6378-82.

Teo, B. K. (1986). "EXAFS : basic principles and data analysis." Springer-Verlag, Berlin ; New York.

Thiele, D. J. (1988). ACE1 regulates expression of the Saccharomyces cerevisiae metallothionein gene. *Mol Cell Biol* **8,** 2745-52.

Thornalley, P. J., and Vasak, M. (1985). Possible role for metallothionein in protection against radiation-induced oxidative stress. Kinetics and mechanism of its reaction with superoxide and hydroxyl radicals. *Biochim Biophys Acta* **827,** 36-44.

Torres, A. S., Petri, V., Rae, T. D., and O'Halloran, T. V. (2001). Copper stabilizes a heterodimer of the yCCS metallochaperone and its target superoxide dismutase. *J Biol Chem* **276,** 38410-6.

Tzagoloff, A., Capitanio, N., Nobrega, M. P., and Gatti, D. (1990). Cytochrome oxidase assembly in yeast requires the product of COX11, a homolog of the P. denitrificans protein encoded by ORF3. *Embo J* **9,** 2759-64.

Tzagoloff, A., and Dieckmann, C. L. (1990). PET genes of Saccharomyces cerevisiae. *Microbiol Rev* **54,** 211-25.

Uchida, Y., Takio, K., Titani, K., Ihara, Y., and Tomonaga, M. (1991). The growth inhibitory factor that is deficient in the Alzheimer's disease brain is a 68 amino acid metallothionein-like protein. *Neuron* **7,** 337-47.

Urbanski, N. K., and Beresewicz, A. (2000). Generation of *OH initiated by interaction of Fe2+ and Cu+ with dioxygen; comparison with the Fenton chemistry. *Acta Biochim Pol* **47,** 951-62.

Uriu-Adams, J. Y., and Keen, C. L. (2005). Copper, oxidative stress, and human health. *Mol Aspects Med* **26,** 268-98.

Valko, M., Morris, H., and Cronin, M. T. (2005). Metals, toxicity and oxidative stress. *Curr Med Chem* **12,** 1161-208.

Vasak, M., Galdes, A., Hill, H. A., Kagi, J. H., Bremner, I., and Young, B. W. (1980). Investigation of the structure of metallothioneins by proton nuclear magnetic resonance spectroscopy. *Biochemistry* **19,** 416-25.

Vulpe, C., Levinson, B., Whitney, S., Packman, S., and Gitschier, J. (1993). Isolation of a candidate gene for Menkes disease and evidence that it encodes a copper-transporting ATPase. *Nat Genet* **3,** 7-13.

Walker, J. M., Huster, D., Ralle, M., Morgan, C. T., Blackburn, N. J., and Lutsenko, S. (2004). The N-terminal metal-binding site 2 of the Wilson's Disease Protein plays a key role in the transfer of copper from Atox1. *J Biol Chem* **279,** 15376-84.

Watanabe, M., Dykes-Hoberg, M., Culotta, V. C., Price, D. L., Wong, P. C., and Rothstein, J. D. (2001). Histological evidence of protein aggregation in mutant SOD1 transgenic mice and in amyotrophic lateral sclerosis neural tissues. *Neurobiol Dis* **8,** 933-41.

Wernimont, A. K., Huffman, D. L., Lamb, A. L., O'Halloran, T. V., and Rosenzweig, A. C. (2000). Structural basis for copper transfer by the metallochaperone for the Menkes/Wilson disease proteins. *Nat Struct Biol* **7,** 766-71.

Wernimont, A. K., Yatsunyk, L. A., and Rosenzweig, A. C. (2004). Binding of copper(I) by the Wilson disease protein and its copper chaperone. *J Biol Chem* **279,** 12269-76.

Williams, J. C., Sue, C., Banting, G. S., Yang, H., Glerum, D. M., Hendrickson, W. A., and Schon, E. A. (2005). Crystal structure of human SCO1: implications for redox signaling by a mitochondrial cytochrome c oxidase "assembly" protein. *J Biol Chem* **280,** 15202-11.

Winge, D. R. (1998). Copper-regulatory domain involved in gene expression. *Prog Nucleic Acid Res Mol Biol* **58,** 165-95.

Yamada, M., Hayashi, S., Hozumi, I., Inuzuka, T., Tsuji, S., and Takahashi, H. (1996). Subcellular localization of growth inhibitory factor in rat brain: light and electron microscopic immunohistochemical studies. *Brain Res* **735,** 257-64.

Yamaguchi, Y., Heiny, M. E., and Gitlin, J. D. (1993). Isolation and characterization of a human liver cDNA as a candidate gene for Wilson disease. *Biochem Biophys Res Commun* **197,** 271-7.

Yamaguchi-Iwai, Y., Serpe, M., Haile, D., Yang, W., Kosman, D. J., Klausner, R. D., and Dancis, A. (1997). Homeostatic regulation of copper uptake in yeast via direct binding of MAC1 protein to upstream regulatory sequences of FRE1 and CTR1. *J Biol Chem* **272,** 17711-8.

Ye, Q., Imriskova-Sosova, I., Hill, B. C., and Jia, Z. (2005). Identification of a disulfide switch in BsSco, a member of the Sco family of cytochrome c oxidase assembly proteins. *Biochemistry* **44,** 2934-42.

Yonkovich, J., McKenndry, R., Shi, X., and Zhu, Z. (2002). Copper ion-sensing transcription factor Mac1p post-translationally controls the degradation of its target gene product Ctr1p. *J Biol Chem* **277,** 23981-4.

Yoshida, M., Saegusa, Y., Fukuda, A., Akama, Y., and Owada, S. (2005). Measurement of radical-scavenging ability in hepatic metallothionein of rat using in vivo electron spin resonance spectroscopy. *Toxicology* **213,** 74-80.

Zhang, B., Egli, D., Georgiev, O., and Schaffner, W. (2001). The Drosophila homolog of mammalian zinc finger factor MTF-1 activates transcription in response to heavy metals. *Mol Cell Biol* **21,** 4505-14.

Zhou, B., and Gitschier, J. (1997). hCTR1: a human gene for copper uptake identified by complementation in yeast. *Proc Natl Acad Sci U S A* **94,** 7481-6.

Zhou, H., Cadigan, K. M., and Thiele, D. J. (2003). A copper-regulated transporter required for copper acquisition, pigmentation, and specific stages of development in Drosophila melanogaster. *J Biol Chem* **278,** 48210-8.

Zhou, P. B., and Thiele, D. J. (1991). Isolation of a metal-activated transcription factor gene from Candida glabrata by complementation in Saccharomyces cerevisiae. *Proc Natl Acad Sci U S A* **88,** 6112-6.

Zhu, H., Shipp, E., Sanchez, R. J., Liba, A., Stine, J. E., Hart, P. J., Gralla, E. B., Nersissian, A. M., and Valentine, J. S. (2000). Cobalt(2+) binding to human and tomato copper chaperone for superoxide dismutase: implications for the metal ion transfer mechanism. *Biochemistry* **39,** 5413-21.

BIOGRAPHICAL SKETCH

I was born in Redding, California on March 25, 1976. For my undergraduate education, I studied at Oregon State University, receiving two Honors Baccalaureate degrees in Biochemistry and Biophysics and in Bioresource Research. My undergraduate thesis was completed in Crop and Soil Science, examining soil changes upon movement to non-thermal residue management in grass seed fields in the Willamette Valley. I also worked in the lab of Dr. Katherine Field studying fecal coliforms in Tillamook Bay, Oregon. For my undergraduate research, I received the Richard Chambers Environmental Grant, the DB DeLoach Scientific Study Grant, and the Oregon State University Research Office Summer Research Grant. During my undergraduate studies, I was a member of the Oregon State University Honors College and a recipient of the Powis Lee and Winifred Carlos Heitmeyer Scholarship. After my undergraduate education, I moved to Madison, Wisconsin for my graduate education at the University of Wisconsin-Madison. Working in the laboratory of Dr. Brian Fox, I completed my Masters in Bacteriology with a thesis on the metallobiochemistry of the extremophilic archaeon, *Ferroplasma acidarmanus*. In 2002, I began my education at the Oregon Graduate Institute at Oregon Health and Science University in the laboratory of Dr. Ninian Blackburn where I received the Charles Patrick Memorial Fund Award and completed the research contained within this thesis. In 2006, I received the Igor Stojiljkovic Memorial Fellowship for my presentation of this research.

Publications

Himes R.A., Park G.Y., **Barry A.N.**, Blackburn N.J., and K.D. Karlin, "Synthesis and X-ray absorption spectroscopy structural studies of Cu(I) complexes of histidylhistidine peptides: the predominance of linear 2-coordinate geometry." *J Am Chem Soc*, **2007**, 129(17):5352-3.

Stasser J.P., Eisses J.F., **Barry A.N.**, Kaplan J.H., Blackburn N.J., "Cysteine-to-serine mutants of the human copper chaperone for superoxide dismutase reveal a copper cluster at a domain III dimer interface" *Biochemistry*, **2005**,44(9):3143-52.